Slow pyrolysis of agro-food waste to produce biochar and activated carbon for adsorption of pollutants from model wastewater

A Thesis Submitted to the
College of Graduate and Postdoctoral Studies
In Partial Fulfilment of the Requirements
For the Degree of Master of Science
In the Department of Chemical and Biological Engineering
University of Saskatchewan
Saskatoon

By

Biswa Ranjan Patra

PERMISSION TO USE

In presenting this thesis towards the partial fulfilment of the requirements for Master of Science degree from the University of Saskatchewan, the author agrees that the libraries of the University of Saskatchewan may make it freely available for reference. The author further agrees that the copying of this thesis in any manner, entirely or partially, for academic purpose may be granted by Dr. Ajay Dalai who supervised this thesis work, or in his absence, by the Head of the Department of Chemical and Biological Engineering or by the Dean of the College of Graduate Studies and Research at the University of Saskatchewan. However, it is understood that any copying or publication or use of this thesis or parts thereof for financial gains shall not be permitted without the author's written approval. It is also understood that the author would be recognized and so will the University of Saskatchewan be for any scholarly use of any material available in this thesis.

Request for permission to copy or to make other use of the material in this thesis in whole or in part should be addressed to:

Head of the Department
Chemical and Biological Engineering
University of Saskatchewan
57 Campus Drive
Saskatoon, Saskatchewan S7N 5A9 Canada
OR
Dean College of Graduate and Postdoctoral Studies
University of Saskatchewan
Room 116 Thorvaldson Building, 110 Science Place
Saskatoon, Saskatchewan S7N 5C9 Canada

ABSTRACT

The increasing human population has induced more demand for food, and to cope with that demand agricultural production has been increased. The wastes generated from such activities resulted in environmental pollution and emanated the deterioration of the climate. Therefore, effective management and utilization of different kinds of wastes are crucial to mitigate greenhouse gas generation challenges upon natural decomposition and waste accumulation. Conversion of biogenic wastes to biofuels and bioproducts can address the energy crisis and play a role in environmental remediation. In this study, the first phase of work was focused on exploring the characteristics of food waste (mixture of onion peel, carrot peel, bell pepper stalks, potato peel, celery head and leaves, watermelon shell, orange peel, pumpkin seeds and pistachio shells) and agricultural crop residues (e.g., canola hull and oar hull) to determine their candidacy for slow pyrolysis to produce biochar, bio-oil, and gaseous products. Process parameters of slow pyrolysis such as temperature, reaction time and heating rate were investigated for food waste to obtain maximum biochar yields. Furthermore, the obtained favourable conditions were utilized for the slow pyrolysis of individual food wastes and agricultural residues, and their detailed characterization was performed. Maximum biochar yields of 28.4, 28.8, and 29.1 wt. % were recorded for food waste, canola hull and oat hull, respectively, at favourable temperature, heating rate and reaction time of 600 °C, 5 °C/min and 60 min, respectively. In the second phase of this study, the biochar derived from food waste and agricultural residue at favorable conditions was used as the precursor for activation study to produce high-quality activated carbon. Steam-led physical activation and KOH-led chemical activation of biochar were conducted, and process parameters such as temperature (700-900 °C) and activation time (60-120 min) were investigated using Taguchi L_{18} (2^1 X 3^2) method. BET surface area and product yield were determined for each activated carbon product. The highest BET surface area of 1760 m^2/g (food waste), 1718 m^2/g (canola hull), 1334 m^2/g (oat hull) with yields of 48.8, 48.6 and 51.3 wt.%, respectively, were obtained at favourable conditions for KOH led activation. Furthermore, the performance test for the biochar and activated carbon were substantiated through the dye adsorption study using model wastewater.

ACKNOWLEDGEMENT

I take this opportunity to convey my profound gratitude to my supervisors, Dr. Ajay K. Dalai and Dr. Venkatesh Meda, for providing me with the opportunity to pursue my master's degree. I would always be grateful for their exemplary guidance, monitoring and constant encouragement throughout my thesis work.

I would like to express my deep gratitude to my advisory committee members, Dr. Hui Wang and Dr. Amira Abdelrasoul, for their valuable suggestions and help in enhancing the quality throughout the course of this research work. I would also like to acknowledge Dr. Sonil Nanda for being an exceptional mentor, a friend and an elder brother to me. His guidance and support facilitated me in accomplishing this research work. His expertise and guidance helped me in conducting quality work and sharpening my writing skills.

I would like to express my gratitude to Ms. Rosa Huyen P. Do and Ms. Dushmanthi Jaysinghe for teaching me laboratory skills, assisting me with my characterizations and being constant sources of support inside the laboratory. I would also like to express my special thanks to my colleagues Alivia Mukherjee, Jude Okolie and Falguni Pattnaik for their tremendous help and support in the lab and outside the lab facility. I would also like to extend my gratitude in acknowledging Canada Research Chairs (CRC) program, Agriculture and Agri-Food Canada (AAFC) and BioFuelNet Canada for funding this bioenergy research. I would also like to extend my thanks to Saskatchewan Structural Sciences Centre (SSSC) for providing the S-NMR and XRD facilities.

And finally, I dearly appreciate and convey my hearty thanks to my parents and my entire family, along with my friends and others who helped me directly or indirectly in completing this research work.

TABLE OF CONTENTS

List of Tables

List of figures

NOMENCLATURE

Analysis of variance	ANOVA
Degree of freedom	DF
Gram per hour	g/h
Gram per minute	g/min
Applied Test Systems	ATS
Municipal solid waste	MSW
Design of experiment	DOE
Revolutions per minute	rpm
Signal-to-noise ratio	S/N
FW	Food waste
Canola hull	CH
Oat hull	OH
Activated carbon	AC

CHAPTER 1: INTRODUCTION

1.1 Research Background

With currently 7.8 billion people, the global population has undergone tremendous growth over the last few decades (Worldometer 2020). This anomalous growth of population, along with a significant rise in incomes of the global population, has driven the global food and energy demand in developed and developing countries. The global demand for food-water-energy nexus is escalating, which is considered central to sustainable development. The main reason behind this escalation is the unprecedented growth of population, change in income, change in dietary choices, and very importantly, the increasing urbanization. The economy and economic growth are mainly dependent upon energy. This global energy demand is fulfilled by fossil fuels (coal, natural gas, petroleum, and other liquid fuels). When it comes to achieving the global food demand, agricultural crop production markets are also shaping and proliferating in a way we have not seen before. The food and energy demand has led to the deterioration of the environment due to pollution and greenhouse gas emissions. Now, the world is facing the problems of increased CO_2 emissions, water pollution, greenhouse gas emissions, and climate change, which need to be addressed in an eco-friendly approach. It is also evident that the contamination of water bodies by organic and inorganic chemicals has attracted global attention (Inyang and Dickenson, 2015). To solve this enormous environmental sustainability and global energy problem, it requires a cascading approach to utilize the natural resources efficiently. Biochar production for environmental remediation like carbon sequestration, treatment of wastewater, soil enrichment and bioenergy products from biomass feedstocks is possibly a reasonable approach in climate change mitigation of greenhouse gases, adsorption of pollutants, waste management and carbon capture (Qambrani et al., 2017).

The two major conversion technology to transform biomass into bioproducts are biochemical and thermochemical conversion. Biochemical conversion involves some disadvantages like tedious preprocessing phases and longer time, lesser yield, and energy-intensive process. In contrast, thermochemical conversion technology emerged as an efficient method in converting biomass into value-added bioproducts. Pyrolysis, one of the thermochemical conversion techniques, converts a variety of waste feedstocks into bio-oil, biochar and gases. Pyrolysis is classified broadly as slow

and fast based on vapour residence time and heating rates. The generated biofuel products vary in their composition depending on the process conditions, namely temperature, heating rate and vapour residence time. Moreover, the high yield of biochar can be achieved using pyrolysis as compared to other conversion technology (Mohanty et al., 2013). The biochar generally possesses a poor porous structure, which restricts its application in the adsorption of pollutants. Therefore, it's highly essential to activate the biochar to enhance its porous structure.

Activated char or carbon is a carbonaceous material derived via physical or thermochemical treatment and exists in the form of aromatic and graphite carbon. It is usually produced from coal, coke or highly porous biochar from lignocellulosic biomass (straw, rice husk, wood, bagasse, shell etc.) and possesses a larger surface area and highly developed porous structure (Yahya et al., 2015). In addition, activated carbon demonstrates high physicochemical and thermal stability, high adsorption capacity and thus finds its application as a catalyst or precursor for catalyst support (Qian et al., 2015). The growing activated carbon market with a size of USD 3.93 billion in 2020 is estimated to reach USD 6.24 billion by 2026 (EMR reports 2020). The innumerable application of activated carbon in chemical, petrochemical, pharmaceutical, cosmeceutical industries, wastewater treatment, water purification, electronic device, and environmental mitigation (Mohan et al., 2014; Nanda et al., 2016) has further fueled the demand. Because of economic and environmental viability, renewable feedstocks-based activated carbon is a suitable replacement for conventional non-renewable-based activated carbon. Furthermore, the high demand for biomass-based activated carbon production can be fulfilled by utilizing agro-food wastes as feedstock.

The commercial production of activated carbon is now leaning towards non-renewable-based feedstocks by limiting the use of fossil fuel-based as it is economically and environmentally sound, entails lower production cost, has high renewable carbon content and high energy efficiency (Hesas et al., 2015). The activated carbon from biochar is synthesized via physical and chemical activation. The physical activation usually involves a carbonization process at an inert atmosphere followed by thermal treatment at high temperatures (800-1100 °C) in the presence of oxidizing agents such as steam, CO_2, and air (Hesas et al., 2015; Yahya et al., 2015). The steam activation leads to the widening of the micropores into meso-and macropores, while CO_2 activation results in the development of micropores (Azargohar and Dalai, 2008). In contrast, the chemical activation

process involves the activation of carbonized biochar at a temperature 450-900 °C with impregnation of a chemical or dehydrating agent like KOH, K_2CO_3, NaOH, Na_2CO_3, $AlCl_3$, $ZnCl_2$, $MgCl_2$ and H_3PO_4 (Yahya et al., 2015; Nanda et al., 2016). The activating agent KOH has been extensively preferred as it obtains highly porous activated carbon with high BET surface area (reaching 3000 m^2/g), more eco-friendly as compared to other chemical agents. It is also found to be effective in the removal of dyes and pharmaceutical wastes (Choma et al., 2015; Li et al., 2017; Nourmoradi et al., 2018; Liu et al., 2019).

Biochar has emerged as a prominent feedstock for the generation of porous activated carbon (Shen et al., 2018). The porous structure of the activated carbon is dependent on process parameters, and the Taguchi design approach can expedite the process by eliminating the needless set of experiments and also provides detailed information about the interaction of the factors influencing the response variable. Furthermore, in Design of Experiment (DOE), the selection of the best level for each factor is made based on the response table.

1.2 Knowledge Gaps

Based on the literature review in Chapter 2, the following knowledge gaps were identified:

a) There are a limited number of studies focusing on the slow pyrolysis of food waste and agricultural residues like canola hull and oat hull to produce biochar. Additionally, the characterization studies carried out for bio-oil and gaseous products from these feedstocks are relatively limited.

b) To the best of our knowledge, scarce literature is available on the activation of agro-food waste-derived biochar. Furthermore, chemical and physical activation using the Taguchi design approach has not been attempted in a single study for the food waste precursor. In addition, the adsorption of pollutants (dyes) using biochar and activated biochar derived from food waste and agricultural residues (canola and oat hull) is scarce in the literature.

1.3 Hypotheses

a) Given the abundance of food wastes, canola hull, and oat hull in Saskatchewan, utilization of these precursors to produce biochar and via slow pyrolysis would provide high-quality biochar.

A detailed study on bio-oil and gaseous products, along with biochar, can enable potential applications. Nonetheless, the valorization of waste biomasses could eliminate the waste disposal problem and global warming issues.

b) Activation of slow pyrolyzed agro-food waste biochar can enhance the structural properties of the produced activated carbon and can be used as an efficient adsorbent for dye removal from wastewater. Furthermore, the use of the Taguchi approach in optimizing activation process parameters can amplify the surface area of the resulting activated carbon by reducing the needless set of experiments.

1.3 Research Objectives

a) The research objective is to conduct slow pyrolysis of food waste and agricultural residue (canola hull and oat hull) with the investigation of process conditions like temperature, heating rate and reaction time to produce high-quality biochar. Furthermore, the biofuel products obtained from the pyrolysis of agro-food residues were subjected to a thorough physicochemical characterization to explore their potential application in environmental and energy applications.

b) Based on the physicochemical properties and composition, the slow pyrolyzed agro-food waste biochar samples will be activated using chemical activation (KOH as chemical agent) and physical activation (Steam as an oxidizing agent). The Taguchi design approach will be used to optimize the process parameters of the activation. The performance tests of the biochar and the resulting activated carbon with a high BET surface will be done for the adsorption of dyes from model wastewater.

CHAPTER 2: LITERATURE REVIEW

Most of the content of this chapter has been published as a review article in Environmental Chemistry Letters:

Patra, B. R., Mukherjee, A., Nanda, S., Dalai, A. K. (2021). Biochar production, activation and adsorptive applications: a review. *Environmental Chemistry Letters*, 19, 2237-2259. https://doi.org/10.1007/s10311-020-01165-9

Contribution of the M.Sc. candidate:

Most of the writing of this phase was done by Biswa Ranjan Patra with the help of Ms. Alivia Mukherjee (Ph.D. Scholar). Dr. Sonil Nanda added his expertise in shaping the manuscript and contributed in developing high impactful graphs and figures. All the corrections and reviews from Dr. Ajay K. Dalai helped in enhancing the quality of the manuscript.

Contribution of this chapter in the overall M.Sc. Work:

This phase of the work was focused on the literature related to this research. A detailed discussion on biomass types and composition along with thermochemical conversion routes for biomass conversion was done. Furthermore, the activation of biochar, bio-products characterization and wastewater treatment were described.

2.1 Types of biomass and their compositions

Biomass is an organic or non-organic solid material from living or living organisms of recent times and their by-products. Different types of waste such as animal manure, sewage sludge, many industrial, domestic waste, and wastepaper are also treated as biomass because these wastes are also derived from organic or non-organic compounds, like natural biomass. Biomass feedstocks are the world's most significant and sustainable energy resource for the production of heat, biofuel and electrical power. Generally, five significant components primarily govern the chemical properties of lignocellulosic biomass: cellulose, hemicellulose, lignin, ash and volatiles/extractives (Williams et al., 2016). Cellulose, a sugar of six-C connected by glycoside bonds, is composed of monomers of glucose. Hemicellulose is made up of sugar like hexose and pentose. Hemicellulose is an amorphous heteropolymer, which makes it more susceptible than cellulose. Lignin usually

consists of a phenolic character and is helical in structure, which contains mainly ether and carbon-carbon linkages. Being a source of aromatics or beneficial phenolic by-products, lignin can contribute energy on combustion (Shinya, 2008; Robbins et al.,2012; Williams et al., 2016). Extractives are generally comprised of non-structural water-soluble sugars and proteins, chlorophyll and waxes (ethanol-soluble components). Volatiles from hemicellulose increases the acidic nature of the oil generated via various thermochemical techniques, which leads to an increase of the bio-oil in the viscosity (Carpenter et al., 2014). Ash is generally composed of inorganic material, which diminishes the oil yield and induces reactor fouling.

2.2 Biomass Classification

Some common and abundantly available biomass sources across the world include lignocellulosic biomass, e.g. agricultural crop residues, forestry biomass and energy crops, municipal solid waste, industrial effluents, sewage sludge and cattle manure (Fig. 2.1). These organic refuses have tremendous potential to be used as precursors for waste-to-energy conversion (Bocci et al., 2014).

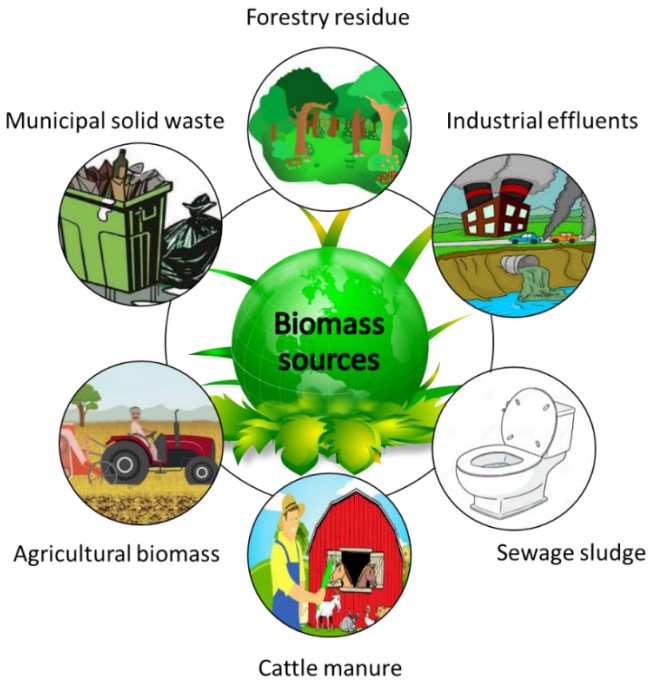

Fig. 2.1: Some common sources of waste biomass

2.2.1 Energy Crops

The annual crops such as maize, hemp, wheat, and sorghum, short-rotation crops like willow, poplar, and eucalyptus and perennial crops like miscanthus, reed canary grass and switchgrass are considered as energy crops (Laurent et al., 2015). Energy crops are grown mainly for energy production purposes. This type of crop is of low cost, and low maintenance is required. The crops are processed into different types of fuel: solid fuels such as pellets and briquettes, liquid fuels such as bioethanol and biodiesel, and gaseous fuel such as biogas. Energy crops can also be converted into energy for the generation of electricity and heat.

2.2.2 Agricultural wastes

Agricultural waste encompasses leftovers after crop harvests, such as husk, leaves, straw, stalks, roots, seed shells, bagasse, peels, stems and woods. Examples of agricultural crops are cotton, rice, wheat, maize, vegetables, sugarcane, nuts, peanuts, paddy, coffee, coconut, lentils etc. Animal husbandry waste such as solid waste (farmyard manure), liquid manure (urinary waste), and wastewater (bedding, process water, silage juices, land disinfectants) are considered as livestock wastes (Pattanaik et al., 2019). Generally, agricultural waste is used for animal feed, natural fertilizers, improving soil texture, and various other processes (Sadh et al., 2018).

2.2.3 Forestry waste and residues

Forest residues consist of stems, stumps, foliage, tops, wood, bark, leaves, un-merchantable wood, and damaged trees. Slash from final fellings, un-merchantable wood, and small trees from thinnings and cleaning are the primary sources of forest residue. Slash is generally fine woody debris from logging operations or through natural forest disturbances. Forest waste like wood can be used for cooking on stoves or open fires and warming houses. The heating value of forest biomass is 16.6 MJ/Kg and can be used for electricity generation (Karaj et al., 2010).

2.2.4 Industrial, commercial and institutional (ICI) waste

This type of waste includes scraps and discards from industries, businesses, construction renovation and demolition (CRD) and institutions like schools, universities, hospitals, hotels, restaurants etc. (Hodge et al., 2016). Municipal solid waste (MSW)from the residential sector is also a significant contributor to the ICI waste generated. Among all the waste, food waste and

paper waste are the major components of the waste generated, which can be treated and reduced using various treatment processes.

2.3 Thermochemical conversion routes for biomass

The presence of high oxygen content in biomass makes it not on par with fossil fuels in terms of energy content. Therefore, it becomes essential that biomass is upgraded through appropriate conversion methods into higher quality fuel or products. Methods like thermochemical conversion/biochemical conversion are employed to densify the energy content of the biomass to bring it closer to the properties of fossil fuels with a neutral carbon footprint.

Therefore, it is highly essential to upgrade biomass through suitable conversion methods into high-quality fuel or products because of the low quality of biomass for energy purposes. Biomass conversion technologies can be divided into three streams, the "Physical conversion route," which involves the application of mechanical forces for the biomass extraction and compaction, the "Thermochemical conversion route," which involves heat and pressure application in densifying biomass, and the "Biochemical conversion route," which involves nature through microorganisms or enzymes for the biomass degradation.

The thermochemical process involves the decomposition of organic compounds of biomass into biofuels at elevated temperatures. As compared to other physical, chemical and biochemical conversion processes, the thermochemical conversion process is a simpler route to generate bio-fuels (Chen et al., 2015). For example, before chemical conversion, there is always a need for an extra purification step to refine the biomass. In the case of biochemical conversion processes, it relies additionally on biocatalysts, such as enzymes and microbial cells, apart from heat and chemicals. In addition, biochemical conversion requires a long period of time to complete the conversion. When it comes to the thermochemical conversion process, it can be applied to a variety of biomass precursors and most importantly, it relies only on heat or physical catalysts, which makes it a more profitable conversion process (Azizi et al., 2018). Thermochemical conversion is generally governed by heat and chemical reaction, which determines the product and energy formation. There are different thermochemical processes, which can be classified in different ways, such as the presence or absence of oxygen during processing, operational pressure, desired end products and processing medium. Gasification, combustion, torrefaction and pyrolysis are the most common subcategories of thermochemical conversion.

2.3.1 Gasification

Gasification, an endothermic process, involves the thermal decomposition of organic materials mainly to combustible synthesis gas or syngas and biochar under reducing conditions in the presence of gasifying agents like oxygen or steam. The gasifying agents are supplied in a sub-stoichiometric amount when compared with the amount required for the complete combustion of CO_2 and water. The gaseous phase contains a mixture of H_2, CO_2, CO and CH_4, as well as traces of C_2H_2, C_2H_4 and C_2H_6. Hydrothermal gasification is also another iteration of gasification that involves supercritical water as the reaction medium. Supercritical water is a fluid phase of water occurring at temperatures and pressures beyond its critical points. The critical temperature and critical pressure of water are 374 ℃ and 22.1 MPa (Reddy et al., 2014). Complex biomass is disintegrated into permanent gases and biochar during supercritical gasification because of a series of hydrothermal reactions such as water-gas shift, hydrogenation, methanation, steam reforming and Boudouard reaction. Supercritical water demonstrates gas-like viscosities and liquid-like densities acting as a green solvent, catalyst and reactant to decompose highly recalcitrant organic matter (Nanda et al. 2017 FTP). Hydrothermal gasification can also eliminate excess energy requirements for the pre-drying of biomass feedstocks because of the aqueous reaction medium (Correa and Kruse 2018).

In the case of conventional thermochemical gasification, the primary oxygenated vapours and liquids comprise hemicellulose and cellulose-derived compounds, i.e. hydroxyl acetaldehyde and levoglucosan, as well as methoxy phenols derived from lignin (De Lasa et al. 2011). At around 350 °C, the aromatization process starts and continues until higher temperatures are attained. At temperatures ranging from 700 °C to 850 °C, the primary vapours and liquids are converted to gaseous olefins, CO_2, H_2, CO, H_2O and condensable oils like phenols and aromatics. A further rise in the temperature from 850 °C to 1000 °C involves the conversion of secondary products to H_2, CH_4, CO, H_2O, CO_2, tar and biochar. Steam gasification of biomass has emerged as an area of interest because of its capability in producing hydrogen-containing gaseous fuel along with biochar of high quality.

Hansen et al. (2015) reported that reactions between biochar and oxygen in the combustion zone of the gasification system played a prominent role in determining the quality of the product gas. Other factors like tar composition, conversion of biochar, gas composition, and heating value

require significant consideration as they determine the operation and performance of gasification. The rise in gasification temperature results in enhancing the content of combustible gas, especially hydrogen along with a substantial increase in its heating value, and the reduction of tar content (Ning et al., 2018). The gasification process usually undergoes in the presence of gasifying agents like air, steam, O_2 and CO_2. Usually, the gasifying agent used in the gasification governs the calorific value and the syngas quality, i.e. ratio of H_2/CO. Kim et al. (2013b) reported that air as a gasifying agent resulted in the production of syngas of low heating value. The dilution of syngas by nitrogen present in the air was the main reason behind its low heating value. However, Choi et al. (2015) found that when steam or an amalgamation of steam and oxygen was used for gasification, a mediocre calorific value syngas was produced. Moreover, the combination of steam and air for gasification produced high hydrogen yields when compared to the use of air alone. Such practice can also lessen the energy required for the gasification process, which is usually supplied by combusting biomass.

2.3.2 Combustion

Combustion is the most known thermochemical technique leading to the direct conversion of fuel to thermal energy. Combustion usually takes place in the existence of oxygen, during which the carbon and hydrogen of the fuel react with the oxygen present in the air to produce CO_2, water, sulphur, and nitrogen to form their corresponding oxides. Unfortunately, due to the high moisture content in most biomasses and MSW, direct combustion is not always the most sensible way to utilize this for energy, as most of this energy will be lost in heating the biomass.

2.3.3 Torrefaction

Torrefaction, a relatively mild thermochemical process, is often proposed as an alternate pretreatment method in upgrading the physiochemical properties of biomass. Torrefaction has attracted tremendous attention because of its energy efficiency and its effectiveness in producing biofuel with uniform-quality energy carriers with coal-like properties (Barbanera and Muguerza 2020). It involves thermal dehydration of lignocellulosic biomass under an inert atmosphere at a moderate temperature, typically in the range of 200–300 °C with a slow to moderate heating rate (Buratti et al., 2018). The operating conditions and biomass composition directly affect the

efficacy of torrefaction. During torrefaction of lignocellulosic materials, hemicellulose is mostly affected due to its amorphous nature and a lower degree of polymerization compared to cellulose and lignin (Chen et al., 2015). Since hemicellulose degrades almost completely during torrefaction, this thermal treatment renders the properties of diverse types of biomass more uniformly with the effects of enriching and changing the form of inorganic species.

Torrefaction of lignocellulosic biomass results in torrefied biomass or char, tar and volatile gases. It results in the production of homogeneous solid fuels with partially reduced biopolymers (e.g. hemicellulose, cellulose and lignin), volatile matter and moisture content and higher carbon content. Some of the advantages of torrefaction are: (i) lowering the moisture content of biomass, (ii) improving hydrophobicity of biomass, (ii) enhancing the energy density, (iii) higher grindability, (iv) higher reactivity, (v) resistance to microbial decomposition due to lower moisture content, and (vi) compacted storage and handling (Chen et al., 2015; Chen et al., 2016; Zhang et al., 2020). Furthermore, the emission of greenhouse gas such as CO_2 and volatile matter from the burning of torrefied char is significantly reduced (Sukiran et al., 2017; Olugbade and Ojo 2020). Moreover, the torrefied char can be extruded into fuel pellets through densification and pelletization (Azargohar et al., 2019).

2.3.4 Pyrolysis

Pyrolysis of biomass is an endothermic process, which includes the thermal degradation of solid organic matter under an inert atmosphere into bio-oil, biochar and producer gas. Pyrolysis produces bio-oil, biochar and non-condensable gases like CO_2, CO, CH_4 and H_2, which can be utilized for combined heat and power generation. The liquid product or bio-oil generally comprises oxygenated hydrocarbons such as phenolic ethers, alkyls, esters, aldehydes, ketones, carboxylic acids, hydrocarbons and a substantial amount of water. The liquid product from pyrolysis generally possesses a calorific value of 16-28 MJ/kg (Mohanty et al., 2013). The calorific value of biochar is generally in the range of 25-30 MJ/kg, depending on the amount of unconverted organic fraction (Jia et al., 2017). During the process of pyrolysis, components like cellulose and hemicellulose mostly form volatile products, while biochar is formed from lignin due to its high stability to thermal degradation. Biochar retains the stable carbon from the biomass and possesses various

uses such as a solid fuel, soil amendment agent, carbon sequestration and precursor for value-added manufacturing products of industrial and commercial interest (Hansen et al. 2015).

The rate and degree of thermal decomposition of biomass during pyrolysis depend on the variations in temperature, heating rate, pressure, vapour residence time, reactor configuration and feedstock properties (Mohanty et al., 2013). Based on temperature, heating rate and vapour residence time, pyrolysis can be categorized typically into slow and fast pyrolysis (Jahirul et al. 2012). Slow pyrolysis is usually categorized by its slow heating rate (i.e. 0.1-1 °C/s) and moderate temperatures (i.e. 300-600 °C) for a longer vapour residence time (> 30 min) in the absence of oxygen (Roy and Dias 2017; Senneca et al., 2018; Safdari et al., 2019). A longer vapour residence time results in a secondary reaction such as polymerization to produce biochar with high carbon content (Yaashikaa et al., 2019). Slow pyrolysis is a preferred route for biochar production due to its high yields compared to that of bio-oil and gaseous products. On the other hand, fast pyrolysis involves a high heating rate (i.e. 10-1000 °C/s), high temperatures (i.e. 300-700 °C) and short vapour residence times (i.e. < 2 s) to thermally degrade the biomass into high yields of bio-oil and producer gas with lower yields of biochar (Ahmad et al., 2014; Roy and Dias 2017).

Slow pyrolysis is also referred to as carbonization because it leads to a higher biochar yield. The stages of carbonization of biomass are categorized into four major steps such as (i) dehydration, (ii) thermal cracking of lighter molecules, (iii) thermal cracking of larger molecules, and (iv) evolution of aromatized and stable carbon with the removal of volatiles (Puligundla et al. 2016). Lignite-like biochar with a high grade of aromatization is generated from carbonization.

Temperature plays a significant role in determining the physicochemical, morphological and structural properties of biochar. Temperature causes dehydration, decarboxylation, decarbonylation, deamination and demethanation of biomass, leading to the evolution of sticking physicochemical features in biochar (Kim et al., 2011). For example, a rise in temperature of pyrolysis, gasification and carbonization leads to a decrease in the biochar properties such as yield, moisture and volatile contents, electrical conductivity and cation exchange capacity (Nanda et al., 2016 WBV). In contrast, a rise in temperature causes an increase in the aromatic carbon content of biochar along with its elemental or ash content, pH value, surface area and porosity (Fig. 2.2).

Biochar produced at low-temperature pyrolysis usually possesses a lower surface area, undeveloped porous structures, acidic pH and low carbon content. The pores in the low-temperature biochar are usually blocked by the formation of tar. Therefore, biochar requires chemical or physical activation to increase its surface area and porosity. The formation of biochar involves crosslinking reactions through condensation and dehydration at low temperatures (Heidari et al., 2019). The biochar becomes progressively more aromatic with higher carbon content as the temperature increases by the elimination of hydroxyl, olefin, aliphatic and carbonyl groups. At higher temperatures, the volatile matter is released, which results in the opening of the pore structure in the biochar.

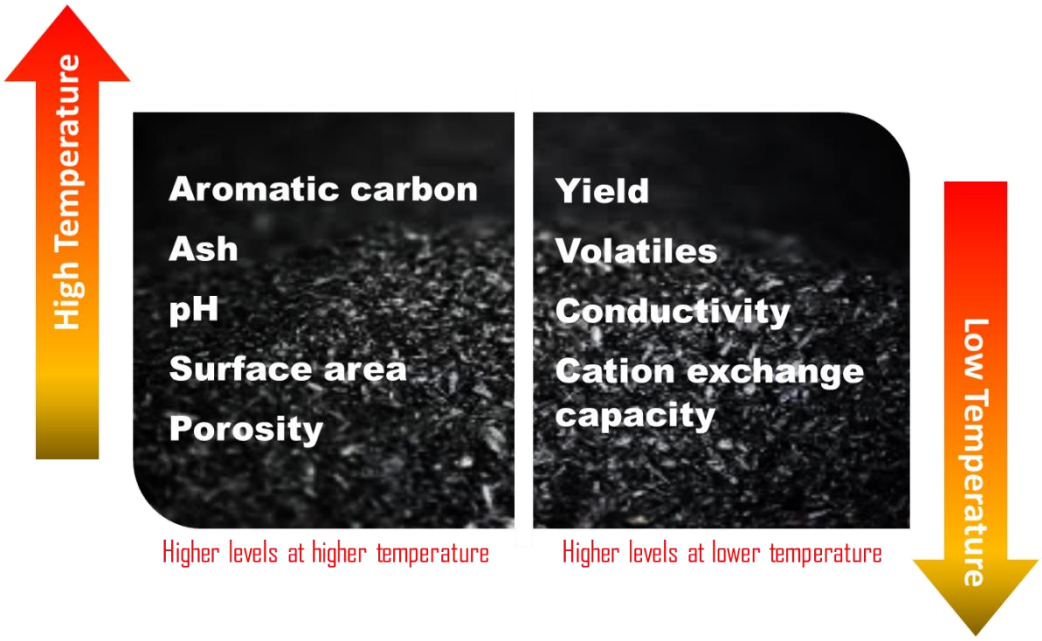

Fig. 2.2: Evolution of physicochemical properties of biochar as a function of temperature.

2.4 Activation of biochar

Activated carbon is a carbonaceous material containing mostly aromatic and graphite forms of carbon thermally or physicochemically treated to have high porosity and larger specific-surface area due to a well-built internal pore structure (Yahya et al., 2015). Activated carbon is typically derived from coal-based precursor or thermally stable lignocellulosic biomass-derived biochar (straw, rice husk, wood, bagasse, shell etc.) to develop organized pore-structure, high specific surface area, favourable pore size distributions, high physiochemical stability, surface reactivity

and high adsorptive capacity (Danish and Ahmad 2018). The development of a larger specific surface area in activated carbons is attributed to the presence of a greater degree of microporosity and mesoporosity generated from the conventional heating techniques. It should be noted that activated carbon is a product of biochar activation through a physical or chemical approach.

Presently, commercial activated carbons are derived from non-renewable-based precursors such as coke or coal-based precursors, which limits their extensive use (Baytar et al., 2018). Although, the source of activated carbon could be non-conventional and renewable sources such as lignocellulosic biomass (e.g. wood, straw, husk, peel, distillery grains, kitchen waste, shell, pith, etc.) and wastes materials such as scrap tires (Rashidi and Yusup 2017). The non-renewable fossil fuel-based precursors are gradually being replaced by waste organic biomasses for the production of activated carbon because of economically feasibility, eco-friendliness, lower regeneration cost, high renewable carbon content, lower production costs and energy requirements (Hesas et al., 2015; Rashidi and Yusup 2017; Mukherjee et al., 2019).

2.4.1 Physical activation

The preparation of activated carbon from biochar through physical activation involves a dual-stage mechanism where the biomass is thermally treated at 600–900 °C under an inert atmosphere to produce biochar for further activation at 800–1100 °C in the presence of suitable activating or oxidizing agents (Yahya et al., 2015; Hesas et al., 2015). The commonly used oxidizing or physical activation agents are steam, CO_2, air or a binary mixture of CO_2 and N_2. During the pyrolysis process, the surface chemical properties of biochar undergo a series of complex and variable changes that further facilitate the activation process (Wang et al., 2019). Extensive research has been conducted on CO_2-based physical activation, which is widely used due to its ease in handling, the requirement of low activation temperature and its carbon recyclability approach (Yahya et al., 2015). However, from an industrial perspective, using a purified stream of CO_2 can increase the process expenditures. Hence, it is recommended to use the flue gas generated after the post-combustion, which contains a binary mixture of N_2 and CO_2 (Puligundla et al., 2016). The steam activation leads to the development of porous structure as it penetrates into the internal structure of the biochar and reacts with the unstable carbon to open and widen the unreachable pores by releasing hydrogen and carbon monoxide. Firstly, the blocked pores get opened with the

development of the micropores, and further micropores are widened to larger meso-and macropores (Azargohar and Dalai 2008).Table 2.1 summarizes some recent studies on the physical activation of biochar.

2.4.2 Chemical activation

Chemical activation involves the impregnation of the precursor with chemical activating agents before the thermal treatment under an inert atmosphere at 450–900 °C. The chemicals agents having the potential as a strong dehydrating agent during activation can be categorized as (i) acids, e.g. sulfuric acid, phosphoric acid, (ii) alkalis, e.g. potassium hydroxide, potassium carbonate, sodium hydroxide, sodium carbonate, and (iii) transition metal salts, e.g. aluminum chloride, zinc chloride and magnesium chloride (Yahya et al., 2015; Nanda et al., 2016). Chemical activation is considered economically viable compared to physical activation since it requires a shorter processing time, lowers the activation temperature, generates high-grade porous activated carbon, high final carbon yields and one-step processing (Bergna et al., 2018). The technique of mixing the dehydrating agent and precursor can significantly influence the properties of activated carbon, such as the yield of solid and carbon, along with the inhibition of tar formation.

Crucial developments in the production of activated carbon have been made over the past few years concerning the type of activating agents, mixing techniques, activation process optimization and utilization of inexpensive carbonaceous precursors (Mukherjee et al., 2019). Table 2.2 summarizes some recent studies on the chemical activation of biochar. Tehrani et al. (2015) studied the effects of process conditions like temperature as well as a physical and chemical activating agent on the characteristics of activated carbon produced from chemical and physical activation of coffee extract residue. The authors used H_3PO_4 and steam as activating agents for chemical and physical activation, respectively. The obtained activated carbon with a highly developed porous structure and surface area enabled its potential application for the removal of various contaminants from a liquid and gaseous stream. The study showed that chemically activated carbon recorded the highest surface area of 696 m^2/g in contrast to the activated carbon derived from physical activation (641 m^2/g). Kumar and Jena (2018) reported high yields (38.1 wt%) of activated carbon with a higher surface area (2869 m^2/g) and total pore volume (1.96 cm^3/g) produced from $ZnCl_2$ assisted chemical activation of Fox nutshell. However, the use of $ZnCl_2$ has adverse impacts on the environment, which has limited use in chemical activation

processes (Azargohar and Dalai 2008). Shahkarami et al. (2015) used whitewood biochar as a precursor for physical and chemical activation processes. KOH (1400 m^2/g) resulted in the highest surface area for the activated carbon, followed by that of steam (840 m^2/g) and CO_2 (820 m^2 /g).

Rambabu et al. (2015) used chemical activation agents (i.e., KOH and NH_3) and physical activation agents (i.e., steam and CO_2) of de-oiled canola meal. The authors found KOH led activation of canola meal with the highest surface area (1230 m^2/g) and pore volume (0.4 cm^3/g). The surface area of the resulting activated carbon was highest in the case of KOH (1230 m^2/g) followed by steam (403 m^2/g), CO_2 (320 m^2/g) and NH3 (19 m^2/g). Muniandy et al. (2014) also reported KOH as a superior activating agent for producing activated carbon from rice husk over NaOH. The study reported a higher surface area of activated carbon produce from KOH (2696 m^2 /g) when compared to that of NaOH (594.9 m^2/g). KOH is extensively used as a chemical activation agent for producing activated carbon with enhanced surface area and adsorption performance. When compared to physical activation, chemical activation tremendously enhances the surface area and porosity of the activated carbon.

Table 2.1 Recent studies on the physical activation of biochar precursor

Feedstock	**Physical agent**	**Activation temperature (°C)**	**Reaction time (min)**	**Key attributes**	**BET surface area (m^2 /g)**	**Total pore volume (cm^3 /g)**	**Average pore size (nm)**	**Yield (wt%)**	**References**
Almond shell	Steam	950	60	Steam flow rate: 130 cm^3 / min	1261	–	–	50	Nazem et al., (2020)
Canola Meal	Steam	800	90	Steam flow rate: 8g/h	403	0.18	2.07	69.5	Rambabu et al., 2015
	CO_2	700	120	CO_2 flow rate:24ml/min	320	0.30	3.67	-	
Coconut shell	CO_2	850	60	CO_2 fow rate: 50 cm^3 / min	1152	0.72	-	2.6	Tsai and Jiang (2018)
Coffee residue	Steam	700	120	Steam/N_2 ratio: 1:2	641	0.33	2.06	13.4	Tehrani et al., (2015)
Pine nut shell	Steam	850	80	Steam/biomass ratio:1.5:1	1058	-	-	31.2	Chen et al., 2016
Tea waste	Steam	800	30	Steam flow rate: 0.075g / min	995	0.68	2.73	22.42	Zhou et al. (2018)
Spruce, Fir, and Pine stem	Steam	900	60	-	1025	0.77	3.0	8	Bardestani and Kaliaguine 2018
Sewage sludge	CO_2	700	60	1:3 (CO_2 to Nitrogen ratio)	239.82	0.39	6.46	-	Zhang et al., 2019
Walnut shell	Steam	950	60	Steam flow rate: 130 cm^3 / min	1248	-	-	45.8	Nazem et al., (2020)
Wood chips	CO_2	800	180	CO_2 flow rate: 90 cm^3/min	590	0.34	3.44	-	Kilpimaa et al., 2015
Pistachio shell	Steam	950	30	Steam flow rate: 130 cm^3 / min	1196	-	-	41.7	Nazem et al., (2020)

2.5 Biomass and bio-products characterization

Biomass, the only renewable and sustainable energy source that can be converted into various fuel forms such as solid, liquid and gas. Biomass is a highly variable and inconsistent material with low energy and high moisture content. The composition of biomass feedstocks is associated with their source, which determines their properties and indicates their potential application. Food waste and agricultural residue possess high potential energy, but regrettably, it has not been explored widely for the generation of bioenergy (Shinya 2008; Qian et al., 2015; Cao et al., 2018). The energy application makes it highly essential for the identification of composition and characterizations of the biomass. Many studies emphasized the use of food waste and agriculture residue as suitable feedstock to produce biochar and bio-oil. Proximate analysis of biomass and bioproducts is conducted to determine the amount of ash, volatile matter, moisture, and fixed carbon content, while ultimate analysis is done to find the percentage content of CHNSO (carbon, hydrogen, nitrogen, sulphur, and oxygen). Saidur et al., 2011 reported carbon content of corn stob, olive husk, sunflower shell, wheat straw, rice husk, soya husks like agricultural residue ranging between 38-51%, while hydrogen, nitrogen, sulphur and oxygen ranged between 4-7 wt.%, 1-4 wt.%, 0.1-0.7 wt.%, and 30-47 wt.%, respectively. The authors also reported ash (2-20 wt.%), volatile matter (70-85 wt.%), fixed carbon (10-25 wt.%), and moisture (3-8 wt.%) content of the agricultural residue. In another study, Lee et al., 2018 reported 29.7 wt.% carbon content for food waste compost, which was enhanced to 51.7 wt.% after pyrolysis at 500 °C. The biochar produced at elevated temperatures possesses high thermal stability, which is determined by thermogravimetric analysis (TGA) (Teh et al., 2014). Furthermore, X-ray diffraction determines the crystallographic structure, Fourier transform infrared spectroscopy analyzes the existence of surface organic functional groups, solid-state ^{13}C nuclear magnetic resonance spectroscopy determines the chemical composition and dynamic properties of solid and scanning electron microscopy determines the morphology of biomass and biochar (Nanda et al., 2014 BER). Furthermore, the surface and textural properties of biochar are determined by using BET analysis. It was found that the surface area of pyrolyzed biochar is relatively low and needs further thermochemical and physical treatment for its enhancement. On the other hand, gas chromatography-mass spectrometry analysis provides a detailed chemical composition of a bio-oil from biomass, gas chromatography provides the composition of gases generated from conversion technologies (Chen et al., 2016).

Table 2.2 Recent studies on the chemical activation of biochar precursors

Feedstock	**Chemical Agent**	**Activation Temperature (º C)**	**Reaction Time (min)**	**Impregnation ratio (Chemical:feedstock) or Chemical concentration**	**BET surface area (m^2/g)**	**Total pore volume (cm^3/g)**	**Average pore size (nm)**	**Yield (wt.%)**	**References**
Canola meal	KOH	800	120	3:1	1230	0.46	1.51	-	Rambabu et al., 2015
Coffee residue	H_3PO_4	600	60	40%	696	0.59	3.37	34.9	Tehrani et al., 2015
Pumpkin seed shell	$ZnCl_2$	500	60	3:1	1564	0.96	24.69	18.6	Demiral et al., 2015
Golden shower	K_2CO_3	800	240	1:1	1413	0.66	1.86	57.7	Tran et al., 2018
Sewage sludge	KOH	700	60	2:1	908	0.83	3.68	-	Zhang et al., 2019
Whitewood	KOH	775	120	0.81:1	1400	0.62	-	35	Shahkarmi et al., 2015
Rice husk	KOH	850	60	5:1	2696	1.29	2.63	17.1	Muniandy et al., 2014
	NaOH	750	60	2:1	595	0.34	8.41	18.2	
Fox nutshell	$ZnCl_2$	600	60	2:1	2869	1.96	2.73	38.12	Kumar and Jena 2015
Pinewood sawdust	H_3PO_4	600	120	2:1	1547	1.17	-	43.3	Cao et al., 2018
Pine wood	$ZnCl_2$	580	120	1:1	1081	0.37	0.57	28.8	Ahmed et al., 2019
	KOH	580	120	4:1	1185	0.35	0.52	19.5	

2.6 Wastewater treatment

Wastewater is generated from domestic, municipal and industrial activities, which consists of harmful pollutants such as organic substances, dyes, pharmaceuticals, hormones and steroids, plastics, sediments, oil and grease, pathogenic microorganisms, heavy metals, microplastics, hydrocarbons, radioactive substances and other toxic substances (Chen et al. 2019; Sun et al. 2019 Nanda and Berruti 2020a). These contaminants have many adverse effects on the environment and ecosystems by affecting the natural habitats and metabolism of plants, animals and human beings. The exposure or consumption of wastewater containing all such contaminants can cause serious health ailments in human beings, including cancer and cardiovascular, neurological and pulmonary disorders (Guo et al. 2016). The treatment of wastewater is often found to be inefficient to complete removal of the toxic compounds, micro-contaminants and nanoparticles. Therefore, advanced treatments are required specific to particular contaminants in the wastewater for its reclamation.
The discharge of wastewater and effluents from dye industries poses numerous threats to the ecosystems as they contain toxic chemicals, organics, acids, bases and other impurities. Textile dyes often show stability to the oxidizing agent and withstand aerobic digestion, which makes their removal difficult (Mohan et al., 2014). Several researchers have used various biochar samples derived from biomass for the removal of dyes such as methylene blue, methyl violet, Remazole orange and reactive red 141 (Xu et al. 2011; Acemioğlu 2019; Gokulan et al. 2019). Table 2.3 summarizes some notable studies on the adsorption of organic contaminants by biochars produced from several organic residues.

Sun et al. (2013) used various biochar samples produced from pyrolysis of Eucalyptus, anaerobic digestion residues (or municipal organic waste) and palm bark at 400 °C to study the adsorption of methylene blue dye. The efficiencies for methylene blue removal by biochar derived from anaerobic digestion residues, palm bark and Eucalyptus were found to be 99.5%, 99.3% and 86.1%, respectively, at optimum conditions i.e.40 °C, 5 mg/L concentration and pH 7. The municipal organic waste-derived biochar showed a maximum adsorption capacity of 9.5 mg/g.
Leng et al. (2015) also studied the adsorption of malachite green using biochar produced from the liquefaction of rice husk using ethanol as a solvent. The adsorption capacity of malachite green was found to be between 32.5 mg/g and 67.6 mg/g. Vyavahare et al. (2018) studied the removal of malachite green dye using biochar produced from different biomasses such as paper waste,

cotton waste, rice husk, sugarcane bagasse and groundnut shells. Among varying pyrolysis temperatures studied, the authors found that pyrolysis of sugarcane bagasse at 800 °C for 60 min showed better performance resulting in maximum sorption of malachite green, i.e. 3000 mg/L. Lin et al. (2018) used pyrolyzed microalgae (*Ulothrix zonata*) derived biochar for the adsorption of various dyes from wastewater. The study also investigated the influence of different pyrolysis temperatures of biochar on the adsorption of dyes. The target dyes were crystal violet, congo red and malachite green. Microalgae-derived biochar showed highly porous structures and thermal stability with developed surface chemical characteristics, which resulted in the removal of the aforementioned dyes from the aqueous solution. The optimum adsorption capacity achieved for the removal of malachite green dye was 5306.2 mg/g with biochar produced at 800 °C, while for crystal violet and Congo red, the maximum adsorption capacities were 1222.5 and 345.2 mg/g, respectively. Kelm et al. (2019) used biochar produced from the gasification of wood waste to remove azo dye (Indosol Black NF_{1200}) from an aqueous solution. The batch adsorption was performed at 28 °C for 3 h at a speed of 200 rpm. The study showed that at lower pH, the experimental adsorption efficiency was found to be 185 mg/g using the Freundlich model. Thus, wood waste-derived biochar was reported as an efficient adsorbent from the removal of individual azo dye contaminated wastewater.

The literature lacks detailed studies on the production of biochar via the slow pyrolysis method. From the literature, it is found that using slow pyrolysis, high-quality biochar with high yield can be achieved. Furthermore, bio-oil and gaseous products can also be obtained whose physicochemical characterization can be determined to explore their potential applications. The biomass such as food waste and agricultural residue contains cellulose, hemicellulose and lignin, which can be converted using thermochemical conversion technologies to valuable biofuel products. The resulting biochar is also found to be a suitable precursor for producing activated carbon. This would replace the dependency on fossil fuel-based precursors to generate activated carbon. Thus, agro-food waste derived biochar can be used for the production of high porous activated carbon and further the generated carbon can be used as an adsorbent for the removal of contaminants from wastewater.

Table 2.3 Adsorption characteristics of dyes by biochar

Feedstock	Conversion technology	Conversion temperature (°C)	Target contaminant	Adsorption temperature (°C)	Adsorption capacity (mg/g)	Adsorption pH	Isotherm	Reference
Rice husk	Liquefaction	340	Malachite green	30	67.6	9	Freundlich	Leng et al. (2015)
Peanut straw	Pyrolysis	350	Methyl violet	25±1	256.4 mmol/g	9.4	Langmuir	Xu et al. (2011)
Soybean straw					178.6 mmol/g	8.4		
Rice hull					123.5 mmol/g	8.3		
Eucalyptus	Pyrolysis	400	Methylene blue dye	40	2.1	7	Langmuir	Sun et al. (2013)
Municipal organic waste					9.5			
Palm bark					2.7			
Blue-green algae (*Spirulina platensis*)	Pyrolysis	450	Congo red	30	51.3	2	Langmuir	Nautiyal et al. (2016)
Sugarcane bagasse	Pyrolysis	800	Malachite green	60	3000 mg/L	7.5	-	Vyavahare (2018)
Wood waste	Gasification	700	Indosol Black NF_{1200}	28	185	2	Langmuir	Kelm et al. (2019)
Green algae (*Ulothrix zonata*)	Pyrolysis	800	Malachite green	35	5306.2	12.3	Freundlich	Lin et al., 2018
			Crystal violet		1222.5			
			Congo red		345.2			

CHAPTER 3: MATERIALS AND METHODS

3.1Properties of Feedstock

The food waste used for slow pyrolysis was a mixture of discarded vegetables and fruits (e.g., onion peel, carrot peel, bell pepper stalks, potato peel, celery head and leaves, watermelon shell, orange peel, pumpkin seeds and pistachio shells) acquired from Marquis Culinary Centre located at the University of Saskatchewan in Saskatoon. The agricultural crop residue like canola hull and oat hull were supplied by Milligan Bio (Foam Lake, Saskatchewan) and Richardson Milling Limited (Portage la Prairie, Manitoba), respectively. The moisture content of as-received food waste was in the range of 50-60 wt%, whereas canola hull and oat hull had moisture contents of less than 10 wt%. The food waste and agricultural biomass were dried in a temperature-controlled chamber at 45 °C for 24 h. The biomass precursors were grounded and then sieved to 1.0 mm particle size and kept in neat glass bottles at ambient temperature for further use.

3.2 Batch slow pyrolysis schematic and procedure

Slow pyrolysis of biomass was operated in a laboratory-scale tubular reactor positioned inside an ATS Series 3210 electrical furnace. Fig. 3.1 represents the schematic of the pyrolysis reactor employed in this study. The setup includes a fixed bed reactor made of Inconel tubing, which is 850 mm long with 20 mm internal diameter and 26 mm outer diameter. The inside temperature of the rector bed was recorded by employing an Omega Type-K thermocouple (Spectris Canada, Inc., Laval, Canada) and controlled by an ATS temperature control system (Applied Test Systems, Butler, USA). The ATS temperature control system also allowed regulating the heating rate. The heating rate was calculated by monitoring the increase in the reactor bed temperature as a function of time. The pyrolysis set-up included other components like mass flow meter, pressure gauge, pressure relief valves and check valves. The temperature and mass flow rate were calibrated prior to the experiments (Fig. A1 and Fig. A2). During pyrolysis experiments, the hot vapours exited the reactor into a stainless steel SS316 condenser placed inside an ice bath. The permanent gases were purged through a water column saturated with brine solution (17 wt%) and collected using gas bags for analysis in a gas chromatography (GC) device. The condensed liquids (i.e., aqueous and organic phase of bio-oil) collected inside the condenser were collected after each experiment. Approximately 20 g of ground biomass was fed into the pyrolysis reactor per experiment. The experiments were conducted under a constant flow of N_2 gas at 30 mL/min to create an inert

atmosphere. Different temperatures (300-600 °C), reaction time (30-60 min) and the heating rate (5-20 °C/min) were investigated for producing biochar. Initial experiments for process investigation were performed using food waste as the feedstock, whereas oat hull and canola hull were pyrolyzed at optimal conditions. The weight of biochar (retained inside the pyrolysis reactor), bio-oil (collected inside the condenser) and gases were estimated through the gravimetric method. The bio-oil was kept in clean and sealed glass bottles under refrigeration to prevent polymerization reaction while the biochar was stored at room temperature.

3.3 Activation and batch adsorption

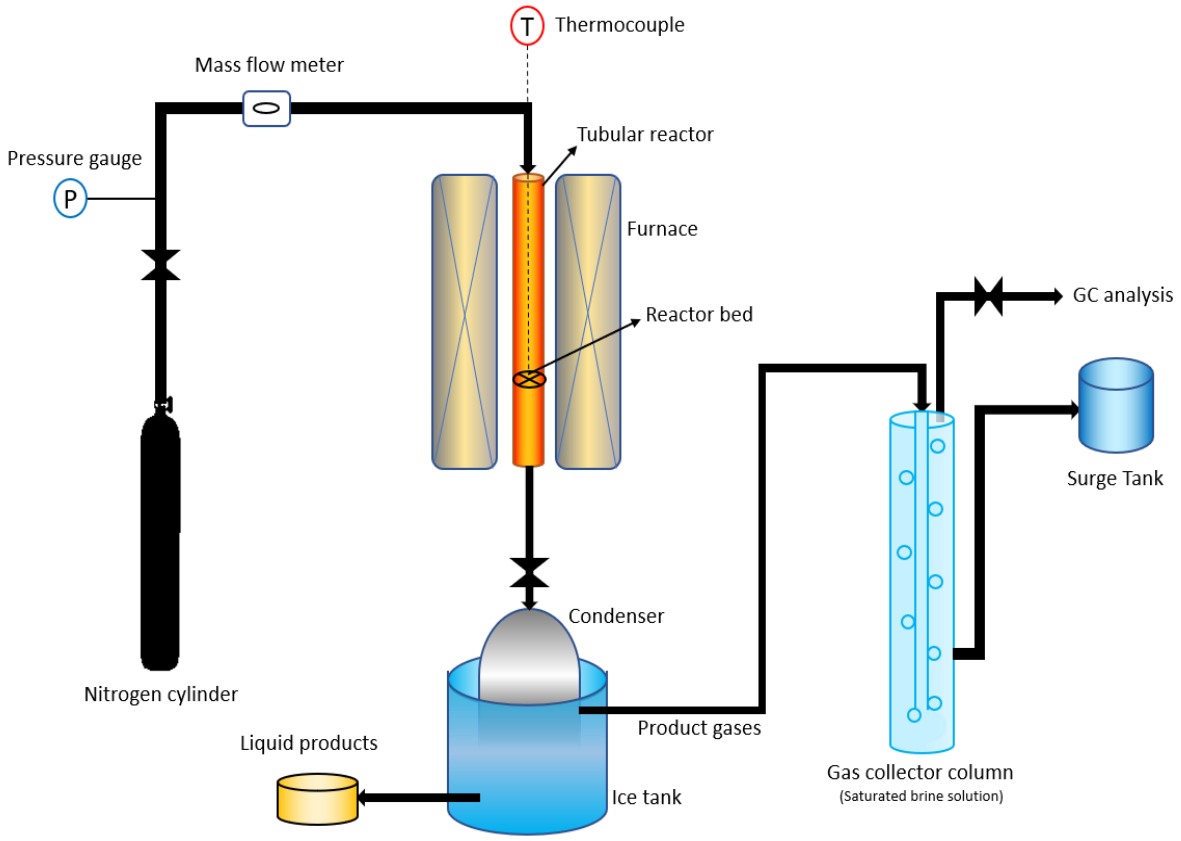

Fig. 3.1: Schematic representation of the slow pyrolysis reactor assembly

The food waste biochar prepared at favourable conditions (Temp: 600 °C, Reaction Time: 60 min, Heating rate: 5 °C/min) were subjected to activation study. Steam and KOH were used as the oxidizing agent and chemical agent, respectively, for the physical and chemical activation of

biochar at temperature: 700-800 °C, activation time: 60-120 min, and heating rate of 3 °C/min. The nitrogen flow rate was maintained at 150 mL/ min.

3.4 Physical activation procedure

A biochar sample of 5 g was placed inside the activation reactor (specifications similar to the reactor used for chemical activation) under a constant flow of nitrogen at 150 mL/min. A constant heating rate of 3 °C/min was used to elevate the reactor temperature to the desired test temperatures (i.e., 700-900 °C). After reaching desired activation temperature, the steam injection was initiated at a flow rate of 2:1 steam-to-biochar ratio (Chen et al., 2016). The activation process was conducted for the desired activation time (i.e., 60-120 min). The temperature of the resulting activated carbon sample was brought down to room temperature under the nitrogen flow after the completion of the experiments. The activated carbon samples produced from steam activation of food waste biochar, canola hull biochar and oat hull biochar at optimized conditions are represented as FW-AC-Steam, CH-AC-Steam and OH-AC-Steam, respectively.

3.5 Chemical Activation procedure

About 5 g of biochar sample was impregnated with potassium hydroxide (KOH) at a 1:1 KOH-to-biochar ratio (Muniandy et al., 2014; Rambabu et al., 2015) and the impregnated biochar was mixed with 100 mL of deionized water. The mixture was then agitated for 8 h at room temperature to enhance the impregnation of KOH into the biochar particles. The resulting slurry was dried overnight at 110 °C in an oven. The dried impregnated biochar was activated in an Inconel fixed bed reactor having the following dimensions: 850 mm long, 20 mm internal diameter, and 26 mm outer diameter. An ATS Series 3210 electrical furnace (Applied Test Systems, Butler, USA) was used with the Inconel tubular reactor placed inside it. An ATS temperature control system was used to regulate the temperature of the split furnace. The reactor bed temperature was determined using an Omega Type-K thermocouple (Spectris Canada, Inc., Laval, Canada).

The activation of biochar was conducted at variable temperatures (i.e., 700-900 °C) and activation time (i.e., 60-120 min) under a fixed nitrogen flow rate of 150 mL/min. The heating rate of 3 °C/min was used to reach the set temperature. After the completion of the activation experiments, the temperature of the resulting activated carbon sample was reduced to room temperature under a continuous nitrogen flow. The activated carbon was weighed and washed with deionized water

followed by 0.1 M HCl to maintain a pH value of 6-7. The rinsed activated carbon sample was dried for 12 h inside an oven at 110 °C. The activated carbon samples produced from KOH activation of food waste biochar, canola hull biochar and oat hull biochar at optimized conditions are represented as FW-AC-KOH, CH-AC-KOH and OH-AC-KOH, respectively.

3.6 Biomass and product characterization

3.6.1 Proximate and ultimate analyses

The contents of ash, moisture, fixed carbon and volatile matter in biomass, biochar, and activated carbon samples were measured by following ASTM methods (ASTM E871-82; ASTM E1755-01; ASTM D3175-11). The moisture content was measured by heating 1 g of solid sample in a crucible placed inside a furnace at 105 °C for 2 h and calculating the difference in weight. The ash contents in biomass and biochar were measured by heating the samples at 575±10 °C for 4 h, followed by calculating the weight losses. The volatile matter was determined by heating the samples at 950±10 °C for 7 min. The calculation for fixed carbon was done by differentiating moisture, ash and volatile matter contents. Ultimate analysis (i.e., C, H, N, S and O) of biomass, biochar and bio-oil samples was done using a Vario EL III elemental analyzer (Elementar Americas, Inc., Ronkonkoma, USA). Furthermore, using the formula as shown in Eq. (3.1) (Ferrera-Lorenzo et al., 2014), the higher heating values (HHV) of biomass, biochar and bio-oil samples were calculated.

$$\text{HHV (MJ/kg)} = [(3.55\text{C}^2) - (232 * \text{C}) - (2230 * \text{H}) + (51.2 * \text{C wt\%} * \text{H}) + (131 * \text{N}) + 20600] * 0.001 \quad (3.1)$$

Where C, H and N are the ultimate compositions for carbon, hydrogen and nitrogen, respectively represented in wt %.

3.6.2 Thermogravimetric analysis (TGA)

TGA analysis was performed with a TGA Q500 instrument (TA Instruments, New Castle, USA) to evaluate the thermal stability of biomass and biochar. The devolatilization of biomass and biochar samples was conducted under N_2 atmosphere (flow rate of 60 mL/min) with heating up to 600 °C (heating rate of 10 °C/min).

3.6.3 X-ray diffraction analysis (XRD)

XRD was carried out to understand the crystallographic structural segments in the biomass and biochar. A Bruker D8 Advance Series II XRD instrument (Bruker Optics Inc, Billerica, USA) was used to conduct the analysis. The crystallographic structures of the samples were analyzed by using XRD diffractometer with CuKα monochromatic radiation (λ = 0.15406 nm) produced at 40 kV and 40 mA. At a scanning frequency of 1.4°/min, the XRD patterns were determined with 2θ wide-angle at a range of 10° and 60°.

3.6.4 Solid-state ^{13}C nuclear magnetic resonance spectroscopy (NMR)

Solid-state ^{13}C NMR spectroscopy was implemented in a Bruker Avance 500 MHz NMR spectrometer to evaluate carbon-containing groups in biomass and biochar samples. The ^{13}C CP/TOSS NMR analysis was executed at 6 kHz of spinning speed. The decoupling CP/TOSS analysis was done with 2048 scans in a time frame of 90 min. The data were processed by using Topspin 3.5 software.

3.6.5 Fourier transform infrared spectroscopy (FTIR)

FTIR analysis was executed to analyze the existence of surface organic functional groups in biomass, biochar and bio-oil samples. Bruker VERTEX 70v FTIR spectrometer (Bruker Optics Inc, Billerica, USA) was used for conducting the FTIR analysis. The infrared spectra were generated at 4 cm^{-1} resolution between 600 and 3600 cm^{-1}.

3.6.6 Surface area and porosity analyses

Brunauer-Emmett-Teller (BET) and Barret-Joyner-Halenda (BJH) analyses were done using Micromeritics ASAP 2020 apparatus (Micromeritics Instrument Corporation, Norcross, USA). BET method revealed the surface and textural properties of biochar samples, while the BJH method elucidated pore size and volume. The adsorption-desorption isotherm of N_2 at –196 °C was used to perform the BET analysis. Before analyzing, the biochar samples were subjected to degassing at 300 °C under a vacuum pressure of 500 mmHg for 4 h to remove the moisture and any absorbed gases present in the samples after pyrolysis.

3.6.7 Scanning electron microscopy (SEM)

SEM imaging of biomass, biochar and activated carbon samples was acquired via a Hitachi SU8010 SEM (Hitachi High-Technologies Corporation, Tokyo, Japan) functioned under a high vacuum at 3 kV voltage. A Q150T ES sputter coater (Quorum Technologies Inc., Laughton, U.K.) was used to coat the solid samples with a gold layer. Samples were placed double-sided carbon tape affixed on pin stubs, and loosely attached particles were blown off under compressed air.

3.6.8 Gas chromatography for gases

Gas chromatography analysis was conducted to quantitatively study the composition of gases generated from slow pyrolysis of food waste at different temperatures. The analysis was carried out in an Agilent 7890A series gas chromatography (GC) instrument (Agilent Technologies, Santa Clara, USA) accoutred with two thermal conductivity detectors and one flame ionization detector and the columns such as Varian capillary CP-Al_2O_3/KCl, HayeSep Q 80/100, Molecular Sieve 13X 45/60). Helium and nitrogen were used as the carrier gas.

The higher heating values (HHV) of non-condensable gases was elucidated from their composition using Eq. (3.2) (Chen et al., 2016):

$$\mathrm{HHV\ (MJ/Nm^3)} = \mathrm{H_2(vol\%)} * \mathrm{HHV_{H_2}} + \mathrm{CO(vol\%)} * \mathrm{HHV_{CO}} + \mathrm{CH_4(vol\%)} * \mathrm{HHV_{CH_4}} + \mathrm{C_{2+}(vol\%)} * \mathrm{HHV_{C_{2+}}} \quad (3.2)$$

3.6.9 Gas chromatography-mass spectrometry (GC-MS) for bio-oil

GC-MS analysis of bio-oil was conducted to investigate their chemical composition in a TRACE™ 1310 gas chromatograph device equipped with a TSQ Duo Mass Spectrometer (Thermo Fisher Scientific, Waltham, USA). At a flow rate of 1.2 mL/min, helium was used as the carrier gas. The sample injection (1 μL) was done at 250 °C with a 50:1 ratio. The mass spectroscopy data were assimilated in a range of 50-650 m/z. The National Institute of Standards and Technology (NIST) library was used for peak identification with the help of Chromeleon™ 7.2 software.

3.6.10 pH and electrical conductivity

The pH value and electrical conductivity (EC) of biochar samples were measured using an Elite PCTS pH/conductivity meter (ThermoFisher Scientific, Mississauga, Canada) after mixing the biochar in deionized water for 24 h at a 1:5 ratio of biochar and water with sporadic agitation (Nanda et al., 2014 BR).

3.7 Biochar and activated carbon batch adsorption study

The adsorptive performance was studied for the activated carbon samples derived from food waste and agricultural biomass along with their biochar precursors and a commercial activated carbon. The commercial activated carbon used in this study was an acid-washed lignite-based activated carbon with a surface area of 655 m^2/g (Darco, Sigma-Aldrich, St. Louis, Missouri, USA). Different dyes such as methylene blue, methyl violet and Rhodamine B were used as model dye pollutants for adsorption studies. Batch experiments for the adsorption study were conducted using 250 mL conical flasks comprising a specific amount (100 mL) of dye solution at a fixed initial concentration (250 mg/L) along with a specific dosage of 0.2 g of biochar and activated carbon. The flasks were agitated under room temperature at 150 rpm in an orbital shaker. After attaining equilibrium at various time intervals, the sample solutions were filtered using 0.2 μm syringe filters before analysis in a UV-Visible spectrophotometer (GENESYS 50, Thermo Fisher Scientific, Waltham, USA). The percent removal of dye was calculated using Eq. (3.3). The UV-Visible spectrophotometer was set to specific wavelengths for the adsorption of the methylene blue (664 nm) (Canales-Flores and Prieto-Garcia 2020), methyl violet (581 nm) (Astuti et al., 2019) and Rhodamine B (554 nm) (Ding et al., 2014).

$$\%\ \text{Dye removal}\ (D_R)\ = \frac{C_0 - C_t}{C_0} * 100 \qquad (3.3)$$

Where C_0 (mg/L) is the initial concentration of the dye solution at time t = 0 and C_t (mg/L) is the concentration of dye solution at a specific time interval (Kausar et al., 2019).

3.8 Taguchi Design

The design of experiment (DOE) is an efficient experimental design technology, which enables the obtained data's accuracy for an effective statistical analysis. The process conditions can be efficiently optimized with minimum experiments by using DOE. Furthermore, through the DOE, the interactive effects between process parameters could be determined (Karmakar et al., 2018). In addition, an equation that establishes the relationship between a set of process parameters and the response could be derived from the DOE.

Taguchi method is one of the most robust optimization techniques, specifically this study adapted the Taguchi approach for optimizing the activation process conditions. Selected process conditions and levels were assimilated into an L_{18} orthogonal array in order to examine the impact of different factors on the response. In Taguchi design, the inner and outer designs of orthogonal arrays are being taken into consideration to minimize the noise and design factors in experiments performed. The pictorial representation of Taguchi design facilitates its efficacy in interpreting the interaction of different factors and in exhibiting the resulting responses from the experiments (Moralı et al., 2018).

The Taguchi design method helps in determining the performance of the process by diminishing the impact of the noise factors while increasing the quality and stability. In all experimental runs, the experimental values are used to measure the quality loss values for each quality characteristic. The product-related quality loss is due to the variation in the functionality of the product from its subsequent target. Furthermore, the value of the loss function gets transformed into the signal-to-noise ratio (S/N), and it is described as the ratio of the mean value of the attributes of the response to the standard deviation (Canales-Flores and Prieto-García 2020). S/N ratio combined with the analysis of variance (ANOVA) and can be utilized to obtain the optimal conditions. In addition, the S/N ratio lessens the variability and aids in enhancing the mean measurement (Karmakar et al., 2018). The nature of the quality characteristics utilized in analyzing the S/N ratio is classified as higher-the-better, nominal-the-best, and lower-the-better.

The intent of this optimization study is to enhance the activated carbon's BET surface area. The steps involved in the Taguchi design approach for the optimization of process conditions are

categorized into four distinct steps. The first step was to specify the process parameters and their levels together with the response (surface area) variable. Secondly, the Taguchi design type was selected based on the factors and their levels, and parameters chosen in this study were activating agent (Physical activating agent: Steam and Chemical activating agent: KOH), temperature (700-900 °C), activation time (60-120 min). The L_{18} Taguchi design was used for the optimization study. In this third step, the experimental data were statistically designed by using Minitab® Statistical Software version 16 (Minitab, LLC, State College, PA, USA). The Taguchi design's final step is validating the experimental results at optimal conditions by performing an additional set of experiments at those conditions.

CHAPTER 4: SLOW PYROLYSIS OF AGRO-FOOD WASTES AND PHYSICOCHEMICAL CHARACTERIZATION OF BIOFUEL PRODUCTS

Most of the content of this chapter has been submitted as a research article:
Biswa R. Patra, Sonil Nanda, Ajay K. Dalai, and Venkatesh Meda 2021. Slow pyrolysis of agro-food wastes and physicochemical characterization of biofuel products (Accepted for Publication in Chemosphere, June, 2021). DOI:https://doi.org/10.1016/j.chemosphere.2021.131431

Contribution of the M.Sc. candidate:

Slow pyrolysis, physicochemical characterization, testing of the materials and data analysis was done by Biswa Patra. The reactor setup was modified by Biswa Patra and Dr. Sonil Nanda. Biswa Patra did the manuscript writing. The experimental planning, discussion on experimental data and correction of the manuscript were done by Drs. Ajay Dalai, Venkatesh Meda and Sonil Nanda.

Contribution of this chapter in the overall M.Sc. Work:

This phase of the research work was focused on exploring the slow pyrolysis of food waste and agricultural residues like canola hull and oat hull. The study also intended for the investigation of process parameters like temperature, heating rate and reaction time, and characterization of biofuels.

4.1 Abstract

Effective management and utilization of food waste and agricultural crop residues are highly crucial to mitigate the challenges of greenhouse gas generation upon natural decomposition and waste accumulation. Conversion of biogenic wastes to biofuels and bioproducts can address the energy crisis and promote environmental remediation. This study was focused on exploring the characteristics of food waste and agricultural crop residues (e.g., canola hull and oar hull) to determine their candidacy for slow pyrolysis to produce biochar and bio-oil. Process parameters of slow pyrolysis such as temperature, reaction time and heating rate were investigated to obtain maximum biochar yields. Maximum biochar yield of 28.4 wt% was recorded at temperature, heating rate and reaction time of 600 °C, 5 °C/min and 60 min, respectively. Furthermore, the physicochemical characterization of biochar, bio-oil and gases were performed. The carbon

content and thermal stability of biochar were found to increase at higher temperatures. Moreover, bio-oil generated at higher temperatures showed the presence of phenolics and aromatic compounds.

4.2 Introduction

The global demand for food, water and energy is escalating with the growth in population, urbanization and industrialization. The current energy demand for heat, power and transportation sector is predominantly fulfilled by fossil fuels, which promotes a rise in greenhouse gas emissions and global warming. Methane, a major contributor of greenhouse gas, results from the natural decomposition of organic residues such as food waste and agricultural biomass. A tremendous amount of food waste, a portion of municipal solid waste, is obtained globally. In the North American context, the U.S., Canada and Mexico produce nearly 415, 396 and 249 kg of food waste per person every year (Weber 2018). Similarly, considerable amounts of agricultural residues (e.g., straw, husk, leaves, roots, peels, bagasse, shells, hull, etc.) are generated every year worldwide. Natural decomposition of food wastes and agricultural refuse in landfills results in the following issues: (i) odor leading to public annoyance, (ii) breeding of pests, flies and microorganisms, and (iii) methane, which is a potent greenhouse gas than CO_2 (Nanda et al., 2021 JHM). In most developing countries, the agricultural residues are burnt in the farms to reduce the volume of the waste and retain carbon in the soil, which also liberates CO_2 and particulate matter causing air pollution and smog (Patel 2019). However, such practices have adverse impacts on the environment and carbon footprint.

Pyrolysis, one of the thermochemical conversion techniques, can convert a variety of waste feedstocks into bio-oil, biochar and gases. Pyrolysis is classified broadly into slow and fast based on vapor residence time and heating rates. Fast pyrolysis, characterized by higher heating rates (i.e., 10-1000 °C/s) and shorter reaction times (i.e., < 20 s), enhances the yields of bio-oil (Roy and Dias, 2017; Safdari et al., 2019). In contrast, slow pyrolysis leads to maximum biochar production due to its slower heating rates (5-30 °C/min) and longer reaction time (>30 min) (Safdari et al., 2019; Amini et al., 2019). The biofuel products vary in their composition depending on the process conditions, namely temperature, heating rate and vapor residence time (Mohanty et al., 2013; Mlonka-Mędrala et al., 2021).

The growing interest in pyrolysis technology and its renewable energy products such as bio-oil and biochar at a global scale has also resulted in the diversification of precursors including third-generation feedstocks (e.g., food waste and municipal solid waste). Furthermore, new markets, as well as industrial and environmental applications of bio-oil and biochar, are also emerging worldwide compared to their traditional utilities. Biochar finds application as a solid fuel, soil enhancer, CO_2 sequestration agent and precursor for manufacturing specialty materials (e.g., activated carbon, adsorbents, templated carbon, graphene and biocomposites) (Nanda et al., 2016; Sieradzka et al., 2020). Biochar production for environmental remediation, carbon sequestration, wastewater treatment, pollutant adsorption from flue gases, soil enrichment and bioenergy generation are a reasonable approach to mitigate climate change (Qambrani et al., 2017). Therefore, the application of waste biomass for bio-oil and biochar production could be an ecofriendly approach to valorize agro-food wastes, increasing the agricultural industries' profitability and close the loop for waste generation.

With the increased generation of food waste globally, there is a mounting interest in its effective and sustainable management (Okolie et al., 2021). Moreover, only a few notable reports are available on the slow pyrolysis of real food waste generated from commercial institutions as well as agricultural residues such as canola hull and oat hull to produce biochar. Attempting to fill in the knowledge gaps, this study reports the univariate optimization and interactions of process parameters during slow pyrolysis of food waste, canola hull and oat hull on product yield and quality. The main objective of this study was to evaluate the impacts of temperature (300-600 °C), heating rate (5-20 °C/min) and reaction time (30-60 min) on the slow pyrolysis of the agro-food residues and subsequent yields, composition and physical chemistry of biofuel products, especially biochar and bio-oil. This study also sheds light on the advanced physicochemical, spectroscopic, morphological and compositional characterization of bio-oil, biochar and gases obtained from slow pyrolysis of the abovementioned agro-food residues.

4.3 Experimental methodology

4.3.1 Slow pyrolysis procedure

Slow pyrolysis of biomass was operated in a laboratory-scale tubular reactor positioned inside an ATS Series 3210 electrical furnace. Different temperatures (300-600 °C), reaction time (30-60 min) and the heating rate (5-20 °C/min) were investigated and favourable conditions for high qualitybiocharwere obtained. Initial experiments for investigation of process conditions were performed using food waste as the feedstock, whereas oat hull and canola hull were pyrolyzed at optimal conditions (Please refer to Section 3.2 for a detailed procedure).

4.3.2 Proximate and ultimate analysis

The contents of ash, moisture, fixed carbon and volatile matter in biomass, biochar, and samples were measured by following ASTM methods (ASTM E871-82; ASTM E1755-01; ASTM D3175-11). Please refer to Section 3.6.1 for a detailed procedure.

4.3.3 Thermogravimetric analysis (TGA)

TGA analysis was performed with a TGA Q500 instrument (TA Instruments, New Castle, USA) to evaluate the thermal stability of biomass and biochar. Please refer to Section 3.6.2 for a detailed procedure.

4.3.4 X-ray diffraction analysis (XRD)

XRD was carried out to understand the crystallographic structural segments in the biomass and biochar. A Bruker D8 Advance Series II XRD instrument (Bruker Optics Inc, Billerica, USA) was used to conduct the analysis. Please refer to Section 3.6.3 for a detailed procedure.

4.3.5 Solid-state ^{13}C nuclear magnetic resonance spectroscopy (NMR)

Solid-state ^{13}C NMR spectroscopy was implemented in a Bruker Avance 500 MHz NMR spectrometer to evaluate carbon-containing groups in biomass and biochar samples. Please refer to Section 3.6.4 for a detailed procedure.

4.3.6 Fourier transform infrared spectroscopy (FTIR)

Bruker VERTEX 70v FTIR spectrometer (Bruker Optics Inc, Billerica, USA) was used for conducting the FTIR analysis. Please refer to Section 3.6.5 for a detailed procedure.

4.3.7 Surface area and porosity analyses

Brunauer-Emmett-Teller (BET) and Barret-Joyner-Halenda (BJH) analyses were done using Micromeritics ASAP 2020 apparatus (Micromeritics Instrument Corporation, Norcross, USA). Please refer to Section 3.6.6 for a detailed procedure.

4.3.8 Scanning electron microscopy (SEM)

SEM imaging of biomass and biochar samples was acquired via a Hitachi SU8010 SEM (Hitachi High-Technologies Corporation, Tokyo, Japan). Please refer to Section 3.6.7 for detail procedure.

4.3.9 Gas chromatography for gases

Gas chromatography analysis was conducted was carried out in an Agilent 7890A series gas chromatography (GC) instrument (Agilent Technologies, Santa Clara, USA). Please refer to Section 3.6.8 for a detailed procedure.

4.3.10 Gas chromatography-mass spectrometry (GC-MS) for bio-oil

GC-MS analysis of bio-oil was conducted to investigate their chemical composition in a TRACE™ 1310 gas chromatograph device equipped with a TSQ Duo Mass Spectrometer (Thermo Fisher Scientific, Waltham, USA). Please refer to Section 3.6.9 for a detailed procedure.

4.3.11 pH and electrical conductivity

The pH value and electrical conductivity (EC) of biochar samples were measured using an Elite PCTS pH/conductivity meter (ThermoFisher Scientific, Mississauga, Canada). Please refer to Section 3.6.10 for a detailed procedure.

4.4 Results and discussion

4.4.1 Effects of reaction temperature on product yields

Fig. 4.1a depicts the reaction temperature (300-600 °C) effects on the product yields of the pyrolyzed food waste biomass at a constant reaction time and heating rate of 30 min and 5°C/min, respectively. The lowest temperature (300 °C) resulted in the highest yield of biochar (52.4 wt%), whereas the highest temperature (600 °C) revealed the lowest biochar yield (31 wt%). With rising temperatures, the biochar yield decreased due to the thermal cracking of biomass, which enhanced the yields of gases and bio-oil (Nizamuddin et al., 2016). Lee et al. (2018) pyrolyzed food waste compost at 300-500 °C and observed a sharp reduction in biochar yield from 300 °C (44.1 wt%)

to 500 °C (22.5 wt%) because of the intensification on thermal cracking reactions.

As seen from Fig. 4.1a, bio-oil with a maximum yield of 42.4 wt% was found at 500 °C and decreased subsequently with the increasing temperature. The secondary cracking reaction enhances the yield of the gaseous product, which was observed at 600 °C in 30 min with the highest yield of 22.3 wt%. Since biochar is the chief product of interest in the present work, the temperature of 600 °C was considered optimal for further studies owing to its highest yields.

4.4.2 Effects of reaction time on product yields

The reaction time was also considered as an essential factor affecting pyrolysis product yields. Although not pronounced, a rise in the reaction time to 60 min resulted in a slight escalation in the biochar yield from the pyrolysis of food waste biochar at temperature and constant heating rate of 600 °C and 5 °C/min, respectively (Fig. 4.1b). The highest yield of biochar (29 wt%) was recorded at 30 min of reaction time, while the lowest yield (28.4 wt%) was noticed at 60 min. A prolonged reaction time enables secondary cracking of volatiles vapours liberated from the biomass, thus leading to the production of permanent gases (Nanda et al., 2016 WBV). Therefore, the gas yields significantly improved at 60 min (30.6 wt%) when compared to 30 min (22.3 wt%). Similarly, a gradual decrease in the bio-oil yield was also noticed at 30 min (36.3 wt%) compared to 60 min (32.4 wt%). According to several reports, the physicochemical properties of biochar (e.g., carbon content, calorific value, porosity, pore volume and thermal stability) are enhanced at higher temperatures despite its low yields (Qian et al., 2015). Hence, 60 min was considered as an optimal reaction time for understanding the consequences of heating rate.

4.4.3 Effects of heating rate on product yields

Fig. 4.1c demonstrates the impact of heating rate (5-20 °C/min) on the product distribution from the pyrolysis of food waste generated at the optimum temperature (600 °C) and reaction time (60 min). There was a steady decrease in the yield of biochar with the rise in the heating rate from 5 °C/min (28.4 wt%) to 20 °C/min (22 wt%). Consequently, bio-oil (35.9 wt%) and gases (35.8 wt%) were at their maximum yields at 20 °C/min. In another study, Amini et al. (2019) recorded a slight increased bio-oil and gas yield with an increased heating rate from 5 °C/min to 30 °C/min. One of the secondary pyrolysis reactions, i.e., repolymerization of cracked vapours liberated from biomass, occurs at low heating rates (Mohanty et al., 2013). The primary products of

repolymerization reactions are biochar and tar. In contrast, high heating rates lead to rapid quenching of volatile vapours released from the thermal cracking of biomass, which causes an increase in bio-oil and gas yields (Singh et al., 2020 CJCE). Considering the biochar yield and properties, the process parameters for slow pyrolysis (i.e., temperature, reaction time and heating rate) in this study were found as 600 °C, 60 min and 5 °C/min (Fig. 4.1). Subsequently, the agricultural crop residues such as canola hull and oat hull were pyrolyzed at the above-mentioned process conditions. Without any significant difference, the biochar yield from oat hull (29.1 wt%) was comparatively highest than that from canola hull (28.8 wt%) and food waste biomass (28.4 wt%) at the optimal conditions.

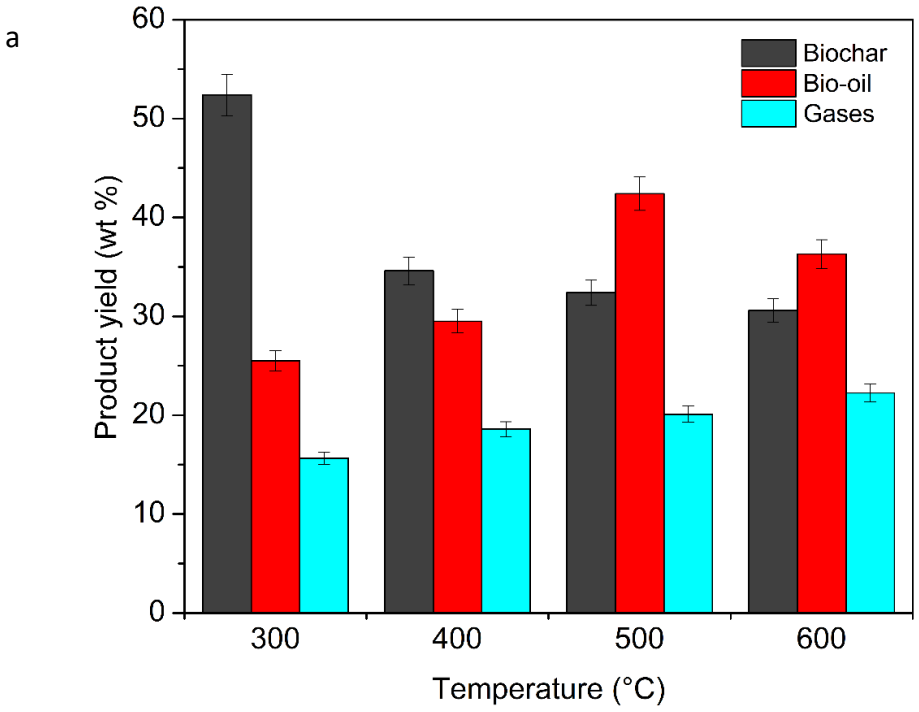

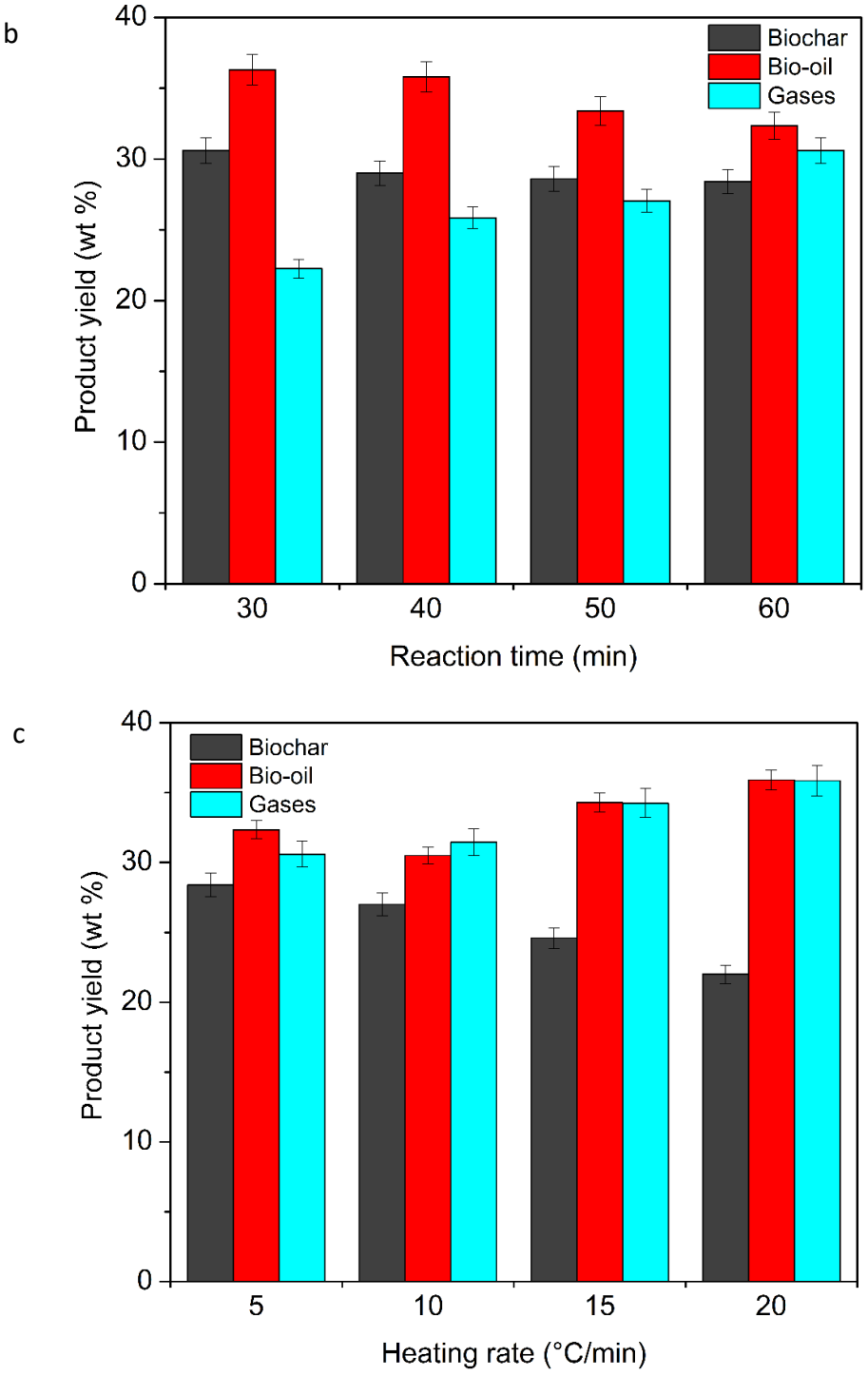

Fig. 4.1: Product distribution from slow pyrolysis of food waste at variable (a) temperature at 30 min and 5 °C/min heating rate, (b) reaction time at 600 °C and 5 °C/min heating rate, and (c) heating rate at 600 °C and 60 min of reaction time

The obtained favourable conditions were used to pyrolyze individual food waste like pistachio shell, onion peel, bell pepper, and carrot, which contributed a major portion in the food waste matrix used for the investigation study (Table A1). Interestingly, pyrolysis of pistachio shell was found to have the highest biochar and bio-oil yield among all other food waste precursors pyrolyzed at favourable conditions. In the case of other individual food waste, the yield of biochar was observed to be lower at favourable conditions.

4.5 Characterization of biochar

4.5.1. Proximate and ultimate analysis

Table 4.1 summarizes the proximate analysis for food waste, canola hull and oat hull along with their corresponding biochar samples. The moisture content of food waste biomass after drying was recorded as 8.7 wt%, which was reduced in the biochar samples with the increasing temperature. Food waste-derived biochar generated at 300°C in 30 min retained 7.3 wt% moisture content when compared to that at 600 °C in 30 min (5.1 wt%) and 600 °C in 60 min (4.3 wt%). Similarly, the volatile matter reduced from 77.2 wt% in food waste biomass to 54.1 wt% in the biochar produced at 300 °C in 30 min and 16 wt% at 600 °C in 30 min and 11.4 wt% at 600 °C in 60 min. Higher temperatures resulted in significant dehydration of hydroxyl groups and the release of volatile compounds of low molecular weight, thereby reducing the moisture and volatiles content (Tomczyk et al., 2020). The ash content of food waste (9 wt%), canola hull (9.2 wt%) and oat hull (5.4%) biomasses were relatively lower than that of their corresponding biochar samples produced at 600 °C in 60 min as 30.5 wt%, 17.4 wt%, and 14.6 wt%, respectively. The high ash content in the biochar samples resulted from the gradual concentration of inorganic constituents present in the biomass (Rafiq et al., 2016). Likewise, the content of fixed carbon in food waste (5.1 wt%), canola hull (4 wt%) and oat hull (6.8 wt%) improved in their biochar samples generated at 600 °C in 60 min as 53.8 wt%, 58.2 wt% and 64 wt%, respectively. The trend of the proximate composition obtained agreed with other studies (Wilk et al., 2017; Amini et al., 2019; Xue et al., 2019).

Table 4.2 depicts the ultimate analysis of food waste, canola hull and oat hull, as well as their corresponding biochar samples. A considerable enhancement in the carbon content of biochar

increased with a rise in pyrolysis temperature. It was observed that the carbon content in the food waste biochar increased from 51.7 wt% (at 300 °C) to 58.4 wt% (at 600 °C) in 30 min. The carbon content of food waste-derived biochar produced at 600 °C in 60 min further amplified to 60.7 wt%. The enhanced carbon content with increasing temperature signifies a higher degree of carbonization of biochar with the development of condensed and aromatic carbon structures (Azargohar et al., 2019). At favourable slow pyrolysis conditions (i.e., 600 °C, 60 min and 5 °C/min), oat hull biochar revealed the highest carbon content (67 wt%) followed by canola hull biochar (63.5 wt%) and food waste biochar (60.7 wt%).

The hydrogen content reduced from 5 wt% to 3.6 wt% in the case of food waste biochar samples generated at 300 °C and 600 °C in 30 min, respectively (Table 4.2). Similarly, the oxygen content of food waste biochar showed a drastic reduction from 21.2 wt% (at 300 °C and 30 min) to 7.1 wt% (600 °C and 30 min) and 2.5 wt% (600 °C and 60 min). An increase in the pyrolysis temperature impacts the oxygenated bonds by decomposing them into low molecular weight by-products (as volatile vapours) which causes a reduction in their composition in the biochar (Suliman et al., 2016). Nitrogen content in the biochar also decreased with increasing temperatures. Compared to oat hull, canola hull and food waste biomass contained higher nitrogen levels owing to their proteins, lipids and fat contents (Azargohar et al., 2013 EF). The HHV of biochar samples also intensified with the increased pyrolysis temperature (Table 4.2). For example, the HHV of food waste-derived biochar increased with the following pyrolysis temperatures: 300 °C (20.5 MJ/kg) < 400 °C (21.2 MJ/kg) < 500 °C (22 MJ/kg) < 600 °C (22.2 MJ/Kg). It was observed that at optimal process conditions (i.e., 600 °C, 60 min and 5 °C/min), oat hull biochar demonstrated the greatest HHV (26.8 MJ/kg) followed by canola hull biochar (25.6 MJ/kg) and food waste biochar (23 MJ/kg). This trend was analogous to that of the increase in the carbon content of the biochar (Table 4.2). A VanKrevelen diagram was plotted to illustrate the correlation between HHV and the variation in atomic H/C and O/C ratios for different agro-food biomass and biochar samples (Fig. 4.2). The severity of the pyrolysis process resulted in the enhancement of aromaticity of biochar with a reduced atomic H/C ratio. Furthermore, the atomic O/C ratio reduced significantly with a temperature rise. The lowest O/C ratio in biochar indicates the lower number of polar functional groups on its surface, which makes it less hydrophilic (Yao et al., 2010).

Table 4.1: Proximate analysis of biomass and biochar samples generated from slow pyrolysis of food waste, oat hull and canola hull

Sample	Moisture (wt%)	Ash (wt%)	Volatile matter (wt%)	Fixed carbon (wt%)
Food waste (FW) biomass	8.7 ± 0.2	9.0 ± 0.9	77.2 ± 0.9	5.1 ± 0.1
FW Biochar-300 °C-30 min	7.3 ± 0.1	18.9 ± 0.1	54.1 ± 0.6	19.7 ± 0.6
FW Biochar-400 °C-30 min	6.7 ± 0.4	24.1 ± 0.3	38.2 ± 0.3	31.0 ± 0.6
FW Biochar-500 °C-30 min	5.9 ± 0.1	25.3 ± 0.4	22.7 ± 0.6	46.1 ± 0.1
FW Biochar-600 °C-30 min	5.1 ± 0.1	28.0 ± 0.1	16.0 ± 0.7	50.9 ± 0.5
FW Biochar-300 °C-60 min	6.7 ± 0.2	20.9 ± 0.3	48.0 ± 0.9	24.4 ± 0.2
FW Biochar-600°C-60 min	4.3 ± 0.1	30.5 ± 0.3	11.4 ± 0.3	53.8 ± 0.3
Canola hull (CH) biomass	7.6 ± 0.3	9.2 ± 0.3	79.2 ± 0.4	4.0 ± 0.5
CH Biochar-600 °C-60 min	5.7 ± 0.1	17.4 ± 0.3	18.7 ± 0.4	58.2 ±0.9
Oat hull (OH) biomass	5.8 ± 0.3	5.4 ± 0.4	82.0 ± 0.3	6.8 ± 0.3
OH Biochar-600 °C-60 min	3.5 ± 0.04	14.6 ± 0.3	17.9 ± 0.1	64.0 ± 0.2

Table 4.2: Ultimate analysis of biomass and biochar samples generated from slow pyrolysis of food waste, oat hull and canola hull

Sample	Ultimate composition (wt%)					Atomic ratios		HHV (MJ/kg)	pH	EC (mS/s)
	C	H	N	S	O	O/C	H/C			
Food waste (FW) biomass	40.8	4.1	3.9	0.2	42.0	0.8	1.2	17.0	-	-
FW Biochar-300 °C-30 min	51.7	5.0	2.9	0.3	21.2	0.3	1.2	20.6	7.9	4.3
FW Biochar-400 °C-30 min	53.5	4.8	2.6	0.3	14.7	0.2	1.1	21.1	8.3	4.8
FW Biochar-500 °C-30 min	57.0	4.0	2.5	0.3	10.9	0.1	0.8	22.0	9.4	6.9
FW Biochar-600 °C-30 min	58.4	3.6	2.5	0.4	7.1	0.1	0.7	22.2	10.2	8.2
FW Biochar-300 °C-60 min	54.1	4.6	3.1	0.4	16.9	0.2	1.0	21.3	8.1	4.3
FW Biochar-600 °C-60 min	60.7	3.6	2.2	0.5	2.5	0.03	0.7	23.0	11.2	8.7
Canola hull (CH) biomass	42.5	5.1	2.2	0.6	40.5	0.7	1.4	17.2	-	-
CH Biochar-600 °C-60 min	63.5	4.8	3.6	0.4	10.3	0.1	0.9	25.6	10.9	8.3
Oat hull (OH) biomass	43.2	5.5	0.2	0.1	45.7	0.8	1.5	17.1	-	-
OH Biochar-600 °C-60 min	67.0	4.8	0.7	0.3	12.6	0.1	0.9	26.8	9.4	6.4

Note: The date presented are average of triplicate measurements with standard error less than 3%. All the biochar samples were generated at a heating rate of 5 °C/min.

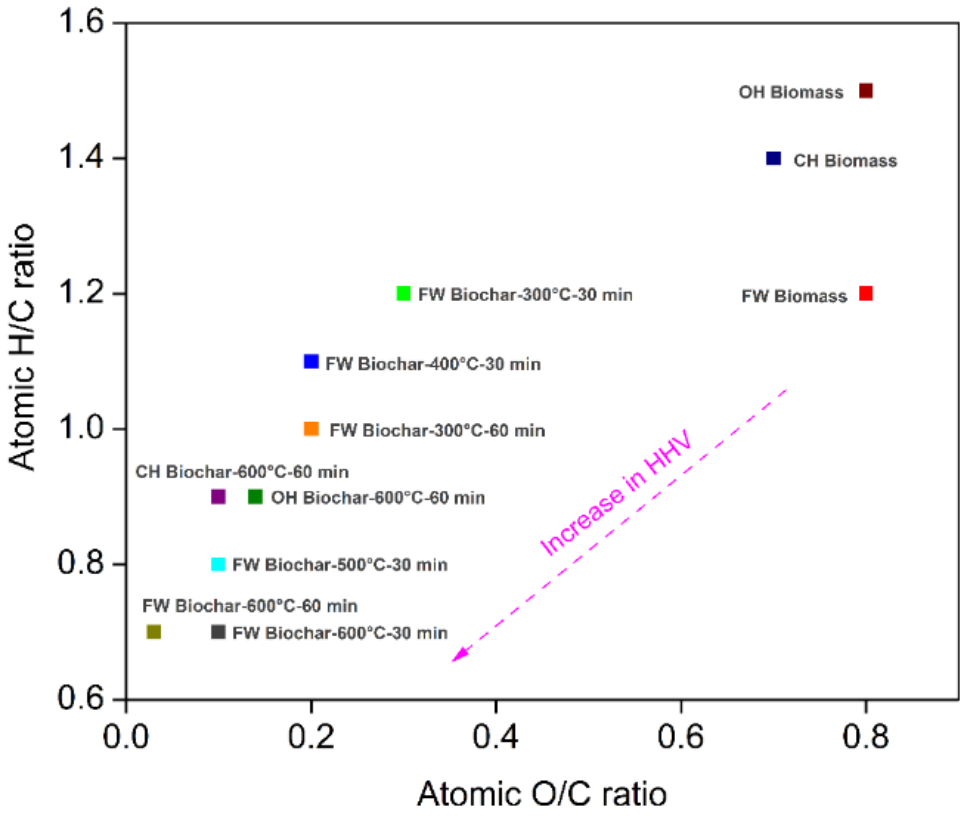

Fig. 4.2: VanKrevelen plot for the correlation of heating value and the atomic ratios of biomass and biochar samples

4.5.2. pH and electrical conductivity

It was observed that pyrolysis temperature had an impact on the pH of biochars (Table 4.2). The pH of food waste-derived biochar increased with the rise in pyrolysis temperatures in the following trend: 300 °C (7.9) < 400 °C (8.3) < 500 °C (9.4) < 600 °C (10.2). Higher temperatures result in the occurrence of alkali and alkaline earth metals in biochar and ash, which makes the biochar alkaline, while lower temperatures result in carboxylic and other acidic functional groups in biochar, which decreases the pH value (Tomczyk et al., 2020). Similarly, the electrical conductivity (EC) of the biochar samples also increased with rising pyrolysis temperature (Table 4.2). The EC value of food waste-derived biochar enhanced with the pyrolysis temperatures in the following order: 300 °C (4.3) < 400 °C (4.8) < 500 °C (6.9) < 600 °C (8.2). Higher pyrolysis temperature has a direct impact on the basic cations present in biochar, which are released in soluble form or converted into insoluble inorganic compounds and minerals (Usman et al., 2015). At optimal slow pyrolysis conditions (i.e., 600 °C, 60 min and 5 °C/min), food waste biochar

demonstrated the highest EC value (8.7), followed by canola hull biochar (8.3) and oat hull biochar (6.4). The increasing EC trend with rising pyrolysis temperature was also stated by other authors (Azargohar et al., 2013 EF; Usman et al., 2015; Intani et al., 2018).

4.5.3. Thermogravimetric analysis

Thermogravimetric analysis was performed to evaluate the thermal stability and devolatilization pattern for biomass and biochar samples generated from food waste at different temperatures and reaction times (Fig. 4.3). Four stages for weight loss in biomass and biochar samples can be inferred from this study. The first stage involves the reduction of entrapped moisture at a temperature around 100-150 °C (Shak and Wu 2014). The second stage involved devolatilization (i.e., removal of volatile compounds) and thermal decomposition of hemicellulose and cellulose at 200-450 °C. The third stage relates to the decomposition of crystalline cellulose and lignin along with complex aromatic or polymeric compounds (Teh et al., 2014).

In this study, food waste biomass started degrading at approximately 70 °C until 180 °C leading to the removal of moisture and volatiles. A sharp decrease in weight loss at 180 °C was observed until 350 °C. The overall weight loss for food waste biomass was around 70% at 600 °C. The magnitude of weight losses reduced for biochar samples produced at higher temperatures due to removal of moisture, volatile matter and conversion of biopolymers and fibers (i.e., cellulose, hemicellulose and lignin) during pyrolysis. For example, the approximate weight losses for biochar samples were in the following sequence: 300 °C-30 min (55 wt%) > 400 °C-30 min (55 wt%) > 500 °C-30 min (15 wt%) > 600 °C-30 min (10 wt%) > 600 °C-60 min (5 wt%). The lower weight loss for biochar samples as compared to raw biomass indicates enhanced thermal stability and aromaticity because of higher pyrolysis temperatures. The devolatilization pattern for biochar produced at pyrolysis conditions (i.e., 600 °C, 60 min and 5 °C/min) indicated its superior thermal stability, aromatic nature, greater HHV and porosity when compared to biochar samples produced at lower temperatures. The aromatic rings that are formed in biochar generated at high temperatures make them suitable for various applications including carbon sequestration and activation (Qian et al., 2015; Tripathi et al., 2016). Moreover, a biomass conversion process is thermochemically viable depending on the energy input, conversion efficiency, utility of the

byproducts, high quality and marketability of the desired products as well as the minimization of waste generation (Nanda et al., 2015a; Suryawanshi et al., 2020; Okolie et al., 2021b).

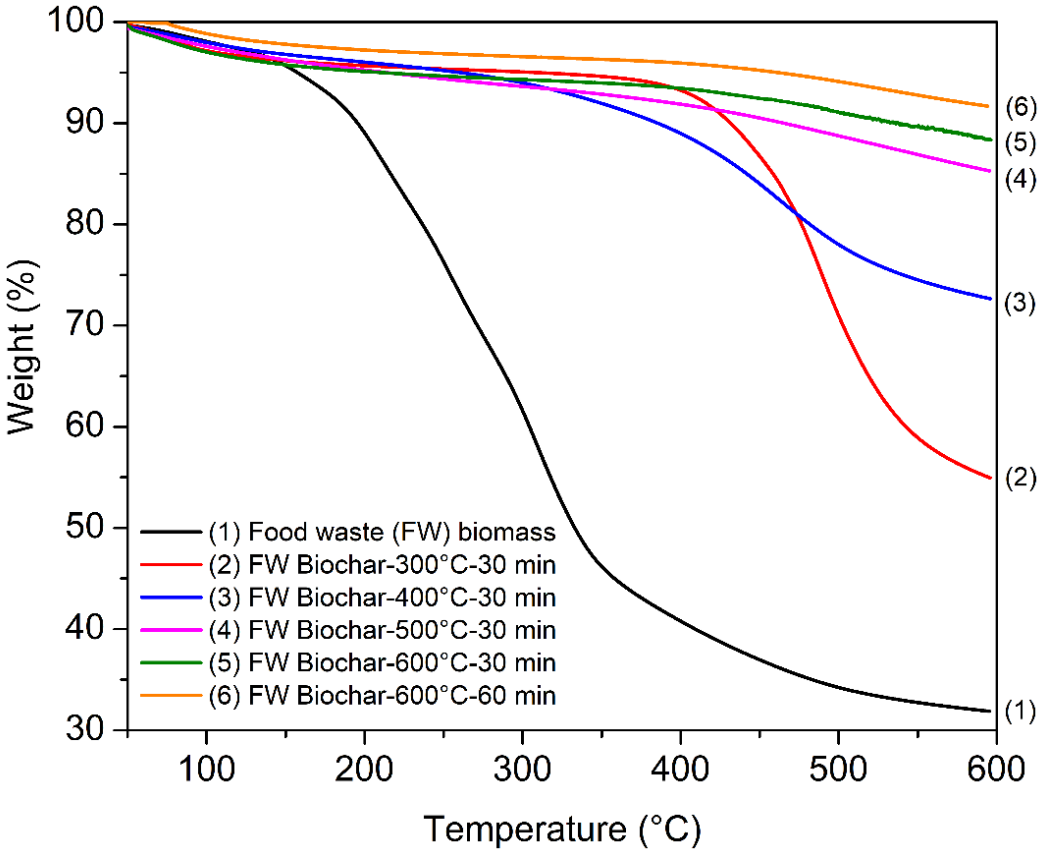

Fig. 4.3: Thermogravimetric analysis of food waste biomass and biochar generated from pyrolysis at variable temperatures and reaction times and 5°C/min heating rate

4.5.4. X-ray diffraction analysis

The XRD patterns of food waste biomass and its biochar samples generated at variable temperatures and reaction time are illustrated in Fig. 4.4. The raw food waste biomass showed two peaks of crystalline cellulose at 2θ of 15.3° and 22.4° (Nanda et al., 2017 FPT). However, these peaks were significantly obliterated in the biochar samples indicating its thermal decomposition. The sharp intensified 2θ peak at 28.1° in the biochar samples was attributed to anhydrite, i.e., $CaSO_4$ (Liu et al., 2020). The 2θ peaks at 30.3°, 40.7° and 50.2° for biochar samples were attributed to calcites, i.e., $CaCO_3$ (Nanda et al., 2017 FPT; Nanda et al., 2013 BR). Other 2θ peaks generated in biochar samples produced at 500°C and 600°C include peaks at 29.1° (sylvite, KCl), 31.4°

(NaCl), 43.2° (periclase, MgO) and 45.1° (halite, NaCl) (Lee et al., 2017; Shin et al., 2020). The occurrence of these alkaline metals also confirms the alkaline nature of biochar produced at higher temperatures.

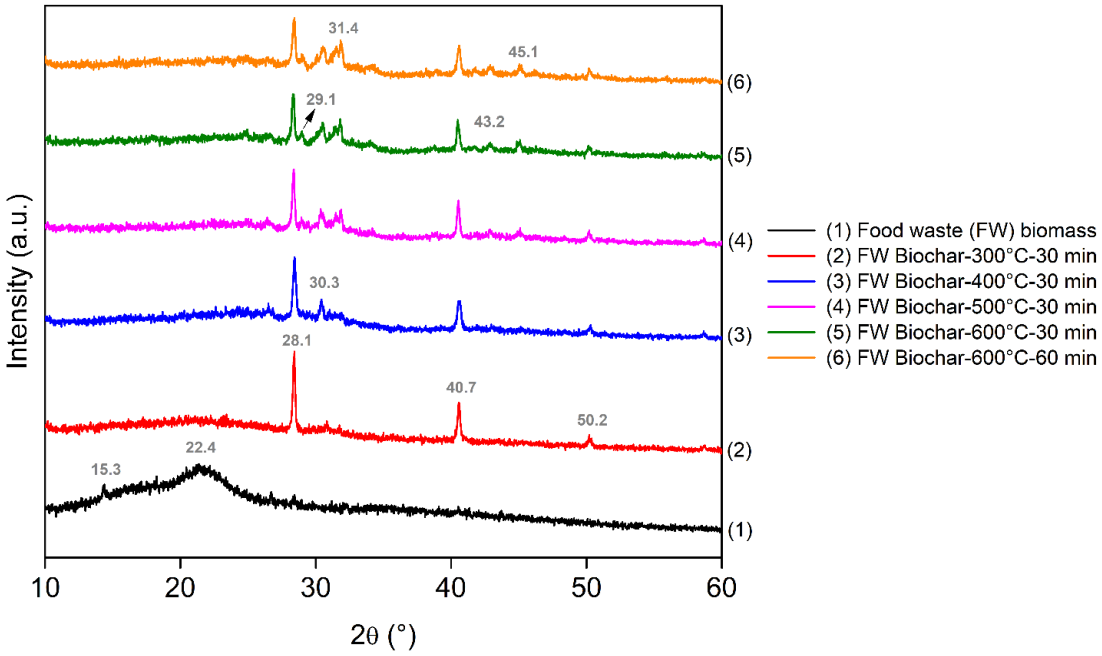

Fig. 4.4: XRD patterns of food waste biomass and biochar generated from pyrolysis at variable temperatures and reaction times and 5 °C/min heating rate

4.5.5. Solid-state nuclear magnetic resonance spectroscopy

Fig.4.5 depicts the solid-state ^{13}C NMR spectra of food waste biomass and biochar samples generated at different temperatures. The identified carbon-containing chemical groups include aliphatics (10-90 ppm), aromatic-vinylic (95-155 ppm), as well as acids and esters (160-180 ppm) (Nanda et al., 2017 FPT). The carbon composition belonging to these identified chemical groups are depicted in Table 4.3 as the relative percent composition of carbon. The aliphatics (77.8%), as well as acids and esters (10.3%), were at higher concentration in food waste biomass, whereas their concentrations diminished in biochar produced at elevated temperatures due to thermal decomposition. In contrast, the aromatic and vinylic carbon groups were at the highest concentration in the biochar generated at 600 °C (66.3%) when compared to that of the biochar generated at 300 °C (50.1%) and food waste biomass (12%). The occurrence of the peak at 95-155 ppm in the biochar samples owing to the aromatic and vinylic carbon is another confirmation of

its thermal stability and higher carbon content as inferred from previous observations in this study (Fig. 4.5). The aromatic carbon presence in biochar plays a colossal role in the effective adsorption of organic contaminants (Rao et al., 2017). The peak around 162 ppm in biochar produced at 600 °C is ascribed to the oxygen substituted aromatic carbon derived from the phenolic composition (Zhou et al., 2017). The peak around 170 ppm in food waste biomass indicates the presence of carboxylic acid, fatty acid and the carbonyl group of anhydrides (Yang et al., 2019).

Table 4.3: Solid-state ^{13}C CP/TOSS NMR spectroscopy of food waste biomass and biochar

Sample	Aliphatic	Aromatic-vinylic	Acid-ester
	Total integrated peak area (%)		
Food waste (FW) biomass	77.8	12.0	10.3
FW Biochar-300 °C-30 min	43.0	50.1	6.9
FW Biochar-600 °C-60 min	26.8	66.3	6.9

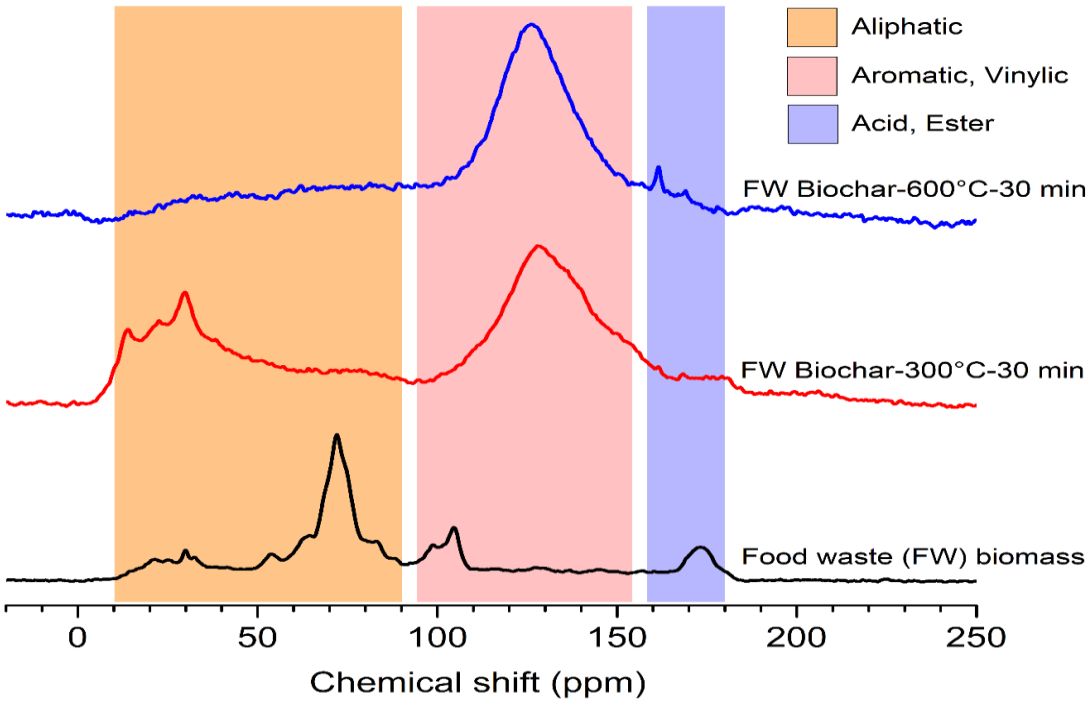

Fig. 4.5: Solid-state ^{13}C CP/TOSS NMR spectroscopy of food waste biomass and biochar

4.5.6. Fourier transform infrared spectroscopy

Fig. 4.6 illustrates the FTIR spectral bands for food waste biomass and biochar samples. Food waste biomass unveiled some distinctive bands that were gradually eliminated in the biochar

samples. The band ascribed to O−H groups was detected at 3300 cm^{-1} for food waste biomass due to the presence of carboxylic acids, alcohols and moisture. The identified spectral bands at 2920 and 2852 cm^{-1} were ascribed to alkanes ($–CH_2$) or other functional groups belonging to $−CH_n$ (Siddiqui et al., 2019). The intensity of such peaks gradually diminished with the rise in temperature in the biochar and their aromatization. The absorbance band at 2361 cm^{-1} showed the existence of C≡C alkynes (Thangalazhy-Gopakumar et al., 2015). Components such as alkenes (i.e., 1395 and 1415 cm^{-1}) and ketones (i.e., 1736 cm^{-1}) lost their strengths in the biochar samples produced at high temperatures. This evidenced the biochar modification and conversion of carbonaceous compounds into the bio-oil phase (Fan et al., 2018; Placido et al., 2019). Hemicellulose was identified at 1736 cm^{-1} (Nanda et al., 2015 JBMB). The bands at 1570, 1574, 1577 and 1605 cm^{-1} in the biomass were ascribed to C=C aromatic lignin, and their absence in the biochar indicates the thermal decomposition of lignin (Nanda et al., 2017 FPT). The bands between 1020-1050 cm^{-1} showed the presence of alcohols, esters, carboxylic acids and ethers, which diminished in the biochar samples. The absorbance bands at 873 and 878 cm^{-1} represented C=C aromatics peculiar to biochar due to aromatization and increase in carbon content as confirmed from TGA (Fig. 4.3), solid-state ^{13}C NMR (Fig. 4.6) and CHNSO (Table 4.2) observations.

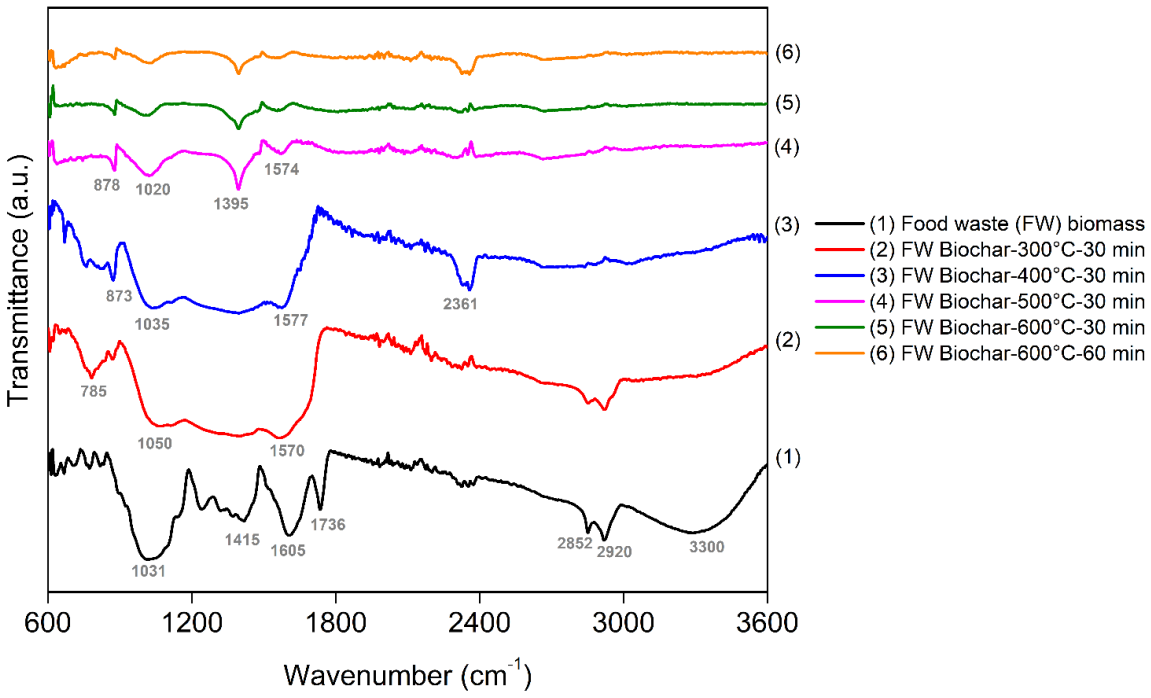

Fig. 4.6: FTIR spectroscopy of (a) food waste biomass and biochar and (b) bio-oil samples generated from pyrolysis at variable temperatures and reaction times and 5°C/min heating rate

4.5.7. Surface area and porosity analyses

Pyrolysis temperature and time also affected the physical properties of biochar. The biochar samples showed an increasing trend in surface area and total pore volume with the rising pyrolysis temperature (Table 4.4). For instance, at a constant 30 min reaction time and 5°C/min heating rate, the BET surface area of food waste-derived biochar amplified with the variation in temperature as follows: 300 °C (0.85 m^2/g) < 400 °C (2.18 m^2/g) < 500 °C (2.87 m^2/g) < 600 °C (4.35 m^2/g). The BET surface area was highest (4.91 m^2/g) in food waste biochar produced at the pyrolysis conditions of 600 °C, 60 min and 5 °C/min. Depending upon the adsorption capacities of biochar, especially those generated at higher temperatures, it could be used for the removal of contaminants from wastewater, degraded soil and flue gases (Qian et al., 2015). Furthermore, it can also be used as feedstocks for the preparation of activated biochar.

Table 4.4: Surface area and porosity measurement for biochar generated from slow pyrolysis of food waste, canola hull and oat hull

Biochar sample	BET surface area (m^2/g)	Total pore volume (cm^3/g)
FW Biochar-300 °C-30 min	0.85	0.002
FW Biochar-400 °C-30 min	2.18	0.002
FW Biochar-500 °C-30 min	2.87	0.003
FW Biochar-600 °C-30 min	4.35	0.007
FW Biochar-600 °C-60 min	4.91	0.009

4.5.8. Scanning Electron Microscopy

High temperatures result in thermal cracking reactions, including dehydration, devolatilization, decarboxylation, deamination and aromatization (Nanda et al., 2016 WBV). These reactions result in the removal of hydrogen, oxygen and nitrogen-containing functional groups and improvement in carbon-containing groups. These reactions render porosity, fragmentation, surface disintegration of biochar while improving its thermal stability. This phenomenon is well illustrated from these SEM images of food waste-derived biochar generated at 300 °C and 600 °C (Fig.4.7). The surface morphology of food waste biomass seems more uniform when compared to its biochar samples. Moreover, biochar generated at 600 °C showed more cracked, disoriented and fragmented morphology when compared to biochar produced at 300 °C.

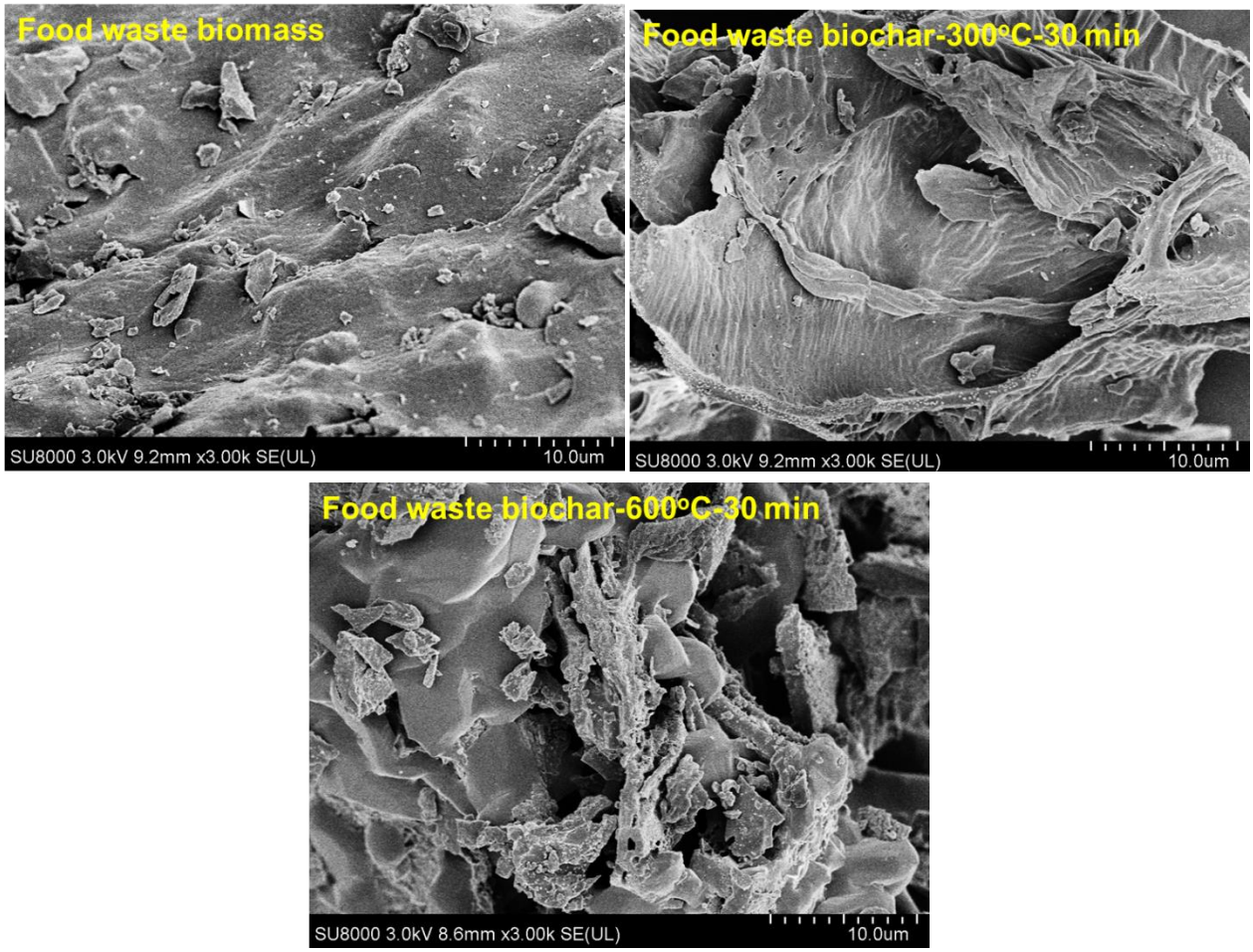

Fig. 4.7: SEM images of food waste biomass and biochar generated from pyrolysis at variable temperatures

4.6. Analysis of bio-oil and product gases

4.6.1. Ultimate analysis for bio-oil

Table 4.5 shows the ultimate composition of the organic phase of bio-oil generated from agro-food residues. The carbon content of food waste-derived bio-oil increased with the rise in pyrolysis temperature and reaction time as follows: 300 °C-30 min (57.6 wt%) < 400 °C-30 min (61 wt%) < 500 °C-30 min (63.5 wt%) < 600 °C-30 min (65.5 wt%) < 600 °C-60 min (66.9 wt%). The hydrogen contents also increased with pyrolysis temperature because of a greater degree of cross-linking and the development of higher molecular weight compounds (Nanda et al., 2014 BR). Like hydrogen and carbon contents, the levels of nitrogen also increased in food waste-derived bio-oils produced at elevated temperatures. Nitrogen in food waste arises from proteins, amino acids and fatty acids. Due to significant levels of nitrogen and oxygen in the bio-oils, it can become imperative to implement catalytic hydrodenitrogenation and hydrodeoxygenation as bio-oil upgrading techniques for the removal of such heteroatoms (Hansen et al., 2020). The HHV of food waste-derived bio-oil showed a rising trend from 23.5 MJ/kg at 300 °C to 31.3 MJ/kg at 600 °C in 30 min. The bio-oil produced from food waste at 600 °C in 60 min exhibited an HHV of 32.4 MJ/kg. At the same optimal conditions, bio-oil derived from canola hull and oat hull revealed HHVs of 21.4 and 29.7 MJ/kg, respectively.

Table 4.5: Ultimate analysis of bio-oil (organic phase) generated from slow pyrolysis of food waste

Bio-oil sample	C (wt%)	H (wt%)	N (wt%)	S (wt%)	O (wt%)	HHV (MJ/kg)
FW Bio-oil-300 °C-30 min	57.6	5.5	4.3	0.1	32.5	23.5
FW Bio-oil-400 °C-30 min	61.0	7.7	5.4	0.3	25.6	27.2
FW Bio-oil-500 °C-30 min	63.5	8.1	5.6	0.1	22.7	29.2
FW Bio-oil-600 °C-30 min	65.5	8.8	6.0	0.2	19.5	31.3
FW Bio-oil-600 °C-60 min	66.9	8.9	6.2	0.3	17.7	32.4
CH Bio-oil-600 °C-60 min	51.3	6.9	4.7	0.4	36.7	21.4
OH Bio-oil-600 °C-60 min	72.9	4.6	1.6	0.2	20.7	29.7

Note: The date presented are average of triplicate measurements with a standard error less than 3%.

4.6.2. Fourier transform infrared spectroscopy for bio-oil

Fig. 4.8 shows the FTIR spectral bands of the organic phase of food waste bio-oil produced by slow pyrolysis at different temperatures and reaction times. Unlike biomass and biochar, the spectra of bio-oil samples resembled each other with a few dissimilarities. For example, the bands at 2852, 2920 and 2960 cm^{-1} ascribed to C−H groups indicating the presence of methylene and methyl groups (Aboulkas et al., 2017). The spectral band identified at 3300 cm^{-1} indicated the existence of water, carboxylic acids, phenolics and alcohols. The peak at a wavenumber of 1708 cm^{-1} was ascribed to C=O groups signifying the existence of ketones, esters, aldehydes and carboxylic acids (David et al., 2018). The peaks at 1375, 1456, and 1555 cm^{-1} were attributed to C−H vibrations indicating alkanes (Mishra et al., 2020). The peak identified at 1046 cm^{-1} attributed to C−O indicating alcohol and phenolic compounds appeared for bio-oils produced at higher temperatures (i.e., 500-600 °C) (Zhang et al., 2018). The bands at 650 and 749 cm^{-1} indicated the occurrence of aromatic compounds in bio-oil samples (Mishra et al., 2020).

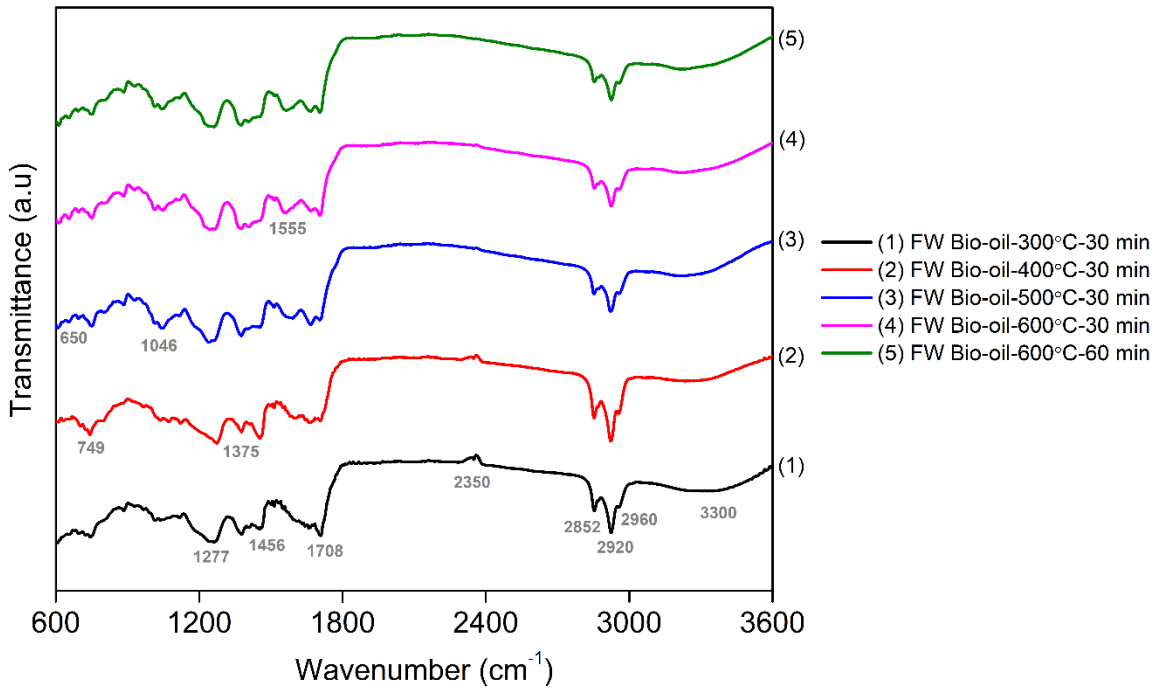

Fig. 4.8: FTIR spectroscopy of bio-oil samples generated from pyrolysis at variable temperatures and reaction times and 5°C/min heating rate

4.6.3. Gas chromatography-mass spectrometry for bio-oil

The bio-oil is generally considered as a complex blend of different chemical compounds such as phenolics, sugars, alcohols, carboxylic acids, esters, aldehydes, ketones and ethers (Kelkar et al., 2014). Moreover, the compounds found in bio-oil can be categorized into aliphatics, monoaromatics, polyaromatics and nitrogenates (Nanda et al., 2014 BR). The complexity of temperature-dependent reactions in pyrolysis such as decomposition, fragmentation and repolymerization result in a wide variety of organic compounds in bio-oils. Table 4.6 and Table 4.7 summarize the list of some notable compounds found in the organic phase of food waste-derived bio-oil generated at 300 °C and 600 °C in 30 min. The identified compounds of the organic phase with relative areas greater than 1% are reported in these tables. Bio-oil produced at 300 °C revealed octadecanoic acid; ricinoleic acid; 3,5-dimethyl cyclohexanone; 1,2,4-trimethyl benzene; 2-ethylhexanol; nonane; 1,2-dimethyl cyclohexane and hexadecanoic acid, methyl ester, oxacyclododecan-2-one and 3,5-dimethyl-cyclohexanone, to name a few major components (Table 4.6).

Table 4.6: Major organic compounds identified through GC-MS analysis of bio-oil (organic phase) generated from pyrolysis of food waste at 300 °C, 5 °C/min and 30 min of reaction time

Compound	Relative area (%)	Retention time (min)
2,2,6,6-tetramethyl-4-piperidinone	1.8	8.7
2-methyl-phenol	1.9	7.3
Hydrocortisone acetate	2.2	41.9
2,3-dimethyl-phenol	2.2	9.7
3-methyl-phenol	2.5	7.9
Ethyl-cyclohexane	2.5	2.4
Decane	2.5	2.9
3-ethyl-phenol	3.2	10.3
3,5-dimethyl-cyclohexanone	3.2	2.3
(Z)-9-Hexadecen-1-ol	3.4	30.0
3,5-dimethyl-cyclohexanone	3.5	2.4
Oxacyclododecan-2-one	3.9	6.0
Hexadecanoic acid, methyl ester	4.2	27.1
1,2-dimethyl cyclohexane	4.3	3.3
Nonane	4.3	3.5
2-ethylhexanol	4.4	3.0
1,2,4-trimethyl benzene	4.5	5.5
3,5-dimethyl cyclohexanone	5.1	2.6
Ricinoleic acid	5.6	30.1
Octadecanoic acid	6.5	27.7

Table 4.7: Major organic compounds identified through GC-MS analysis of bio-oil (organic phase) generated from pyrolysis of food waste at 600 °C, 5 °C/min and 30 min of reaction time

Compound	Relative area (%)	Retention time (min)
1,2-dimethyl-cyclohexane	1.9	3.2
Nonane	1.8	3.5
9-Octadecenoic acid (Z)-, methyl ester	2.0	29.5
Pentadecane	2.1	18.6
3,5-dimethyl cyclohexanone	2.1	2.6
2-methyl phenol	2.2	7.3
Hydrocortisone acetate	2.3	41.9
2,3-dimethyl phenol	2.3	9.8
Heptadecane	2.4	23.1
2,2,6,6-tetramethyl 4-piperidinone	2.4	8.7
Indole	2.5	13.4
Hexadecanoic acid, methyl ester	2.6	27.1
3-ethyl phenol	3.1	10.3
3-methyl phenol	3.1	7.9
Phenol	4.4	5.5
(Z)-9-Hexadecen-1-ol	5.6	30.0
Gibberellic acid	7.0	17.7
Digitoxin	7.1	26.6
Ricinoleic acid	8.0	30.1
Octadecanoic acid	8.1	27.7

On the contrary, the bio-oil produced at 600 °C predominantly contained octadecanoic acid; ricinoleic acid; digitoxin; gibberellic acid; (Z)-9-hexadecen-1-ol; phenol; 3-methyl phenol; 3-ethyl phenol; hexadecanoic acid, methyl ester and indole (Table 4.7). The observations agreed with the literature (Mishra et al., 2020). In this study, the bio-oil generated at a higher temperature (i.e., 600 °C) contained greater levels of acids, alcohols and phenols (Mishra et al., 2020; Tomczyk et al., 2020).

Hexadecanoic acid and octadecanoic acid found in food waste-derived bio-oil find application in the manufacturing of soaps, detergents and cosmetic products, while phenols can be used to produce plastics, cosmetics and disinfectants (Mishra et al., 2020). Furthermore, ricinoleic acid can be used in pigment and textile finishing (Schio et al., 2019). The presence of compounds like ethers, esters and ketones in the bio-oil can impact the fuel quality meant for transportation purposes, thus requiring further upgrading. Several technologies can be applied to recovery the

value-added components from the aqueous and organic phases of bio-oil. Examples include fractional distillation, column chromatography, solvent extraction, membrane separation, ionic liquid separation and supercritical CO_2 extraction (Feng and Meier 2017; Chan et al., 2018; Cesari et al., 2019; Tao et al., 2020).

4.6.4. Gaschromatography for gases

Fig. 4.9 illustrates the temperature effects on the composition of gases released from the pyrolysis of food waste at a steady heating rate and reaction time of 5 °C/min and 30 min, respectively. It was observed that CO_2 and CO were the major gases compared to other permanent gases. Cellulose and hemicellulose degradation in the primary stages of pyrolysis results in the generation of CO_2 and CO, whereas at elevated temperature, slower degradation of lignin contributes to the release of CH_4 and H_2 (Chen et al., 2014). Therefore, with the rising pyrolysis temperature, the yield of CO_2 decreased significantly from 35.7 vol% at 300 °C to 15.8 vol% at 600 °C. It was also observed that the concentration of CO steadily increased from 4 vol% at 300 °C to 9.7 vol% at 600 °C. Similarly, the yields of CH_4 and H_2 increased notably with the rise in pyrolysis temperature, i.e., up to 4.1 vol% and 0.9 vol% at 600 °C, respectively. The increase in CH_4 concentration in the gaseous product with rising temperature indicated the release of methoxy groups, which involves the rupture of C–C bonds and lignin decomposition (Chen et al., 2016). The hydrogenation of CO_2 and CO induces the formation of C_{2+} hydrocarbons in the gaseous stream with the highest yield (2.6 vol%) recorded at 500 °C. Chen et al. (2016) also found a decreasing trend in C_{2+} hydrocarbons and CO_2 yield with the increasing pyrolysis temperature after 500 °C. The HHV of different gas phases obtained from slow pyrolysis of food waste at variable temperatures diverged as: 300 °C (1.1 MJ/Nm^3) < 400 °C (5.6 MJ/Nm^3) < 500 °C (7.8 MJ/Nm^3) < 600 °C (8.4 MJ/Nm^3). The increasing HHV of the gases resulted due to the increase of concentration of H_2 and CH_4 with the increasing pyrolysis temperature.

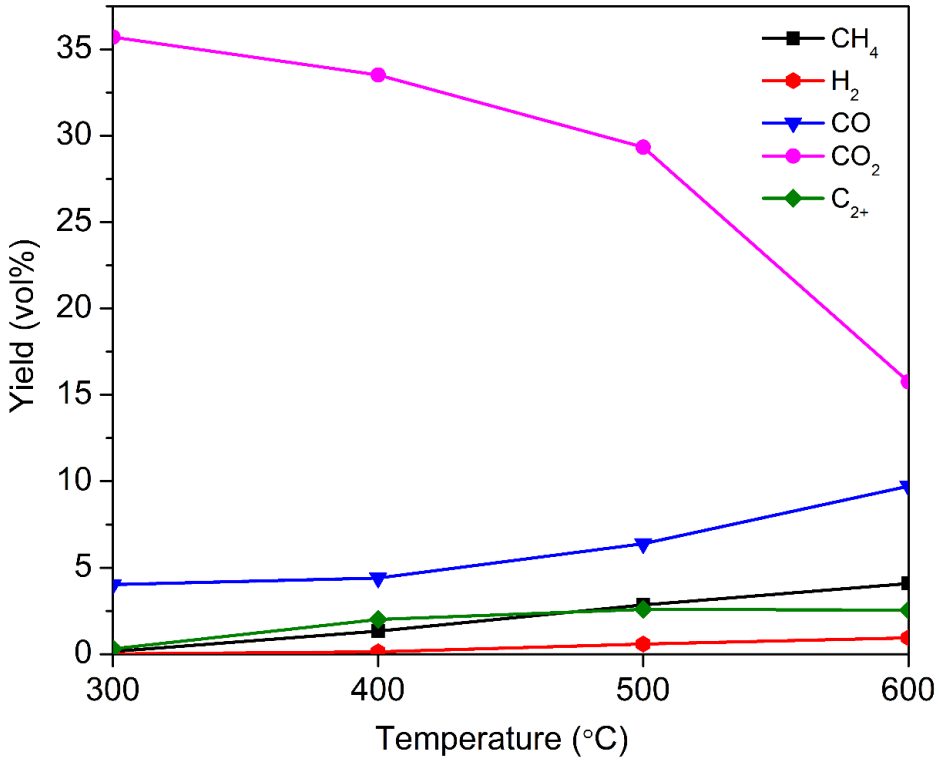

Fig. 4.9: Gas yields from pyrolysis of food waste at variable temperatures for 30 min of reaction time and 5 °C/min heating rate

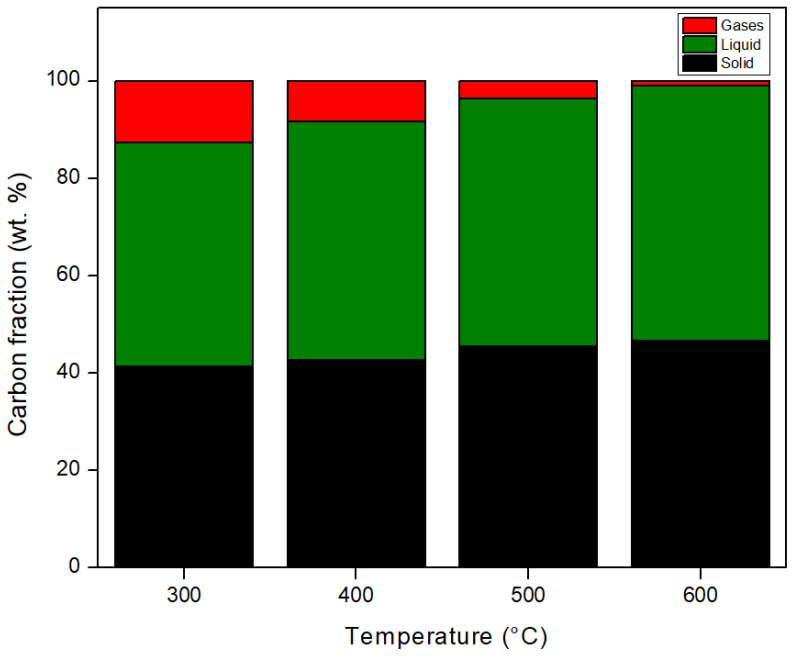

Fig. 4.10: Carbon balance of products obtained from slow pyrolysis of food waste (temperature: 300-600 °C, residence time: 30 min, heating rate: 5 °C /min)

The carbon balance for the slow pyrolysis of food waste products at a temperature range of 300 - 600 °C, a heating rate of 5 °C/min and a residence time of 30 min is presented in Fig. 4.10. With rising temperature the carbon content in all three products increased. About 41-46 wt.% of carbon in the feedstock was retained or fixed in the biochar, indicating high degree of carbonization of biochar. Similarly, the carbon content of bio-oil was found in the range of 46-52 wt.%. The lowest carbon content was found to be in gaseous product.

4.7. Conclusions

This study described the investigation of process conditions such as temperature, reaction time and heating rate for slow pyrolysis of food waste, canola hull and oat hull. Maximum biochar yield (52.4 wt%) from food waste was reported at lower temperatures (300 °C), shorter reaction time (30 min) and slower heating rate (5 °C/min). Although biochar produced from slow pyrolysis of food waste at 300 °C with 5 °C/min in 30 min resulted in the highest yields (52 wt%), it had the lowest carbon content (51.7 wt%), inferior HHV (20.6 MJ/kg), lowest surface area (0.85 m^2/g), lowest aromatic-vinylic content (12%), slightly alkaline pH (7.9) and lowest electrical conductivity (4.3 mS/s). On the contrary, biochar produced from food waste at 600 °C with 5 °C/min in 60 min resulted in the lower yields (28 wt%) while demonstrating greater carbon content (60.7 wt%), superior HHV (23 MJ/kg), highest surface area (4.91 m^2/g), maximum aromatic-vinylic content (66.3%), alkaline pH (11.2), highest electrical conductivity (8.7 mS/s) and enhanced thermal stability. These physicochemical features of biochar produced at 600 °C in 60 min are beneficial for its application as an adsorbent, catalyst support, soil amendment agent or precursor for activated carbon.

Oat hull biochar (26.8 MJ/kg) revealed comparatively greater HHV than that of canola hull biochar (25.6 MJ/kg) and food waste biochar (23 MJ/kg) obtained at 600 °C and 60 min (i.e., optimized slow pyrolysis conditions). Besides, the bio-oil produced at elevated temperatures (600 °C) was enriched with acids, alcohols and phenols. The gaseous product obtained at 600 °C also showed greater yields of CH_4 and H_2 with an HHV of 8.4 MJ/Nm^3. The findings suggest that food waste, canola hull and oat hull could be used as potential feedstocks for slow pyrolysis to produce high-value biochar for environmental applications as well as bio-oil and pyro-gas for energy and fuel applications.

CHAPTER 5: PROCESS OPTIMIZATION FOR ACTIVATION OF AGRO-FOOD WASTE BIOCHAR AND PERFORMANCE TEST FOR DYE ADSORPTION

Most of the content of this chapter has been submitted as a research article:

Biswa R. Patra, Sonil Nanda, Ajay K. Dalai, and Venkatesh Meda, 2021. Process optimization of agro-food waste biochar and performance test using dye adsorption (Accepted for publication in Chemosphere, May, 2021). DOI:https://doi.org/10.1016/j.chemosphere.2021.131531

Contribution of the M.Sc. candidate:

Activation, Taguchi design, physicochemical characterization, testing of the materials and data analysis were carried out by Biswa Ranjan Patra. The reactor setup was modified by Biswa Ranjan Patra and Dr. Sonil Nanda. Biswa Ranjan Patra wrote the manuscript. Experimental planning, data analyses and correction of the manuscripts were supervised by Drs. Ajay Dalai, Venkatesh Meda and Sonil Nanda.

Contribution of this chapter in the overall M.Sc. Work:

This phase of the research work was focused on Taguchi optimization of activation process parameters for the generation of activated carbon using pyrolyzed food waste and agricultural residues like canola hull and oat hull biochar as a precursor. The study also intended for the biochar and activated carbon performance tests for dye adsorption using model wastewater.

5.1. Abstract

5. Abstract:

The optimization of process parameters for biochar activation is crucial for enhancing its surface area and adsorption capacity. This work attempts to investigate the influence of activating agent (e.g., steam and KOH), temperature (700-900 °C) and activation time (60-120 min) using Taguchi L_{18} ($2^1 \times 3^2$) experimental design for the activation of biochar derived from food waste and agricultural crop residues such as canola hull and oat hull. Among all the factors, activating agent and temperature influenced surface area considerably. KOH-assisted chemical activation of biochar at 800 °C for 90 min was found to be optimal with higher specific surface areas of 1760, 1718, and 1334 m^2/g for food waste, canola hull and oat hull derived biochar, respectively. Finally,

the comparative evaluations of the performances of biochar and activated carbon samples were carried out through the adsorption of common dyes such as methylene blue, methyl violet and Rhodamine B. Food waste and canola hull derived activated carbon exhibited a complete removal of methylene blue and methyl violet from model aqueous solution within 1-2 h of contact time at room temperature, where as in case of Rhodamine B only 91-94% removal was achieved.

5.2. Introduction

The increasing human population, excessive usage of fossil fuels and synthetic recalcitrant chemicals have induced the deterioration of the environment. Many complex and robust pollutants from domestic and industrial activities are directly or indirectly discharged into water bodies. Dyes are one of such pollutants that are extensively used in textile, fabric, pharmaceutical, plastics, pulp and paper, printing and food industries. The discharged dyes contain highly toxic compounds, acids, organics, bases and other impurities, which poses many adverse effects on the natural habitats and metabolism of the living organisms in soil and water (Omer et al., 2018).

Water is an essential commodity for all known forms of life. Therefore, significant research is being continually conducted to annihilate the detrimental effects of dyes from wastewater (Abidi et al., 2015; Omer et al., 2018). The conventional wastewater treatment for removal of dyes includes biological methods (e.g., anaerobic and aerobic digestion), physical methods (e.g., sedimentation, coagulation, filtration, ion exchange, adsorption, and reverse osmosis) and chemical methods (e.g., oxidation, ozonation, photochemical and electrochemical degradation) (Katheresan et al., 2018; Crini and Lichtfouse 2018). Activated carbon is considered an advanced treatment method to treat wastewater and sequester specific pollutants such as dyes (Wang et al., 2018; Baysal et al., 2018; Shen and Fu, 2018; Liu et al., 2019; Singh et al., 2021). Activated char or carbon is a highly porous carbonaceous material derived via physical or chemical activation. The physical activation involves carbonization of biochar or biomass, usually at 800-1100 °C under an inert atmosphere in the presence of oxidizing agents such as steam, CO_2 or air (Hesas et al., 2015; Nanda et al., 2016). In contrast, the chemical activation process involves the activation of carbonized biochar or biomass typically at 450-900 °C with impregnation of a chemical or dehydrating agent such as KOH, K_2CO_3, NaOH, Na_2CO_3, $AlCl_3$, $ZnCl_2$, $MgCl_2$ and H_3PO_4 (Nanda

et al., 2016). In contrast to other chemical activating agents, KOH has been extensively used for obtaining activated carbon with higher specific surface area (up to 3000 m^2/g) and effective in the removal of organic and inorganic contaminants from wastewater (Choma et al. 2015; Li et al. 2017; Liu et al. 2019).

The worldwide market size of activated carbon reached U.S.$ 3.93 billion in 2020, with an estimation to reach U.S.$ 6.24 billion by 2026 (Expert Market Research, 2020). The commercial production of activated carbon is inclined towards renewable feedstocks such as lignocellulosic biomass by limiting the use of fossil-based carbon, e.g., coal and petroleum coke (Nanda et al., 2016b). The use of lignocellulosic biomass to produce biochar and activated carbon entails lower production cost, high fixed carbon content, greater energy efficiency, carbon neutrality and carbon sequestration (Kang et al., 2020). A wide variety of renewable waste is available as precursors to produce biochar and activated carbon such as woody biomass, agricultural crop residues, food waste, municipal solid waste and cattle manure (Nanda et al., 2016a, 2016b). Thermochemical conversion of food waste and agricultural biomass to biochar and activated carbon can be considered an effective valorization method to alleviate the disposal challenges while reducing greenhouse gas emissions from their natural decomposition in landfills or open burning.

The physicochemical and structural properties, including porosity, thermal stability and carbon of activated carbon, are largely dependent on the activation process parameters such as activating agent, temperature, time and reactor geometry (Heidarinejad et al., 2020). Therefore, the optimization of such parameters is crucial to prepare high-quality activated carbon for a wide variety of industrial and environmental applications. However, the optimization of process parameters and understanding their correlation could be tedious and time-consuming due to the excessive number of experiments (Moralı et al., 2018). In contrast, the design of experiments (DOE) method is effective when compared to the conventional experimental approaches (Loredo-Cancino et al., 2013). The inclusion of the Taguchi design approach utilizes the orthogonal array, which could expedite the process by eliminating the redundant set of experiments (Moralı et al., 2018). It also provides detailed information about the interaction of the factors that influence the response variable. Furthermore, in DOE, the selection of the best level for each factor is made based on the response table.

In this study, biochar derived from the slow pyrolysis of food waste and agricultural residues (e.g., canola hull and oat hull) were used as the precursors to optimize the process parameters for physical and chemical activation. The optimization of the process parameters such as activation temperature and time was performed using the L_{18} array-based Taguchi DOE method. The resulting activated carbon along with their biochar precursors were comparatively evaluated to study their kinetics for adsorption of dyes such as methylene blue, methyl violet and Rhodamine B.

5.3 Experimental Methodology

5.3.1 Proximate and ultimate analysis

The contents of ash, moisture, fixed carbon and volatile matter in activated carbon samples were measured by following ASTM methods (ASTM E871-82; ASTM E1755-01; ASTM D3175-11). Please refer to Section 3.6.1 for a detailed procedure.

5.3.2 Surface area and porosity analyses

Brunauer-Emmett-Teller (BET) and Barret-Joyner-Halenda (BJH) analyses were done using Micromeritics ASAP 2020 apparatus (Micromeritics Instrument Corporation, Norcross, USA). Please refer to Section 3.6.6 for a detailed procedure.

5.3.3 Scanning electron microscopy (SEM)

SEM imaging of biomass and biochar samples was acquired via a Hitachi SU8010 SEM (Hitachi High-Technologies Corporation, Tokyo, Japan). Please refer to Section 3.6.7 for a detailed procedure.

5.3.4 Adsorption of dyes

The adsorptive performance was studied for the activated carbon samples derived from food waste and agricultural biomass along with their biochar precursors and a commercial activated carbon. UV-Visible spectrophotometer (GENESYS 50, Thermo Fisher Scientific, Waltham, USA) was utilized to determine the concentration of the dye in model wastewater. Please refer to Section 3.7 for a detailed procedure.

5.4. Results and Discussion

5.4.1. Parametric studies

In the present study, biochar samples generated from food waste and agricultural crop residues (e.g., canola hull and oat hull) were used as precursors for activated carbon through physical and chemical activation processes. In a parallel study, biochar samples were produced from the slow pyrolysis of food waste, canola hull and oat hull at optimal temperature, reaction time and heating rate of 600 °C, 60 min and 5 °C/min, respectively based on their greater carbon content (61-67 wt.%). However, the work in this phase is primarily focused on the optimization of the physical and chemical activation of biochar generated from food waste, canola hull and oat hull. The optimization of physical (steam) and chemical (KOH) activation of biochar samples were performed at different temperatures (i.e., 700-900 °C) and activation time (i.e., 60-120 min) using the L_{18} ($2^1 \times 3^2$) Taguchi design method.

The BET surface area (response), total pore volume, pore size and yield obtained at different process conditions is summarized in Table 5.1. It should be noted that the arrangement of the process conditions and their corresponding levels is based on the L_{18} Taguchi design. As illustrated in Table 5.1, keeping all other parameters constant. The increase in the temperature favoured a larger specific surface area in the activated carbon samples while reducing their yield. The increase in the activation temperature boosted the reaction between carbon and potassium compounds, which resulted in the development of the porous sturcture. In steam activation with increasing temperature, the porosity increases as the steam penetrates the internal structure of the biochar and reacts with the unstable carbon to open and widen the unreachable pores by releasing hydrogen and carbon monoxide (Rambabu et al., 2015). Similarly, the use of KOH as an activating agent produced activated carbon with improved surface area. The impregnated KOH at high temperature dehydrates and gets converted into K_2O, and further reduction of K_2O results in elemental potassium. In addition, the series of reactions involved in KOH activation results in several potassium compounds like K, K_2O, and K_2CO_3. The resulting free potassium after penetrating graphene carbon layers leads to the structural graphene layers expansion. Thus, the free metal at high temperatures gets eliminated from the graphene layer by developing a porous structure in the activated carbon (Heidarinejad et al., 2020). Furthermore, the produced activated carbon was subjected to acid wash with 0.1N HCl for the complete elimination of residual K, K_2O and, K_2CO_3,

which makes the pore structure available and further enhanced the surface area. The main effects plots showing the relationship between the surface area of the activated carbon and the process conditions are illustrated in Fig. 5.1. As shown in Fig. 5.1, increasing the reaction temperature led to a positive impact on the surface area of the activated carbon samples.Specifically, when the activation temperature increased from 700 °C to 800 °C, the specific surface area elevated by around 40% (1323-1723 m^2/g). A further increment in temperature to 900 °C caused a slight decline in the specific surface area of the activated carbon samples to 1407 m^2/g. Therefore, the optimal activation temperature based on a higher specific surface area was determined as 800 °C. A decrease in the surface area could be attributed to the weakening of the pore walls and its collapse at higher activation temperatures (Lan et al., 2019).

The activation time also demonstrated a similar trend with activation temperature. In certain cases, a rise in the activation time from 60 min to 120 min resulted in a higher BET surface area at 90 min followed by a decline in 120 min (Table 5.1). With the increase in activation time, a significant improvement in the BET surface area and total pore volume was observed (Fig. 5.1). However, a prolonged activation time of 120 min resulted in a further decrease of the surface area of the activated carbon. The decreasing pattern of the surface area can be correlated to the collapse of the thin pore wall in the biochar (Lan et al., 2019).

The exposure of char in the presence of KOH to 900 °C resulted in a drastic decrease in its surface area from 1820 m^2/g at 60 min to 1407 m^2/g at 120 min with a widening of the pore size (Table 5.1). The prolonged exposure of char at extreme tempearure resulted in collapse of pore walls and formation of ash, which blocks the available pores (Li et al., 2017).The yield of KOH-activated carbon decreased from 62.4 wt.% to 40.3 wt.% with the rising activation temperature (from 700 °C to 900 °C) and time (from 60 min to 120 min). The decrease in yield resulted because of increasing temperature and acid washing, which eliminated the remaining potassium and other inorganic compounds present in the activated carbon. KOH acts as a dehydrating agent during activation by hindering the tar formation on the char surface and improving its surface area (Azargohar and Dalai, 2008; Li et al., 2015). The activated carbon samples obtained from oat hull biochar and canola hull biochar because of KOH activation at the optimized conditions (i.e., 800

°C, 90 min and 3 °C/min) resulted in the BET surface areas of 1334 m^2/g and 1718 m^2/g, respectively.

Table 5.1 Porous characteristics of the food waste derived activated carbon

Activating agent	Temperature (°C)	Activation time (min)	Specific surface area (m^2/g)	Total pore volume (cm^3/g)	Average pore size (nm)	Yield (wt.%)
KOH	700	60	1323	0.67	4.8	62.4
KOH	700	90	1447	0.74	4.1	58.5
KOH	700	120	1398	0.71	4.6	53.8
KOH	800	60	1489	0.75	4.1	52.6
KOH	800	90	1760	0.94	3.7	48.8
KOH	800	120	1723	0.91	3.9	41.4
KOH	900	60	1820	0.95	3.4	50.2
KOH	900	90	1681	0.93	3.8	43.6
KOH	900	120	1407	0.76	3.9	40.3
Steam	700	60	101	0.06	9.1	71.4
Steam	700	90	214	0.11	7.7	63.1
Steam	700	120	262	0.14	5.8	58.7
Steam	800	60	275	0.15	5.2	61.2
Steam	800	90	385	0.28	4.6	54.1
Steam	800	120	529	0.38	3.8	49.3
Steam	900	60	406	0.31	4.2	47.8
Steam	900	90	421	0.32	4.1	43.5
Steam	900	120	348	0.22	4.8	37.4

Note: The data presented are average of triplicate measurements with standard error < 3%.

Rambabu et al. (2015) used both steam and KOH to activate canola meal and observed a similar trend of decreasing surface area and pore volume at higher activation temperature and time. Furthermore, the yield of the activated carbon decreased from 71 wt.% to 37 wt.% with the rising activation temperature from 700 °C to 900 °C. The decrease in yield is related to the propitious impact of temperature on the specific surface area of the activated carbon, which causes the

elimination of volatile compounds by enhancing its porosity. Furthermore, the reduction in yield could also result from ash formation at higher temperatures (Azargohar and Dalai, 2008).

In steam-assisted physical activation of food waste biochar, the porous structure development was observed as the steam penetrated the biochar's internal matrix. The high-temperature steam reacted with the unstable carbon in the biochar to open and widen the unreachable pores by releasing H_2 and CO (Rambabu et al., 2015). The blocked pores initially open as micropores and further widen to mesopores and macropores (Azargohar and Dalai, 2008). The surface area and total pore volume for steam activated carbon increased from 101 m^2/g to 529 m^2/g and 0.06 cm^3/g to 0.38 cm^3/g at 700 °C and 60 min as well as 800 °C and 120 min (Table 5.1). However, a sharp reduction of surface area was observed at 900 °C owing to the collapse of thin pore walls and ash formation (Rambabu et al., 2013). The ash content of activated carbon increased at high temperatures with a decrease in its yield (Nanda et al., 2017). Ash restricts further diffusion of activating carbon by blocking the pores (Valix et al., 2004).

The activation time also showed a significant effect in enhancing the surface area and yield of the activated carbon. In the case of steam activation at 800 °C, an increase in activation time from 60 min to 120 min resulted in the improvement of BET surface area from 275 m^2/g to 529 m^2/g, respectively (Table 5.1). Similarly, there was an upsurge in the pore volume of steam-activated carbon from 0.15 cm^3/g (in 60 min) to 0.38 cm^3/g (in 120 min) at 800 °C. At 900 °C, when the reaction time was increased for steam activation from 60 min to 90 min, the BET surface area showed an inclination from 406 m^2/g to 421 m^2/g after which it decreased to 348 m^2/g at 120 min. However, an increase in the pore size to 4.8 nm was observed. The extreme temperature with prolong time induced the reaction between steam and carbon, and furthermore allowed the penetration of steam into the pores of biochar by enabling the removal of volatile compounds. This resulted in increase in surface area to some extent (Chen et al., 2016). However, beyond a particular level, the extreme conditions resulted in collapse of pore walls causing a decrease in surface area (Lan et al., 2019).The steam activation of canola hull biochar and oat hull biochar at optimal conditions (i.e., 800 °C and 120 min) resulted in the BET surface areas of 733 m^2/g and 558 m^2/g, respectively.

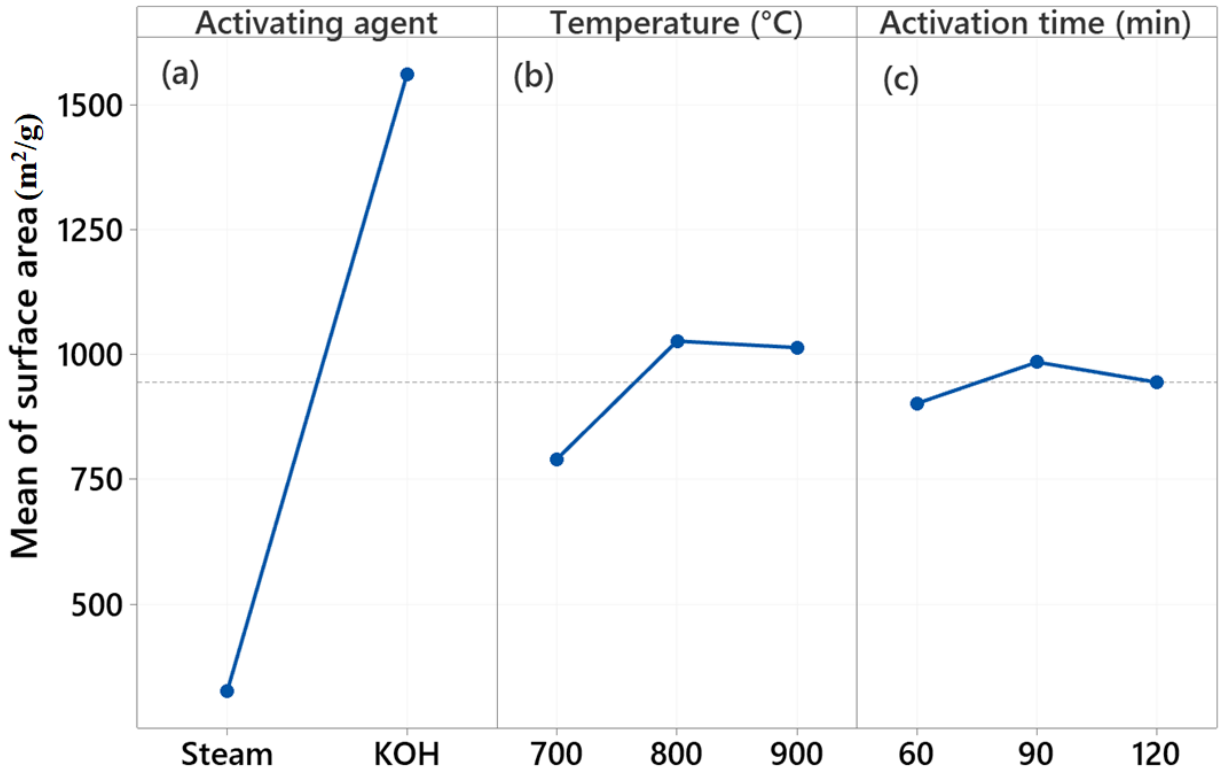

Fig. 5.1. Main effects plot showing BET surface area of the food waste based activated carbon as a function of reaction parameters: (a) activating agent, (b) temperature, (c) activation time

5.4.2 Interactive effects of process parameters on the surface area of activated carbon

Figure. 5.2 illustrates the interaction plot for means of surface area. The figure depicts the interaction of the process parameters like the activating agent, activation temperature and time. The "larger is better" option was considered for the DOE. A strong interaction between the activating agents (i.e., KOH and steam) with temperature is evident from the presented data. In contrast, the interaction between the activating agent and time was found to be weak. With the temperature rise, the response (i.e., BET surface area) recorded a drastic increase up to 800 °C, following which it was insignificant at 900 °C. Similarly, with the rise in the activation time up to 90 min, the surface area changed significantly, beyond which it decreased at 120 min. It was noticed that with rising temperatures, an increase in activation time also played a major role in

developing the porous structure of the activated carbon. However, beyond a particular activation time, a drastic reduction in surface area was noticed because of the breakdown of pore walls at a longer residence time at elevated temperatures. The declining trend of surface area was more significant at 900 °C with increasing activation time from 60 min to 120 min.

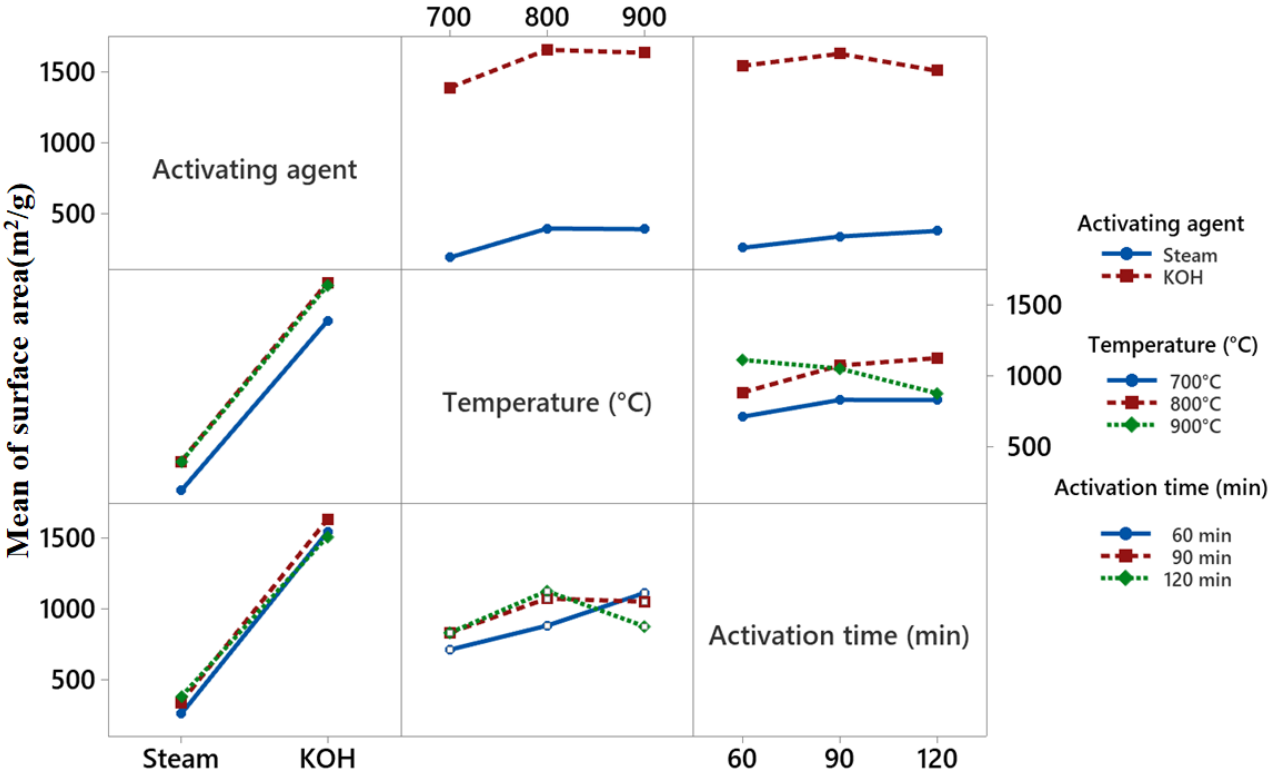

Fig. 5.2. Interactive effects plot between activating agent, temperature and activation time, and their impact on surface area of the activated carbon

5.4.3 Optimization of process parameters and confirmation of experimental results

The optimization of activation conditions is highly essential to obtain activated carbon with higher surface area and porosity. To make a process efficient and economical, all the significant parameters should be at the optimum level. The optimum conditions in terms of higher BET surface area for this activation study using the Taguchi method were activating agent (i.e., KOH), activation temperature (800 °C) and activation time (90 min). Furthermore, the activation experiments were carried out thrice to validate the Taguchi experimental design at the optimum conditions. A comparison was made between the experimentally obtained surface area and the predicted surface area. The experimental value of BET surface area of food waste-derived

activated carbon using KOH at the aforementioned optimum conditions were found to be 1760 m^2/g, while the predicted value from the Taguchi model was 1730 m^2/g (Table 5.1). The difference between the experimental and predicted results is less than 5%, which indicates the predictive power of the model. Therefore, the selected model is efficient in predicting the optimum conditions of biochar activation (Canales-Flores and Prieto-García, 2020).

Food waste-derived activated carbon using KOH at optimum conditions (i.e., 800 °C and 90 min) was found to be highly porous with a total pore volume of 0.94 cm^3/g and average pore size of 3.7 nm (Table 5.1). Moreover, the yield of 48.8 wt.% was highly desirable. From the experiments, it was observed that the physical activation (using steam) was inferior when compared to chemical activation (using KOH) in enhancing the surface area of the activated carbon. The activation temperature also played an important role. A sharp increase in the specific surface area was observed with increasing temperature until 900 °C, beyond which a sharp reduction was recorded. At 900 °C and 60 min, the highest BET surface area of 1820 m^2/g was recorded, which undermines the optimum conditions predicted by the Taguchi model. However, to make the process more economical, lesser energy input is highly desirable, thus the model predicted using Taguchi design conditions are reasonable.

5.4.4 Model verification

The normal probability plot (see Appendix Fig. A3) was used to establish the normality of BET surface area obtained from activation of food waste at different activation temperatures and times. The figure shows the residuals plot versus their expected values at normal distribution. As shown in Fig. A3, all the data points arranged in a straight line indicating the normally distributed BET surface areas.

The impact of each factor and determination of the most prominent process parameters to enhance the surface of the activated carbon was evaluated by utilizing analysis of variance (ANOVA). It also includes the *F*-test (Fisher test) value, which helped in evaluating the efficacy of the chosen model and the influence of the process parameters in the resulting response. The statistical significance of each factor and its influence on the response was determined using the p-value set at a confidence interval of 95%. Moreover, the sequential sum of squares (Seq SS) is the sum of

the square between and within groups obtained for the designed model and individual process parameters to determine the influence of each parameter on the BET surface area. Furthermore, the mean squares were found by dividing the degree of freedom (DF) from the sum of squares. The higher values of the sum of squares and *F*-test value signify any parameter's relative importance on the response. Moreover, a p-value above 5% indicates that the parameter is not significant with respect to the response (Fernández-López et al., 2019).

The degree of freedom (DF = n–1) for each source is the number of total variable observations, while 'n' is the number of factors. In this study, a total of 17 DFs were used for the complete set of parameters. The sum of squares for the model (i.e., 7,255,860) was higher enough to be assessed as significant (Table 5.2). The *F*-test value for the model was found to be 1388, which further indicates the significance of the model. The parameters with less than 0.05 p-value were considered insignificant. The ANOVA results suggested that among all the parameters of interest, only activating agent and temperature affected the response substantially as their p-value was found to be less than 0.05. The activation time was found to have lesser impacts on the surface area of the activated carbon with a p-value of 0.24, which is above 0.05. The activating agent with an *F*-test value of 1388 was revealed to be the most significant parameter with a substantial influence on the BET surface area based on the p-value and the sum of squares values of 0 and 6,852,896, respectively. Moreover, all the interactive terms showed p-values greater than 0.05.

Table 5.2. ANOVA table for the food waste activated carbon sample prepared with different factors and levels

Source	**DF**	**Seq SS**	**Adj SS**	**Adj MS**	**F-test value**	**P-test value**
Activating agent	1	6,852,896	6,852,896	6,852,896	1,388	0
Temperature	2	211,288	211,288	105,644	21.39	0.007
Activation time	2	20,389	20,389	10,195	2.06	0.24
Activating agent*Temperature	2	3,291	3,291	1,646	0.33	0.74
Activating agent*Activation time	2	24,538	24,538	12,269	2.48	0.20
Temperature*Activation time	4	123,707	123,707	30,927	6.26	0.052
Residual Error	4	19,752	19,752	4,938	-	-
Total	17	7,255,860	-	-	-	-
S = 133.124 R-Sq = 96.58% R-Sq(adj) = 94.12%						
(DF= Degree of freedom, Seq SS = Sequential sums of squares, Adj SS= Adjusted sums of squares, Adj MS= Adjusted mean squares)						

The relative importance of each process parameter on the BET surface area was determined from the S/N ratio (Table 5.3). The relative effect of the operating parameters on the response obtained from the Delta statistical method was ranked as follows: activating agent > temperature > activation time. The correlation between the surface area (response) and operating conditions including the activating agent, activation temperature and time is shown in Eq. (5.1) and (5.2). The equations enable the prediction of new observations. Furthermore, the least-squares method was utilized to obtain each predictor's coefficient along with the constant term. The regression equations for both steam and KOH activation showed a positive value for the parameters (i.e.,

temperature and time). This also indicates that an increase in activation time and temperature could elevate the specific surface area of the activated carbon.

Table 5.3. Response table for signal-to-noise ratios (S/N) – larger is better

Level	Activating agent	Temperature (°C)	Activation Time (min)
1	327	791	902
2	1561	1027	985
3	-	1014	945
Delta	1234	236	82
Rank	1	2	3

Steam activation:

$$\text{Surface area } (\text{m}^2/\text{g}) = 628 + 1.115\ \text{Temperature } (°\text{C}) + 0.7\ \text{Activation time (min)} \quad (5.1)$$

$$\text{Yield } (wt.\%) = 119.1 - 0.078\ \text{Temperature } (°\text{C}) - 0.009\ \text{Surface area } (\text{m}^2/\text{g}) \quad (5.2)$$

KOH activation:

$$\text{Surface area } (\text{m}^2/\text{g}) = 606 + 1.115\ \text{Temperature}(°\text{C}) + 0.7\ \text{Activation time (min)} \quad (5.3)$$

$$\text{Yield } (wt.\%) = 126.2 - 0.078\ \text{Temperature } (°\text{C}) - 0.009\ \text{Surface area } (\text{m}^2/\text{g}) \quad (5.4)$$

The validity of the regression analysis is verified using the coefficient of determination (R^2) as well as the adjusted and predicted R^2. The adjusted R^2 is the value modified to account for different predictors in the model. On the contrary, the predicted value of R^2 helps to determine the strength of the equation for predicting new observations. R^2, adjusted and predicted R^2 values were found as 96.6%, 95.8% and 94.1%, respectively. High values of R^2 suggest that the model can predict accurate results for new observations.

5.5 Physicochemical properties of biochar and activated biochar samples

The proximate and ultimate analyses of biochar and activated carbon samples produced from food waste, canola hull and oat hull are tabulated in Table 5.4 and Table 5.5, respectively. Compared to the biochar precursors, the fixed carbon of activated carbon samples was relatively greater in the range of 84-91 wt.% (Table 5.4). In contrast, the non-activated biochar samples had a fixed carbon content in the range of 54-64 wt.%. The volatile matter, moisture and ash contents for the activated carbon at optimized conditions were in the range of 3-12 wt.%, 1-3 wt.%, 5-16 wt.%, respectively. On the other hand, non-activated biochar samples had relatively higher volatile matter, moisture and ash contents of 11-19 wt.%, 4-6 wt.%, 15-31 wt.%, respectively. Biomass usually contains high volatile and moisture contents, which are eliminated during torrefaction and the carbonization process to generate torrefied biomass and biochar (Nanda et al., 2013). However, a complete removal is difficult to attain because of the complex structure of the biomass, which entraps such compounds in it. With the release of volatile compounds, the concentration of inorganic constituents and alkali earth metals increases, inducing high ash content in biochar (Rafiq et al., 2016). In our study, different biochar samples derived via a slow pyrolysis process were used for generating activated carbon. The ash content of the activated carbon was found to be lower than their respective biochar. The reduction in ash content was mainly because of acid wash with diluted HCl (Valix et al., 2004). The influence of KOH as a chemical activation agent showed a strong impact on the densification of elemental carbon content in the resulting activated carbon samples produced from food waste biochar (89.6 wt.%), canola hull biochar (83.7 wt.%) and oat hull biochar (56.9 wt.%) (Table 5.5). On the contrary, steam-activated carbon produced from food waste biochar, canola hull biochar and oat hull biochar had carbon contents of 78.2 wt%, 76.4 wt% and 79.8 wt%, respectively. Activation of biochar results in the further removal of volatile compounds because of dealkylation, dehydration, decarboxylation, decarbonylation and deamination, and an increase in the carbon content by aromatization (Azargohar et al., 2014; Azargohar et al., 2019). Furthermore, the HHV values of activated carbon samples were found to be greater than their corresponding biochar precursors owing to the higher carbon and reduced oxygen contents. This correlation of HHV with atomic H/C and O/C ratios is illustrated through the Van Krevelen diagram (Fig. 5.3). Activated carbon samples generated through KOH activation (26.6-28.9 MJ/kg) had greater HHV than those produced by steam activation (24.6-26.3 MJ/kg). Compared to other biochar and activated carbon samples, food waste-derived activated carbon

demonstrated relatively higher HHV via KOH activation (28.9 MJ/kg) and steam activation (26.3 MJ/kg).

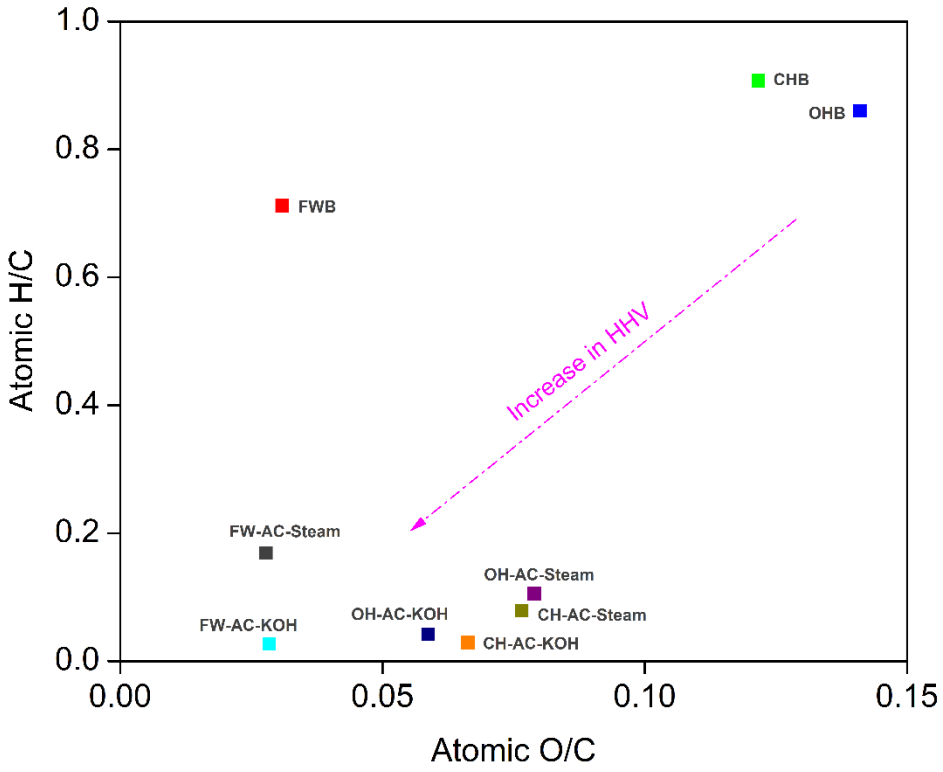

Fig. 5.3: Van Krevelen plot for the correlation of heating value and the atomic ratios of biochar and activated carbon samples. (Note: Activated carbon samples viz. FW-AC-KOH, CH-AC-KOH and OH-AC-KOH are produced at optimal KOH activation at 800 °C and 90 min. Activated carbon samples viz. FW-AC-Steam, CH-AC-Steam and OH-AC-Steam are produced at optimal steam activation at 800 °C and 120 min)

Fig. 5.4 depicts SEM images of food waste, canola hull and oat hull pyrolyzed biochar along with their corresponding KOH and steam activated carbon samples. It was observed that the biochar precursors retained relatively less fragmented morphologies and surface structure with underdeveloped pores compared to their resulting activated carbon samples. The activation of biochar using KOH induced the development of microporous structures with high surface area (Table 5.1). In contrast, steam-activated carbon showed less incidence of microporous structures.

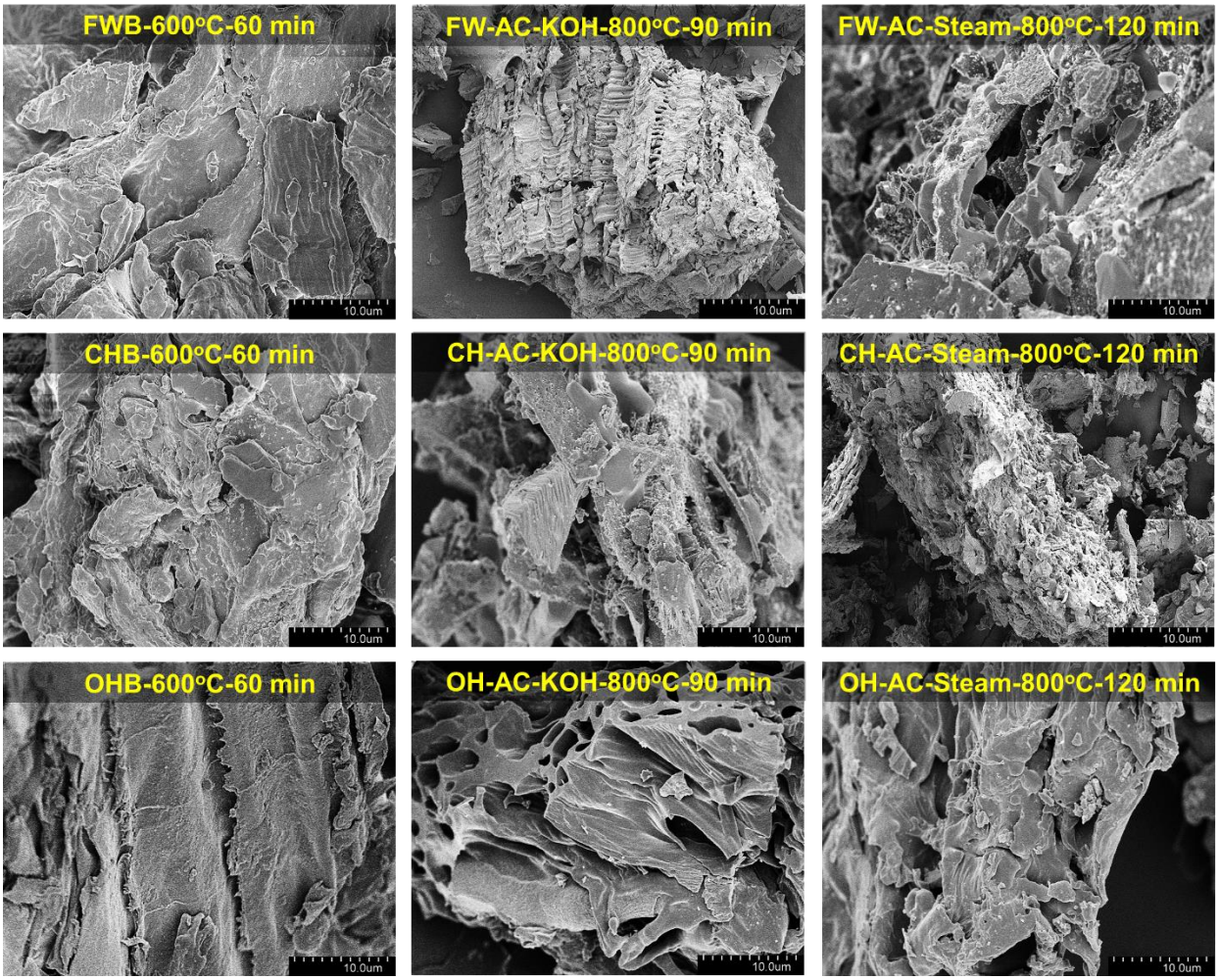

Fig. 5.4: SEM micrographs of biochar and activated carbon samples (Note: Activated carbon samples viz. FW-AC-KOH, CH-AC-KOH and OH-AC-KOH are produced at optimal KOH activation at 800 °C and 90 min. Activated carbon samples viz. FW-AC-Steam, CH-AC-Steam and OH-AC-Steam are produced at optimal steam activation at 800 °C and 120 min)

Table 5.4: Proximate analysis of biochar and activated carbon samples

Sample	Temperature (°C)	Activation time (min)	Moisture (wt.%)	Ash (wt.%)	Volatile matter (wt.%)	Fixed carbon (wt.%)
Food waste biochar	600	60	4.3	30.5	11.4	53.8
Canola hull biochar	600	60	5.7	17.4	18.7	58.2
Oat hull biochar	600	60	3.5	14.6	17.9	64.0
Food waste activated carbon (KOH activation)	800	90	2.9	5.6	4.7	86.8
Canola hull activated carbon (KOH activation)	800	90	2.2	7.6	5.8	84.4
Oat hull activated carbon (KOH activation)	800	90	1.1	4.9	3.4	90.6
Food waste activated carbon (Steam activation)	800	120	3.3	16.4	7.1	73.3
Canola hull activated carbon (Steam activation)	800	120	2.6	13.5	12.4	71.5
Oat hull activated carbon (Steam activation)	800	120	2.4	10.2	10.5	76.9

Note: The data presented are average of triplicate measurements with standard error < 3%.

Table 5.5: Ultimate analysis of biochar and activated carbon samples

Sample	Temperature (°C)	Activation time (min)	Carbon (wt.%)	Hydrogen (wt.%)	Nitrogen (wt.%)	Sulfur (wt.%)	Oxygen (wt.%)	HHV (MJ/kg)
Food waste biochar	600	60	60.7	3.6	2.2	0.5	2.5	23.0
Canola hull biochar	600	60	63.5	4.8	3.6	0.4	10.3	25.6
Oat hull biochar	600	60	67.0	4.8	0.7	0.3	12.6	26.8
Food waste activated carbon (KOH activation)	800	90	89.6	0.2	1.1	0.1	3.4	28.9
Canola hull activated carbon (KOH activation)	800	90	83.7	0.2	1.0	0.1	7.4	26.6
Oat hull activated carbon (KOH activation)	800	90	86.9	0.3	0.9	0.2	6.8	28.0
Food waste activated carbon (Steam activation)	800	120	78.2	1.1	1.3	0.1	2.9	26.3
Canola hull activated carbon (Steam activation)	800	120	76.4	0.5	1.6	0.2	7.8	24.6
Oat hull activated carbon (Steam activation)	800	120	79.8	0.7	0.8	0.1	8.4	26.1

Note: The data presented are average of triplicate measurements with standard error < 3%

5.6 Performance study of the biochar and activated carbon for the removal of dyes from model wastewater

The adsorption test for biochar and activated carbon derived from food waste, canola hull and oat hull as well as a commercial activated carbon (CAC), were studied using adsorption of industrial dyes as model pollutants. Fig. 5.5 illustrates the percentage removal of model pollutants such as methylene blue, methyl violet and Rhodamine B at different time intervals. It was observed that the contact time played an immense role in the adsorption of dyes onto biochar and activated carbon, and adsorption increased with the contact time until an equilibrium was reached. After a certain point of time, further adsorption was seized with an almost constant value where the adsorbed dyes from the aqueous solution attained the state of dynamic equilibrium. The adsorption of dyes onto the adsorbent undergoes different steps. Initially, the bulk diffusion occurred where the transportation of adsorbate (dyes) from the bulk of the aqueous solution to the liquid film surrounding the solid adsorbent occurred (Karthikeyan et al., 2010). Subsequently, the intraparticle diffusion of the dyes from the liquid film to the surface occurred via pore diffusion and surface diffusion. The final step involved the interaction with the active sites present on the adsorbent.

Activated carbon samples viz. FW-AC-KOH, CH-AC-KOH and OH-AC-KOH were produced at optimal KOH activation at 800 °C and 90 min. Activated carbon samples viz. FW-AC-Steam, CH-AC-Steam and OH-AC-Steam were produced at optimal steam activation at 800 °C and 120 min. It was observed that at a dosage of 2 g/L, food waste (FW-AC-KOH) and canola hull (CH-AC-KOH) derived activated carbon with a surface area of 1760 m^2/g and 1718 m^2/g, respectively exhibited complete removal of methylene blue (Fig. 5.5a) and methyl violet (Fig. 5.5b) from model aqueous solution within 1-2 h of contact time at room temperature. While in the case of Rhodamine B (Fig. 5.5c), the adsorption increased with the contact time up to 2 h and attained equilibrium thereafter. Nearly 94% and 91% removal of dye were achieved with FW-AC-KOH and FW-AC-KOH, respectively.

A similar trend for Rhodamine B adsorption onto rice husk-based activated carbon was reported by Ding et al. (2014). The authors observed a rise in adsorption capacity with the rising temperature of the model aqueous solution, which enabled the mobility of Rhodamine B molecules and shortened the equilibrium time for the adsorption. Furthermore, the rapid adsorption of methylene blue, methyl violet and Rhodamine B at the beginning can be ascribed to their high initial

concentration, which extended the required driving force for dyes to overcome the mass transfer resistance between the liquid phase and adsorbents (Wang et al., 2018). In addition, with the increased adsorbent surface area and the total number of active sites, the total adsorptive capability of dyes was enhanced (Gao et al., 2018). The KOH activated oat hull (i.e., OH-AC-KOH) exhibited lesser adsorption capacity with a contact time ranging from 0 to 6 h and showed removal percentages of 81%, 79% and 72% for methylene blue, methyl violet and Rhodamine B, respectively. The diminished adsorption capacity of OH-AC-KOH compared to FW-AC-KOH and CH-AC-KOH was because of its lower surface area (1334 m^2/g) and total pore volume (0.66 cm^3/g). Similarly, steam activated carbon (e.g., FW-AC-Steam, CH-AC-Steam and OH-AC-Steam) demonstrated a lower removal percentage of the dyes because of their relatively lower surface area and total pore volume compared to KOH-activated carbon samples (Table 5.1). The commercial activated carbon with a surface area of 655 m^2/g showed an inferior performance when compared to the activated carbon derived from food waste, canola hull and oat hull using steam and KOH. Among other steam-activated carbon, OH-AC-Steam with surface area and total pore volume of 733 m^2/g and 0.35 cm^3/g, respectively, showed 55-65% of removal of all three dyes (Fig. 5.5). The non-activated biochar samples with underdeveloped adsorption sites and lower BET surface area showed poor adsorption performance (2-7 m^2/g). However, oat hull-derived biochar (249 m^2/g) showed 20-35% removal of the three dyes. In the pristine adsorbents (i.e., activated carbon), the availability of active sites and empty pores resulted in rapid adsorption at 0-2 h of contact time. The adsorption decelerated gradually (2-6 h) with the reducing available adsorption sites.

Several studies have reported the adsorption of methylene blue, methyl violet and rhodamine B using biochar and activated carbon (Table 4). Foroutan et al. (2019) used Sargassum *oligocystum* derived activated carbon with magnetic Fe_3O_4 nanoparticles for the adsorption of methyl violet and methylene blue. The authors reported 99.4% and 98.7% removal for methylene blue and methyl violet, respectively from an initial concentration of 20 mg/L and adsorbent dosage of 0.15 g/100 mL. In another study, Pathania et al. (2017) used *Ficus carica* bast derived activated carbon for the adsorption of methylene blue with an initial concentration of 500 mg/L and reported 85% removal with 0.5 g/100 mL of adsorbent dosage. The authors investigated different experimental factors and found that temperature, pH, contact time and adsorbent dosage as significant factors impacting the removal of dye compounds. Wu et al. (2020) reported 96% removal of rhodamine

B from aqueous solution using cassava slag-derived biochar at a dose of 4 g/L. Most of the studies used a high dosage of biochar or activated carbon to achieve a higher percentage of dye removal. On the contrary, in our current work, a low dosage of 2 g/L achieved high removal of dyes such as methylene blue, methyl violet and rhodamine B within a short contact time.

The analytical tolerance of dye adsorption is related to its percentage and rate of removal after attaining equilibrium. Overall, the adsorption of dyes by an adsorbent (i.e., biochar or activated carbon) is mostly impacted by factors such as its surface area and porosity, adsorbent loading, initial dye concentration in the solution, pH value, agitation speed and contact time. Most of the studies on adsorption of dyes have implemented a neutral pH of 7-8 (Foroutan et al., 2019; Kelm et al., 2019), room temperature around 25-30°C (Omer et al., 2018; Yang et al., 2020) and agitation speed of 100-200 rpm (Pathania et al., 2017; Kelm et al., 2019). Therefore, in the present study, satisfactory adsorption of dyes by the activated carbon samples was found at neutral pH (7), room temperature, agitation speed of 150 ppm and contact time of 1-2 h.

Table 5.6: Comparison table for dye removal using various biochar and activated carbon products

Feedstock	Adsorbent material	BET surface area (m^2/g)	Target contaminant	Adsorption temperature (°C)	Adsorption pH	Adsorbent dosage	Dye concentration (mg/L)	Removal of dyes (%)	References
Food waste	Activated carbon	1760	Methylene blue	25	7	0.02 g/100 mL	250	99.7	This study
			Methyl violet					99.8	
			Rhodamine B					94.6	
Canola hull		1718	Methylene blue					99.5	
			Methyl violet					99.7	
			Rhodamine B					91.4	
Oat hull		1334	Methylene blue					81.4	
			Methyl violet					79.3	
			Rhodamine B					72.2	
Oat hull	Biochar	249	Methylene blue					29.2	
			Methyl violet					28.1	
			Rhodamine B					22.6	
Chitin	Biochar	33	Methyl violet	25	6.8	0.5 g/L	50	96.9	Zazycki et al. (2019)

Sargassum oligocystum	Activated carbon	127	Methyl violet	25	7	0.15 g/100 mL	20	99.4	Foroutan et al. (2019)
			Methylene blue					98.7	
Ficus carica bast	Activated carbon	-	Methylene Blue	30	7.8	0.5 g/100 mL	500	85	Pathania et al. (2017)
Eucalyptus	Biochar	10.4	Methylene Blue	40	7	8 g/L	5	78.3	Sun et al. (2013)
Palm bark		2.5						89.8	
Cassava slag	Biochar	3.2	Rhodamine B	25	4	4 g/L	500	96	Wu et al. (2020)
Rice husk	Activated carbon	1803	Rhodamine B	20	7	0.02/20 mL	100	95.3	Ding et al. (2014)
							600	63.7	

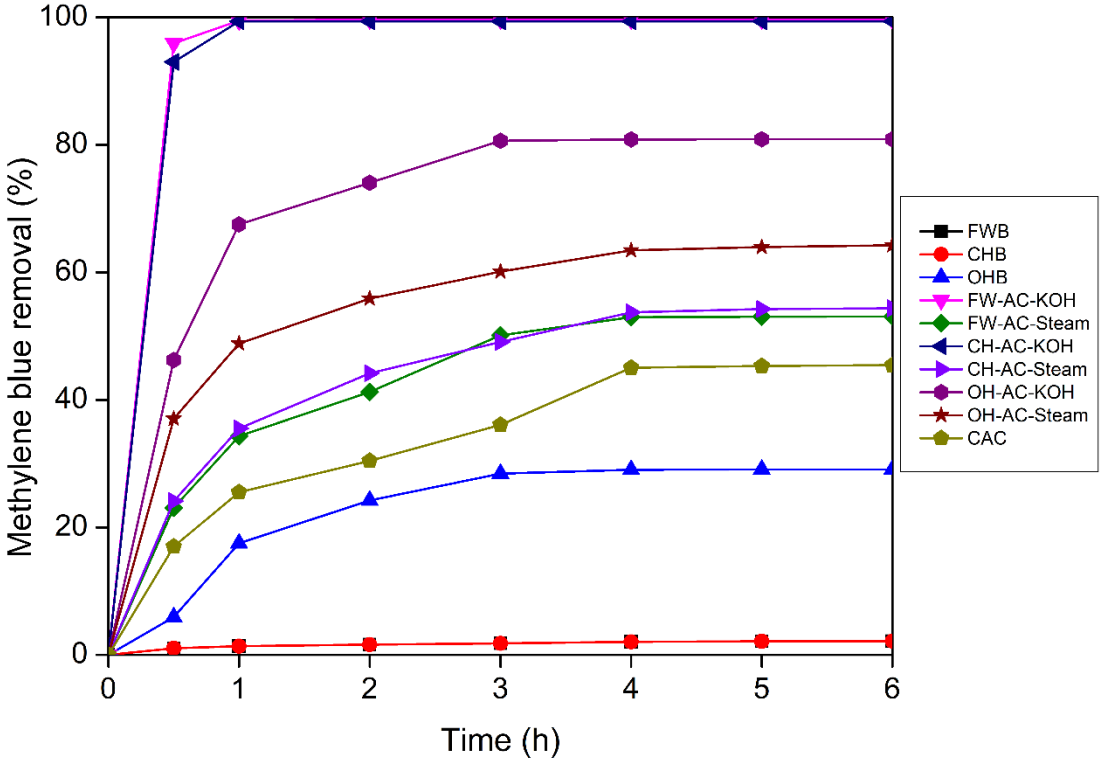
Methylene blue removal (%)
Time (h)
FWB
CHB
OHB
FW-AC-KOH
FW-AC-Steam
CH-AC-KOH
CH-AC-Steam
OH-AC-KOH
OH-AC-Steam
CAC

(a)

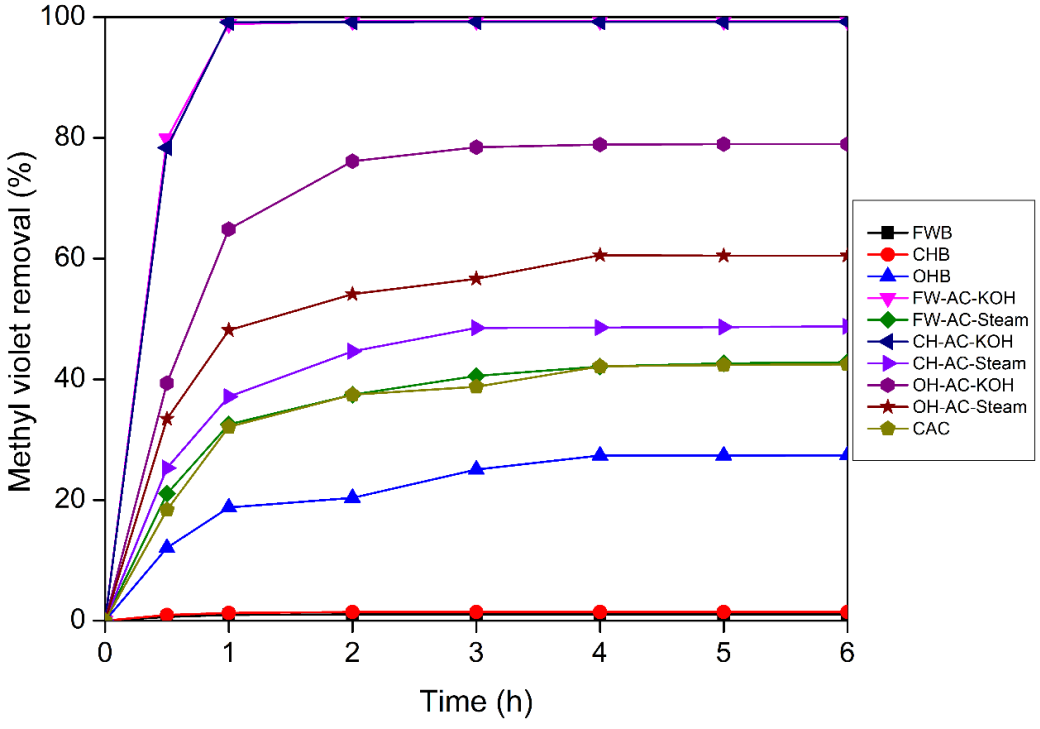
Methyl violet removal (%)
Time (h)
FWB
CHB
OHB
FW-AC-KOH
FW-AC-Steam
CH-AC-KOH
CH-AC-Steam
OH-AC-KOH
OH-AC-Steam
CAC

(b)

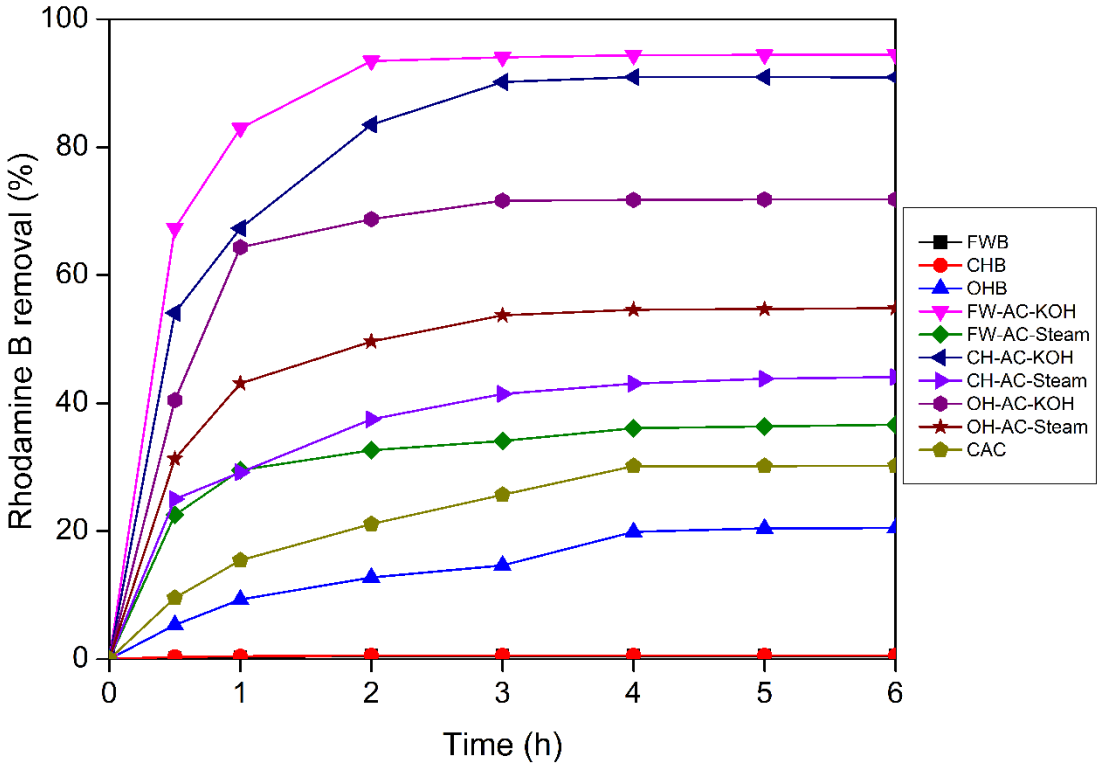

(c)

Fig. 5.5. Performance test of biochar and activated carbon for the adsorption of (a) methylene blue, (b) methyl violet, and (c) Rhodamine B. (Note: Dye removal profiles of different biochar and activated carbon at a dosage of 2 g/L, concentration of 250 mg/L and volume of 100 mL)

5.7 Conclusions

The L_{18} ($2^1 \times 3^2$) Taguchi design method was employed for the first time to optimize the activation conditions for biochar derived from food waste, canola hull and oat hull. The Taguchi-based DOE was efficient in optimizing process parameters of activated carbon. The experimental and predictable values of BET surface area of food waste-based activated carbon at optimum conditions were 1760 m^2/g and 1730 m^2/g, respectively. Furthermore, the high value of R^2 (97%) demonstrated the model's accuracy for new observations. The relative efficacy and impact of the operating parameters on the response (surface area) were ranked as follows: activating agent > temperature > time. Almost complete adsorption of methylene blue, methyl violet and Rhodamine B dyes was observed using activated carbon generated from KOH activation of food waste biochar and canola hull biochar within 0-2 h of contact time.

CHAPTER 6: SUMMARY, OVERALL CONCLUSIONS AND RECOMMENDATIONS

6.1 Summary

In this study, an approach has been made to valorize agro-food residue to generate valuable bio-products for environmental remediation. In the initial phase of this work, slow pyrolysis was employed as thermochemical conversion technology to produce high quality biochar. This phase intended to investigate and favourable slow pyrolysis conditions like temperature (300-600 °C), heating rate (5-20 °C/min), and reaction time (30-60 min) using food waste as a precursor. The biochar produced products (600 °C in 60 min with 5 °C/min of heating rate) exhibited high magnitudes of thermal stability, calorific value, carbon content, aromaticity, pH, electrical conductivity, surface area and pore volume. Furthermore, agriculture residue like canola hull and oat hull were pyrolyzed at the obtained conditions. All the bio-products were subjected to physico-chemical, porosity, different spectroscopic and microscopic characterization to explore their potential applications. The obtained biochar exhibited low surface area and undeveloped porous structure. Thus, the second phase of the work was focused on activation of the biochar from agro-food residue to enhance its surface area and porous structure. The process conditions like activating agent (Steam and KOH), temperature (700-900 °C), activation time (60-120 min) were investigated using Taguchi L_{18} (2^1 X 3^2) method for the activation of food waste-derived biochar. Furthermore, the obtained optimization conditions were utilized for the activation of biochar derived from agricultural residue. The KOH-led chemical activation of biochar at temperature 800 °C and time 90 min was found as optimized conditions and BET surface area of 1760 m^2/g (food waste), 1718 m^2/g (canola hull), 1334 m^2/g (oat hull) with a yield of 48.8, 48.6 and 51.3 wt.%, respectively, were obtained. The performance study of biochar and activated carbon were conducted to explore the effectiveness of such precursors in removing dye pollutants like methylene blue (MB), methyl violet (MV), and Rhodamine B (RhB) from model wastewater. It was found that the activated carbon produced from food waste and canola hull at the Taguchi optimized conditions showed almost complete removal of the dyes at 0-2h of contact time.

6.2 Conclusions

This study described the investigation of process parameters such as temperature, reaction time and heating rate for slow pyrolysis of food waste, canola hull and oat hull biomasses. Maximum biochar yield (52.4 wt%) from food waste was reported at lower temperatures (300 °C), shorter reaction time (30 min) and slower heating rate (5 °C/min). However, the resulting biochar was found to have less thermal stability, low carbon content, inferior heating value, low pH and electrical conductivity, as well as residual biopolymeric contents from the biomass precursor. On the contrary, biochar produced at 600 °C in 60 min with 5 °C/min of heating rate revealed relatively greater magnitudes of thermal stability, calorific value, carbon content, aromaticity, pH, electrical conductivity, surface area and pore volume. The rising temperature resulted in increased HHV for the biochar samples, which was found maximum for oat hull biochar (26.8 MJ/kg) when compared to canola hull biochar (25.6 MJ/kg) and food waste biochar (23 MJ/kg) obtained at the favourable conditions. The findings suggest that food waste biochar as well as canola hull and oat hull, could be used as potential feedstocks for slow pyrolysis to produce biochar for several applications and can also be used for the production of activated carbon.

The process parameters for activation of biochar were optimized for both chemical (Temp: 900 °C, activation time: 90 min) and physical activation (Temp: 800 °C, activation time:120 min) using the Taguchi design method (L18). The KOH activated food waste and canola hull biochar showed a better surface area of 1760 m^2/g and 1730 m^2/g, respectively and showed better adsorption of dye compounds such as methylene blue, methyl violet and Rhodamine B. The relative efficacy and impact of the operating parameters on the response (surface area) were ranked as Activating agent > Temperature > Activation time. Almost complete adsorption of methylene blue, methyl violet, and rhodamine B dyes was observed with adsorbents like FW-ACK and CH-ACK within 0-2 h of contact time. The complete removal of dye from water indicates the prominent role of surface area and active sites in adsorbing the model compounds. Therefore, it can be concluded that the KOH-treated food waste and canola hull-activated carbon were promising adsorbents.

6.3 Recommendations

- For future slow pyrolysis studies, the more detailed characterization of bio-oil and gas can conclude their specific application. Biochar can also be tested as catalyst support.A detailed equilibrium adsorption study with different dye concentrations and adsorbent dosage can be conducted to find out the optimum adsorbent dosage based on the concentration of dye in wastewater.
- The adsorption capacity and the regeneration study of the biochar and activated carbon can be done.
- For the activation of the biochar, microwave ultrasonic pathways can be explored to find out its candidacy in reducing energy inputs. The regeneration study can also be done to make the study cost-effective.
- The techno-economic analysis combined with life cycle analysis should be conducted to evaluate the economic and environmental aspects of the process to explore its potential for industrial applications.

References

Abidi, N., Errais, E., Duplay, J., Berez, A., Jrad, A., Schäfer, G., Trabelsi-Ayadi, M. (2015). Treatment of dye-containing effluent by natural clay. *Journal of Cleaner Production*, *86*, 432-440.

Aboulkas, A., Hammani, H., El Achaby, M., Bilal, E., Barakat, A. (2017). Valorization of algal waste via pyrolysis in a fixed-bed reactor: production and characterization of bio-oil and bio-char. *Bioresource technology*, *243*, 400-408.

Acemioğlu, B. (2019). Removal of a reactive dye using NaOH-activated biochar prepared from peanut shell by pyrolysis process. *International Journal of Coal Preparation and Utilization*,1-23, 1939-2699.

Ahmad, M., Rajapaksha, A. U., Lim, J. E., Zhang, M., Bolan, N., Mohan, D., Ok, Y. S. (2014). Biochar as a sorbent for contaminant management in soil and water: a review. *Chemosphere*, *99*, 19-33.

Ahmed, M. B., Johir, M. A. H., Zhou, J. L., Ngo, H. H., Nghiem, L. D., Richardson, C., Bryant, M. R. (2019). Activated carbon preparation from biomass feedstock: Clean production and carbon dioxide adsorption. *Journal of Cleaner Production*, *225*, 405-413.

Amini, E., Safdari, M. S., DeYoung, J. T., Weise, D. R., Fletcher, T. H. (2019). Characterization of pyrolysis products from slow pyrolysis of live and dead vegetation native to the southern United States. *Fuel*, *235*, 1475-1491.

ASTM D3175-11, Standard method for volatile matter in the analysis sample of coal and coke, ASTM International, Pennsylvania, 2011.

ASTM E1755-01, Standard test method for ash in biomass, ASTM International, Pennsylvania, 2007.

ASTM E871-82, Standard test method for moisture analysis of particulate wood fuels, ASTM International, Pennsylvania, 2006.

Azargohar, R., Dalai, A. K. (2008). Steam and KOH activation of biochar: Experimental and modeling studies. *Microporous and Mesoporous Materials*, *110*(2-3), 413-421.

Azargohar, R., Nanda, S., Dalai, A. K., Kozinski, J. A. (2019). Physico-chemistry of biochars produced through steam gasification and hydro-thermal gasification of canola hull and canola meal pellets. *Biomass and Bioenergy*, *120*, 458-470.

Azargohar, R., Nanda, S., Kang, K., Bond, T., Karunakaran, C., Dalai, A. K., Kozinski, J. A. (2019). Effects of bio-additives on the physicochemical properties and mechanical behavior of canola hull fuel pellets. *Renewable Energy*, *132*, 296-307.

Azargohar, R., Nanda, S., Rao, B. V. S. K., Dalai, A. K. (2013). Slow pyrolysis of deoiled canola meal: product yields and characterization. *Energy & fuels*, *27*(9), 5268-5279.

Azizi, K., Moraveji, M. K., Najafabadi, H. A. (2018). A review on bio-fuel production from microalgal biomass by using pyrolysis method. *Renewable and Sustainable Energy Reviews*, *82*, 3046-3059.

Barbanera, M., & Muguerza, I. F. (2020). Effect of the temperature on the spent coffee grounds torrefaction process in a continuous pilot-scale reactor. *Fuel*, *262*, 116493.

Baysal, M., Bilge, K., Yılmaz, B., Papila, M., Yürüm, Y. (2018). Preparation of high surface area activated carbon from waste-biomass of sunflower piths: kinetics and equilibrium studies on the dye removal. *Journal of environmental chemical engineering*, *6*(2), 1702-1713.

Baytar, O., Şahin, Ö., Saka, C. (2018). Sequential application of microwave and conventional heating methods for preparation of activated carbon from biomass and its methylene blue adsorption. *Applied Thermal Engineering*, *138*, 542-551.

Bergna, D., Varila, T., Romar, H., Lassi, U. (2018). Comparison of the properties of activated carbons produced in one-stage and two-stage processes. *C—Journal of Carbon Research*, *4*(3), 41.

Bocci, E., Sisinni, M., Moneti, M., Vecchione, L., Di Carlo, A., Villarini, M. (2014). State of art of small scale biomass gasification power systems: a review of the different typologies. *Energy Procedia*, *45*, 247-256.

Buratti, C., Barbanera, M., Lascaro, E., Cotana, F. J. W. M. (2018). Optimization of torrefaction conditions of coffee industry residues using desirability function approach. *Waste management*, *73*, 523-534.

Canales-Flores, R. A., Prieto-García, F. (2020). Taguchi optimization for production of activated carbon from phosphoric acid impregnated agricultural waste by microwave heating for the removal of methylene blue. *Diamond and Related Materials*, *109*, 108027.

Cao, L., Iris, K. M., Tsang, D. C., Zhang, S., Ok, Y. S., Kwon, E. E., Poon, C. S. (2018). Phosphoric acid-activated wood biochar for catalytic conversion of starch-rich food waste into glucose and 5-hydroxymethylfurfural. *Bioresource technology*, *267*, 242-248.

Carpenter, D., Westover, T. L., Czernik, S., Jablonski, W. (2014). Biomass feedstocks for renewable fuel production: a review of the impacts of feedstock and pretreatment on the yield and product distribution of fast pyrolysis bio-oils and vapors. *Green Chemistry*, *16*(2), 384-406.

Cesari, L., Canabady-Rochelle, L., Mutelet, F. (2019). Separation of phenols from lignin pyrolysis oil using ionic liquid. *Separation and Purification Technology*, *209*, 528-534.

Chan, Y. H., Yusup, S., Quitain, A. T., Chai, Y. H., Uemura, Y., Loh, S. K. (2018). Extraction of palm kernel shell derived pyrolysis oil by supercritical carbon dioxide: Evaluation and modeling of phenol solubility. *Biomass and bioenergy*, *116*, 106-112.

Chen, D., Chen, X., Sun, J., Zheng, Z., Fu, K. (2016). Pyrolysis polygeneration of pine nut shell: quality of pyrolysis products and study on the preparation of activated carbon from biochar. *Bioresource technology*, *216*, 629-636.

Chen, D., Chen, X., Sun, J., Zheng, Z., Fu, K. (2016). Pyrolysis polygeneration of pine nut shell: quality of pyrolysis products and study on the preparation of activated carbon from biochar. *Bioresource technology*, *216*, 629-636.

Chen, D., Zhou, J., Zhang, Q. (2014). Effects of heating rate on slow pyrolysis behavior, kinetic parameters and products properties of moso bamboo. *Bioresource Technology*, *169*, 313-319.

Chen, H., Chen, X., Qiao, Z., Liu, H. (2016). Release and transformation characteristics of K and Cl during straw torrefaction and mild pyrolysis. *Fuel*, *167*, 31-39.

Chen, J., Liu, Y. S., Deng, W. J., Ying, G. G. (2019). Removal of steroid hormones and biocides from rural wastewater by an integrated constructed wetland. *Science of the Total Environment*, *660*, 358-365.

Chen, W. H., Peng, J., Bi, X. T. (2015). A state-of-the-art review of biomass torrefaction, densification and applications. *Renewable and Sustainable Energy Reviews*, *44*, 847-866.

Choi, Y. K., Cho, M. H., Kim, J. S. (2015). Steam/oxygen gasification of dried sewage sludge in a two-stage gasifier: Effects of the steam to fuel ratio and ash of the activated carbon on the production of hydrogen and tar removal. *Energy*, *91*, 160-167.

Choma, J., Osuchowski, Ł., Dziura, A., Marszewski, M., Jaroniec, M. (2015). Benzene and methane adsorption on ultrahigh surface area carbons prepared from sulphonated styrene divinylbenzene resin by KOH activation. *Adsorption Science & Technology*, *33*(6-8), 587-594.

Correa, C. R., Kruse, A. (2018). Supercritical water gasification of biomass for hydrogen production–Review. *The Journal of Supercritical Fluids*, *133*, 573-590.

Crini, G., Lichtfouse, E., 2019. Advantages and disadvantages of techniques used for wastewater treatment. *Environmental Chemistry Letters*, *17*, 145-155.

da Rosa Schio, R., da Rosa, B. C., Gonçalves, J. O., Pinto, L. A., Mallmann, E. S., Dotto, G. L. (2019). Synthesis of a bio–based polyurethane/chitosan composite foam using ricinoleic acid for the adsorption of Food Red 17 dye. *International journal of biological macromolecules*, *121*, 373-380.

Danish, M., Ahmad, T. (2018). A review on utilization of wood biomass as a sustainable precursor for activated carbon production and application. *Renewable and Sustainable Energy Reviews*, *87*, 1-21.

David, E., Kopac, J. (2018). Pyrolysis of rapeseed oil cake in a fixed bed reactor to produce bio-oil. *Journal of Analytical and Applied Pyrolysis*, *134*, 495-502.

De Lasa, H., Salaices, E., Mazumder, J., Lucky, R. (2011). Catalytic steam gasification of biomass: catalysts, thermodynamics and kinetics. *Chemical reviews*, *111*(9), 5404-5433.

Demiral, I., Aydın Şamdan, C., Demiral, H. (2016). Production and characterization of activated carbons from pumpkin seed shell by chemical activation with ZnCl2. *Desalination and Water Treatment*, *57*(6), 2446-2454.

Ding, L., Zou, B., Gao, W., Liu, Q., Wang, Z., Guo, Y., Liu, Y. (2014). Adsorption of Rhodamine-B from aqueous solution using treated rice husk-based activated carbon. *Colloids and Surfaces A: Physicochemical and Engineering Aspects*, *446*, 1-7.

EMR reports 2020. https://www.expertmarketresearch.com/reports/activated-carbon-market#:~:text=The%20global%20activated%20carbon%20market,forecast%20period%20of%202021%2D2026.

Fan, Q., Sun, J., Chu, L., Cui, L., Quan, G., Yan, J., Iqbal, M. (2018). Effects of chemical oxidation on surface oxygen-containing functional groups and adsorption behavior of biochar. *Chemosphere*, *207*, 33-40.

Feng, Y., Meier, D. (2017). Supercritical carbon dioxide extraction of fast pyrolysis oil from softwood. *The Journal of Supercritical Fluids*, *128*, 6-17.

Fernández-López, J. A., Angosto, J. M., Roca, M. J., Miñarro, M. D. (2019). Taguchi design-based enhancement of heavy metals bioremoval by agroindustrial waste biomass from artichoke. *Science of The Total Environment*, *653*, 55-63.

Foroutan, R., Mohammadi, R., Razeghi, J., Ramavandi, B. (2019). Performance of algal activated carbon/Fe3O4 magnetic composite for cationic dyes removal from aqueous solutions. *Algal Research, 40,* 101509.

Gao, H., Cao, R., Xu, X., Xue, J., Zhang, S., Hayat, T., Li, J. (2018). Surface area-and structure-dependent effects of LDH for highly efficient dye removal. *ACS Sustainable Chemistry & Engineering*, *7*(1), 905-915.

Gokulan, R., Prabhu, G. G., Jegan, J. (2019). Remediation of complex remazol effluent using biochar derived from green seaweed biomass. *International journal of phytoremediation*, *21*(12), 1179-1189.

Guo, X., Yang, Z., Dong, H., Guan, X., Ren, Q., Lv, X., Jin, X. (2016). Simple combination of oxidants with zero-valent-iron (ZVI) achieved very rapid and highly efficient removal of heavy metals from water. *Water research*, *88*, 671-680.

Hansen, S., Mirkouei, A., Diaz, L. A. (2020). A comprehensive state-of-technology review for upgrading bio-oil to renewable or blended hydrocarbon fuels. *Renewable and Sustainable Energy Reviews*, *118*, 109548.

Hansen, V., Müller-Stöver, D., Ahrenfeldt, J., Holm, J. K., Henriksen, U. B., Hauggaard-Nielsen, H. (2015). Gasification biochar as a valuable by-product for carbon sequestration and soil amendment. *Biomass and Bioenergy*, *72*, 300-308.

Heidari, M., Dutta, A., Acharya, B., Mahmud, S. (2019). A review of the current knowledge and challenges of hydrothermal carbonization for biomass conversion. *Journal of the Energy Institute*, *92*(6), 1779-1799.

Heidarinejad, Z., Dehghani, M.H., Heidari, M., Javedan, G., Ali, I., Sillanpää, M., 2020. Methods for preparation and activation of activated carbon: a review. *Environmental Chemistry Letters, 18*, 393–415.

Hesas, R. H., Arami-Niya, A., Daud, W. M. A. W., Sahu, J. N. (2015). Microwave-assisted production of activated carbons from oil palm shell in the presence of CO2 or N2 for CO2 adsorption. *Journal of Industrial and Engineering Chemistry*, *24*, 196-205.

Hodge, K. L., Levis, J. W., DeCarolis, J. F., Barlaz, M. A. (2016). Systematic evaluation of industrial, commercial, and institutional food waste management strategies in the United States. *Environmental science & technology*, *50*(16), 8444-8452.

Intani, K., Latif, S., Cao, Z., Müller, J. (2018). Characterisation of biochar from maize residues produced in a self-purging pyrolysis reactor. *Bioresource technology*, *265*, 224-235.

Inyang, M., Dickenson, E. (2015). The potential role of biochar in the removal of organic and microbial contaminants from potable and reuse water: a review. *Chemosphere*, *134*, 232-240.

Jia, S., Ying, H., Sun, Y., Sun, N., Xu, W., Ning, S. (2017). Co-processing methanol and ethanol in bio-char steam gasification for hydrogen-rich gas production. *International Journal of Hydrogen Energy*, *42*(30), 18844-18852.

Kang, K., Nanda, S., Lam, S.S., Zhang, T., Huo, L., Zhao, L., 2020. Enhanced fuel characteristics and physical chemistry of microwave hydrochar for sustainable fuel pellet production via co-densification. *Environmental Research, 186*, 109480.

Karaj, S., Rehl, T., Leis, H., Müller, J. (2010). Analysis of biomass residues potential for electrical energy generation in Albania. *Renewable and sustainable energy Reviews*, *14*(1), 493-499.

Karmakar, B., Dhawane, S. H., Halder, G. (2018). Optimization of biodiesel production from castor oil by Taguchi design. *Journal of Environmental Chemical Engineering*, *6*(2), 2684-2695.

Karthikeyan, S., Sivakumar, B., Sivakumar, N., 2010. Film and pore diffusion modeling for adsorption of reactive red 2 from aqueous solution on to activated carbon prepared from bio-diesel industrial waste. *E-Journal of Chemistry*, 7, S175-S184.

Katheresan, V., Kansedo, J., Lau, S.Y., 2018. Efficiency of various recent wastewater dye removal methods: a review. *Journal of Environmental Chemistry and Engineering, 6*, 4676-4697.

Kausar, A., Naeem, K., Hussain, T., Bhatti, H.N., Jubeen, F., Nazir, A., Iqbal, M., 2019. Preparation and characterization of chitosan/clay composite for direct Rose FRN dye removal from aqueous media: comparison of linear and non-linear regression methods. *Journal of Materials Research and Technolology*, *8*, 1161-1174.

Kelkar, S., Li, Z., Bovee, J., Thelen, K. D., Kriegel, R. M., Saffron, C. M. (2014). Pyrolysis of North-American grass species: effect of feedstock composition and taxonomy on pyrolysis products. *biomass and bioenergy*, *64*, 152-161.

Kelm, M. A. P., da Silva Júnior, M. J., de Barros Holanda, S. H., de Araujo, C. M. B., de Assis Filho, R. B., Freitas, E. J., da Motta Sobrinho, M. A. (2019). Removal of azo dye from water via adsorption on biochar produced by the gasification of wood wastes. *Environmental Science and Pollution Research*, *26*(28), 28558-28573.

Kilpimaa, S., Runtti, H., Kangas, T., Lassi, U., Kuokkanen, T. (2015). Physical activation of carbon residue from biomass gasification: Novel sorbent for the removal of phosphates and nitrates from aqueous solution. *Journal of Industrial and Engineering Chemistry*, *21*, 1354-1364.

Kim, P., Johnson, A., Edmunds, C. W., Radosevich, M., Vogt, F., Rials, T. G., Labbé, N. (2011). Surface functionality and carbon structures in lignocellulosic-derived biochars produced by fast pyrolysis. *Energy & fuels*, *25*(10), 4693-4703.

Kim, Y. D., Yang, C. W., Kim, B. J., Kim, K. S., Lee, J. W., Moon, J. H., Do Lee, U. (2013). Air-blown gasification of woody biomass in a bubbling fluidized bed gasifier. *Applied energy*, *112*, 414-420.

Kumar, A., Jena, H. M. (2015). High surface area microporous activated carbons prepared from Fox nut (Euryale ferox) shell by zinc chloride activation. *Applied Surface Science*, *356*, 753-761.

Lan, X., Jiang, X., Song, Y., Jing, X., Xing, X., 2019. The effect of activation temperature on structure and properties of blue coke-based activated carbon by CO_2 activation. *Green Process and Synthesis*, *8*, 837–845.

Laurent, A., Pelzer, E., Loyce, C., Makowski, D. (2015). Ranking yields of energy crops: a meta-analysis using direct and indirect comparisons. *Renewable and Sustainable Energy Reviews*, *46*, 41-50.

Lee, Y. E., Jo, J. H., Kim, I. T., Yoo, Y. S. (2017). Chemical characteristics and NaCl component behavior of biochar derived from the salty food waste by water flushing. *Energies*, *10*(10), 1555.

Leng, L., Yuan, X., Zeng, G., Shao, J., Chen, X., Wu, Z., Peng, X. (2015). Surface characterization of rice husk bio-char produced by liquefaction and application for cationic dye (Malachite green) adsorption. *Fuel*, *155*, 77-85.

Li, Z., Gao, X., Wu, L., Wang, K., Kobayashi, N. (2017). Preparation of activated carbons from poplar wood by chemical activation with KOH. *Journal of Porous Materials*, *24*(1), 193-202.

Lin, Y. C., Ho, S. H., Zhou, Y., Ren, N. Q. (2018). Highly efficient adsorption of dyes by biochar derived from pigments-extracted macroalgae pyrolyzed at different temperature. *Bioresource technology*, *259*, 104-110.

Liu, G., Pan, X., Ma, X., Xin, S., Xin, Y. (2020). Effects of feedstock and inherent mineral components on oxidation resistance of biochars. *Science of The Total Environment*, *726*, 138672.

Liu, L., Li, Y., Fan, S. (2019). Preparation of KOH and H3PO4 modified biochar and its application in methylene blue removal from aqueous solution. *Processes*, *7*(12), 891.

Loredo-Cancino, M., Soto-Regalado, E., Cerino-Córdova, F. J., García-Reyes, R. B., García-León, A. M., Garza-González, M. T. (2013). Determining optimal conditions to produce activated carbon from barley husks using single or dual optimization. *Journal of environmental management*, *125*, 117-125.

Mishra, R. K., Mohanty, K. (2020). Pyrolysis of Manilkara zapota seeds over ZSM-5 to produce high-quality bio-oil and chemicals. *Fuel*, *280*, 118594.

Mlonka-Mędrala, A., Evangelopoulos, P., Sieradzka, M., Zajemska, M., Magdziarz, A. (2021). Pyrolysis of agricultural waste biomass towards production of gas fuel and high-quality char: Experimental and numerical investigations. *Fuel*, *296*, 120611.

Mohan, D., Sarswat, A., Ok, Y. S., Pittman Jr, C. U. (2014). Organic and inorganic contaminants removal from water with biochar, a renewable, low cost and sustainable adsorbent–a critical review. *Bioresource technology*, *160*, 191-202.

Mohanty, P., Nanda, S., Pant, K. K., Naik, S., Kozinski, J. A., Dalai, A. K. (2013). Evaluation of the physiochemical development of biochars obtained from pyrolysis of wheat straw, timothy grass and pinewood: effects of heating rate. *Journal of analytical and applied pyrolysis*, *104*, 485-493.

Moralı, U., Demiral, H., Şensöz, S. (2018). Optimization of activated carbon production from sunflower seed extracted meal: Taguchi design of experiment approach and analysis of variance. *Journal of Cleaner Production*, *189*, 602-611.

Mukherjee, A., Okolie, J. A., Abdelrasoul, A., Niu, C., Dalai, A. K. (2019). Review of post-combustion carbon dioxide capture technologies using activated carbon. *Journal of Environmental Sciences*, *83*, 46-63.

Muniandy, L., Adam, F., Mohamed, A. R., Ng, E. P. (2014). The synthesis and characterization of high purity mixed microporous/mesoporous activated carbon from rice husk using chemical activation with NaOH and KOH. *Microporous and Mesoporous Materials*, *197*, 316-323.

Nanda, S., A Kozinski, J., Dalai, A. K. (2016). Lignocellulosic biomass: a review of conversion technologies and fuel products. *Current Biochemical Engineering*, *3*(1), 24-36.

Nanda, S., Azargohar, R., Kozinski, J. A., Dalai, A. K. (2014). Characteristic studies on the pyrolysis products from hydrolyzed Canadian lignocellulosic feedstocks. *BioEnergy Research*, *7*(1), 174-191.

Nanda, S., Berruti, F. (2020). A technical review of bioenergy and resource recovery from municipal solid waste. *Journal of Hazardous Materials*, 123970.

Nanda, S., Berruti, F. (2020). Municipal solid waste management and landfilling technologies: a review. *Environmental Chemistry Letters*, 1-24.

Nanda, S., Dalai, A. K., Berruti, F., Kozinski, J. A. (2016). Biochar as an exceptional bioresource for energy, agronomy, carbon sequestration, activated carbon and specialty materials. *Waste and Biomass Valorization*, *7*(2), 201-235.

Nanda, S., Dalai, A. K., Berruti, F., Kozinski, J. A. (2016). Biochar as an exceptional bioresource for energy, agronomy, carbon sequestration, activated carbon and specialty materials. *Waste and Biomass Valorization*, *7*(2), 201-235.

Nanda, S., Dalai, A. K., Berruti, F., Kozinski, J. A. (2016). Biochar as an exceptional bioresource for energy, agronomy, carbon sequestration, activated carbon and specialty materials. *Waste and Biomass Valorization*, *7*(2), 201-235.

Nanda, S., Gong, M., Hunter, H. N., Dalai, A. K., Gökalp, I., Kozinski, J. A. (2017). An assessment of pinecone gasification in subcritical, near-critical and supercritical water. *Fuel Processing Technology*, *168*, 84-96.

Nanda, S., Gong, M., Hunter, H. N., Dalai, A. K., Gökalp, I., Kozinski, J. A. (2017). An assessment of pinecone gasification in subcritical, near-critical and supercritical water. *Fuel Processing Technology*, *168*, 84-96.

Nanda, S., Maley, J., Kozinski, J. A., Dalai, A. K. (2015). Physico-chemical evolution in lignocellulosic feedstocks during hydrothermal pretreatment and delignification. *Journal of Biobased Materials and Bioenergy*, *9*(3), 295-308.

Nanda, S., Mohanty, P., Pant, K. K., Naik, S., Kozinski, J. A., Dalai, A. K. (2013). Characterization of North American lignocellulosic biomass and biochars in terms of their candidacy for alternate renewable fuels. *Bioenergy Research*, *6*(2), 663-677.

Nautiyal, P., Subramanian, K. A., Dastidar, M. G. (2016). Adsorptive removal of dye using biochar derived from residual algae after in-situ transesterification: alternate use of waste of biodiesel industry. *Journal of environmental management*, *182*, 187-197.

Nazem, M. A., Zare, M. H., Shirazian, S. (2020). Preparation and optimization of activated nano-carbon production using physical activation by water steam from agricultural wastes. *RSC advances*, *10*(3), 1463-1475.

Ning, S., Jia, S., Ying, H., Sun, Y., Xu, W., Yin, H. (2018). Hydrogen-rich syngas produced by catalytic steam gasification of corncob char. *Biomass and Bioenergy*, *117*, 131-136.

Nizamuddin, S., Shrestha, S., Athar, S., Ali, B. S., Siddiqui, M. A. (2016). A critical analysis on palm kernel shell from oil palm industry as a feedstock for solid char production. *Reviews in Chemical Engineering*, *32*(5), 489-505.

Nourmoradi, H., Moghadam, K. F., Jafari, A., Kamarehie, B. (2018). Removal of acetaminophen and ibuprofen from aqueous solutions by activated carbon derived from Quercus Brantii (Oak) a corn as a low-cost biosorbent. *Journal of environmental chemical engineering*, *6*(6), 6807-6815.

Okolie, J. A., Nanda, S., Dalai, A. K., Berruti, F., Kozinski, J. A. (2020). A review on subcritical and supercritical water gasification of biogenic, polymeric and petroleum wastes to hydrogen-rich synthesis gas. *Renewable and Sustainable Energy Reviews*, *119*, 109546.

Okolie, J. A., Nanda, S., Dalai, A. K., Kozinski, J. A. (2020). Chemistry and specialty industrial applications of lignocellulosic biomass. *Waste and Biomass Valorization*, 1-25.

Okolie, J. A., Nanda, S., Dalai, A. K., Kozinski, J. A. (2020). Hydrothermal gasification of soybean straw and flax straw for hydrogen-rich syngas production: Experimental and thermodynamic modeling. *Energy Conversion and Management*, *208*, 112545.

Okolie, J. A., Nanda, S., Dalai, A. K., Kozinski, J. A. (2020). Optimization and modeling of process parameters during hydrothermal gasification of biomass model compounds to generate hydrogen-rich gas products. *International Journal of Hydrogen Energy*, *45*(36), 18275-18288.

Olugbade, T. O., & Ojo, O. T. (2020). Biomass torrefaction for the production of high-grade solid biofuels: a review. *BioEnergy Research*, *13*, 999-1015.

Omer, O. S., Hussein, M. A., Hussein, B. H., Mgaidi, A. (2018). Adsorption thermodynamics of cationic dyes (methylene blue and crystal violet) to a natural clay mineral from aqueous solution between 293.15 and 323.15 K. *Arabian Journal of Chemistry*, *11*(5), 615-623.

Ozdemir, I., Şahin, M., Orhan, R., Erdem, M. (2014). Preparation and characterization of activated carbon from grape stalk by zinc chloride activation. *Fuel processing technology*, *125*, 200-206.

Patel P. Tackling Delhi's Air Pollution Problem. ACS Central Science 2019;5:3–6

Pathania, D., Sharma, S., Singh, P. (2017). Removal of methylene blue by adsorption onto activated carbon developed from Ficus carica bast. *Arabian Journal of Chemistry*, *10*, S1445-S1451.

Pattanaik, L., Pattnaik, F., Saxena, D. K., Naik, S. N. (2019). Biofuels from agricultural wastes. In *Second and Third Generation of Feedstocks* (pp. 103-142). Elsevier.

Placido, J., Bustamante-López, S., Meissner, K. E., Kelly, D. E., Kelly, S. L. (2019). Comparative study of the characteristics and fluorescent properties of three different biochar derived-carbonaceous nanomaterials for bioimaging and heavy metal ions sensing. *Fuel Processing Technology*, *196*, 106163.

Puligundla, P., Oh, S. E., Mok, C. (2016). Microwave-assisted pretreatment technologies for the conversion of lignocellulosic biomass to sugars and ethanol: a review. *Carbon letters*, *17*(1), 1-10.

Qambrani, N. A., Rahman, M. M., Won, S., Shim, S., Ra, C. (2017). Biochar properties and eco-friendly applications for climate change mitigation, waste management, and wastewater treatment: A review. *Renewable and Sustainable Energy Reviews*, *79*, 255-273.

Qian, K., Kumar, A., Zhang, H., Bellmer, D., Huhnke, R. (2015). Recent advances in utilization of biochar. *Renewable and Sustainable Energy Reviews*, *42*, 1055-1064.

Rafiq, M. K., Bachmann, R. T., Rafiq, M. T., Shang, Z., Joseph, S., Long, R. (2016). Influence

of pyrolysis temperature on physico-chemical properties of corn stover (Zea mays L.) biochar and feasibility for carbon capture and energy balance. *PloS one*, *11*(6), e0156894.

Rambabu, N., Azargohar, R., Dalai, A. K., Adjaye, J. (2013). Evaluation and comparison of enrichment efficiency of physical/chemical activations and functionalized activated carbons derived from fluid petroleum coke for environmental applications. *Fuel Processing Technology*, *106*, 501-510.

Rambabu, N., Rao, B. V. S. K., Surisetty, V. R., Das, U., Dalai, A. K. (2015). Production, characterization, and evaluation of activated carbons from de-oiled canola meal for environmental applications. *Industrial Crops and Products*, *65*, 572-581.

Rao, M. A., Simeone, G. D. R., Scelza, R., Conte, P. (2017). Biochar based remediation of water and soil contaminated by phenanthrene and pentachlorophenol. *Chemosphere*, *186*, 193-201.

Rashid, R. A., Jawad, A. H., Ishak, M. A. M., Kasim, N. N. (2016). KOH-activated carbon developed from biomass waste: adsorption equilibrium, kinetic and thermodynamic studies for Methylene blue uptake. *Desalination and Water Treatment*, *57*(56), 27226-27236.

Rashidi, N. A., Yusup, S. (2017). A review on recent technological advancement in the activated carbon production from oil palm wastes. *Chemical Engineering Journal*, *314*, 277-290.

Robbins, M. P., Evans, G., Valentine, J., Donnison, I. S., Allison, G. G. (2012). New opportunities for the exploitation of energy crops by thermochemical conversion in Northern Europe and the UK. *Progress in Energy and Combustion Science*, *38*(2), 138-155.

Roy, P., Dias, G. (2017). Prospects for pyrolysis technologies in the bioenergy sector: A review. *Renewable and Sustainable Energy Reviews*, *77*, 59-69.

Sadh, P. K., Duhan, S., Duhan, J. S. (2018). Agro-industrial wastes and their utilization using solid state fermentation: a review. *Bioresources and Bioprocessing*, *5*(1), 1-15.

Safdari, M. S., Amini, E., Weise, D. R., Fletcher, T. H. (2019). Heating rate and temperature effects on pyrolysis products from live wildland fuels. *Fuel*, *242*, 295-304.

Saidur, R., Abdelaziz, E. A., Demirbas, A., Hossain, M. S., Mekhilef, S. (2011). A review on biomass as a fuel for boilers. *Renewable and sustainable energy reviews*, *15*(5), 2262-2289.

Senneca, O., Cerciello, F., Heuer, S., Ammendola, P. (2018). Slow pyrolysis of walnut shells in nitrogen and carbon dioxide. *Fuel*, *225*, 419-425.

Shahkarami, S., Azargohar, R., Dalai, A. K., Soltan, J. (2015). Breakthrough CO2 adsorption in bio-based activated carbons. *Journal of environmental sciences*, *34*, 68-76.

Shak, K. P. Y., Wu, T. Y. (2014). Coagulation–flocculation treatment of high-strength agro-industrial wastewater using natural Cassia obtusifolia seed gum: treatment efficiencies and flocs characterization. *Chemical Engineering Journal*, *256*, 293-305.

Shen, Y., Fu, Y. (2018). KOH-activated rice husk char via CO2 pyrolysis for phenol adsorption. *Materials today energy*, *9*, 397-405.

Shin, H., Tiwari, D., Kim, D. J. (2020). Phosphate adsorption/desorption kinetics and P bioavailability of Mg-biochar from ground coffee waste. *Journal of Water Process Engineering*, *37*, 101484.

Shinya, Yokoyama. 2008. "The Asian Biomass Handbook A Guide for Biomass Production and Utilization Support Project for Building Asian-Partnership for Environmentally Conscious Agriculture, Entrusted by Ministry of Agriculture, Forestry, and Fisheries The Japan Institute of Energy," 338.

Siddiqui, M. T. H., Nizamuddin, S., Mubarak, N. M., Shirin, K., Aijaz, M., Hussain, M., & Baloch, H. A. (2019). Characterization and process optimization of biochar produced using novel biomass, waste pomegranate peel: a response surface methodology approach. *Waste and biomass valorization*, *10*(3), 521-532.

Sieradzka, M., Gao, N., Quan, C., Mlonka-Mędrala, A., Magdziarz, A. (2020). Biomass thermochemical conversion via pyrolysis with integrated CO2 capture. *Energies*, *13*(5), 1050.

Singh, A., Nanda, S., Guayaquil Sosa, F., Berruti, F. Pyrolysis of Miscanthus and characterization of value-added bio-oil and biochar products. *The Canadian Journal of Chemical Engineering*.

Singh, R. P., Kaskaoutis, D. G. (2014). Crop residue burning: a threat to South Asian air quality. *Eos, Transactions American Geophysical Union*, *95*(37), 333-334.

Sukiran, M. A., Abnisa, F., Daud, W. M. A. W., Bakar, N. A., Loh, S. K. (2017). A review of torrefaction of oil palm solid wastes for biofuel production. *Energy Conversion and Management*, *149*, 101-120.

Suliman, W., Harsh, J. B., Abu-Lail, N. I., Fortuna, A. M., Dallmeyer, I., & Garcia-Perez, M. (2016). Influence of feedstock source and pyrolysis temperature on biochar bulk and surface properties. *Biomass and Bioenergy*, *84*, 37-48.

Sun, J., Dai, X., Wang, Q., van Loosdrecht, M. C., Ni, B. J. (2019). Microplastics in wastewater treatment plants: Detection, occurrence and removal. *Water research*, *152*, 21-37.

Sun, L., Wan, S., Luo, W. (2013). Biochars prepared from anaerobic digestion residue, palm bark, and eucalyptus for adsorption of cationic methylene blue dye: characterization, equilibrium, and kinetic studies. *Bioresource technology*, *140*, 406-413.

Suryawanshi, P.G., Das, S., Borugadda, V.B., Goud, V.V., Dalai, A.K., (2020). Process improvements and techno-economic feasibility of hydrothermal liquefaction and pyrolysis of biomass for biocrude oil production. In: Biorefinery of Alternative Resources: Targeting Green Fuels and Platform Chemicals, Nanda S., Vo, D.V.N., Sarangi, P.K. (Eds.), Springer Nature, Singapore, pp. 221-248.

Tao, J., Li, C., Li, J., Yan, B., Chen, G., Cheng, Z., Hou, L. (2020). Multi-step separation of different chemical groups from the heavy fraction in biomass fast pyrolysis oil. *Fuel Processing Technology*, *202*, 106366.

Teh, C. Y., Wu, T. Y., Juan, J. C. (2014). Potential use of rice starch in coagulation–flocculation process of agro-industrial wastewater: treatment performance and flocs characterization. *Ecological engineering*, *71*, 509-519.

Tehrani, N. F., Aznar, J. S., Kiros, Y. (2015). Coffee extract residue for production of ethanol and activated carbons. *Journal of Cleaner Production*, *91*, 64-70.

Thangalazhy-Gopakumar, S., Al-Nadheri, W. M. A., Jegarajan, D., Sahu, J. N., Mubarak, N. M., Nizamuddin, S. (2015). Utilization of palm oil sludge through pyrolysis for bio-oil and bio-char production. *Bioresource technology*, *178*, 65-69.

Tomczyk, A., Sokołowska, Z., Boguta, P. (2020). Biochar physicochemical properties: pyrolysis temperature and feedstock kind effects. *Reviews in Environmental Science and Bio/Technology*, *19*(1), 191-215.

Tran, H. N., Chao, H. P., You, S. J. (2018). Activated carbons from golden shower upon different chemical activation methods: synthesis and characterizations. *Adsorption Science & Technology*, *36*(1-2), 95-113.

Tran, H. N., Tomul, F., Ha, N. T. H., Nguyen, D. T., Lima, E. C., Le, G. T., Woo, S. H. (2020). Innovative spherical biochar for pharmaceutical removal from water: Insight into adsorption mechanism. *Journal of hazardous materials*, *394*, 122255.

Tripathi, M., Sahu, J. N., Ganesan, P. (2016). Effect of process parameters on production of biochar from biomass waste through pyrolysis: A review. *Renewable and Sustainable Energy Reviews*, *55*, 467-481.

Tsai, W. T., Jiang, T. J. (2018). Mesoporous activated carbon produced from coconut shell using a single-step physical activation process. *Biomass Conversion and Biorefinery*, *8*(3), 711-718.

Usman, A. R., Abduljabbar, A., Vithanage, M., Ok, Y. S., Ahmad, M., Ahmad, M., Al-Wabel, M. I. (2015). Biochar production from date palm waste: charring temperature induced changes in composition and surface chemistry. *Journal of Analytical and Applied Pyrolysis*, *115*, 392-400.

Valix, M., Cheung, W.H., McKay, G., 2004. Preparation of activated carbon using low temperature carbonisation and physical activation of high ash raw bagasse for acid dye adsorption. *Chemosphere, 56,* 493-501.

Vyavahare, G. D., Gurav, R. G., Jadhav, P. P., Patil, R. R., Aware, C. B., Jadhav, J. P. (2018). Response surface methodology optimization for sorption of malachite green dye on sugarcane bagasse biochar and evaluating the residual dye for phyto and cytogenotoxicity. *Chemosphere*, *194*, 306-315.

Wang, L., Wang, Y., Ma, F., Tankpa, V., Bai, S., Guo, X., Wang, X. (2019). Mechanisms and reutilization of modified biochar used for removal of heavy metals from wastewater: a review. *Science of the total environment*, *668*, 1298-1309.

Wang, X., Jiang, C., Hou, B., Wang, Y., Hao, C., Wu, J. (2018). Carbon composite lignin-based adsorbents for the adsorption of dyes. *Chemosphere*, *206*, 587-596.

Weber B. Canada is one of the biggest wasters of food, report finds. The Globe and Mail. 2018. https://www.theglobeandmail.com/canada/article-canada-is-one-of-the-biggest-wasters-of-food-report-finds/ (accessed on 13 January 2021)

Wilk, M., Magdziarz, A. (2017). Hydrothermal carbonization, torrefaction and slow pyrolysis of Miscanthus giganteus. *Energy*, *140*, 1292-1304.

Williams, C. L., Westover, T. L., Emerson, R. M., Tumuluru, J. S., Li, C. (2016). Sources of biomass feedstock variability and the potential impact on biofuels production. *BioEnergy Research*, *9*(1), 1-14.

Worldometer. Current World Population. https://www.worldometers.info/world-population/. Accessed 22 Oct 2020.

Wu, J., Yang, J., Huang, G., Xu, C., Lin, B. (2020). Hydrothermal carbonization synthesis of cassava slag biochar with excellent adsorption performance for Rhodamine B. *Journal of Cleaner Production*, *251*, 119717.

Xu, R. K., Xiao, S. C., Yuan, J. H., Zhao, A. Z. (2011). Adsorption of methyl violet from aqueous solutions by the biochars derived from crop residues. *Bioresource technology*, *102*(22), 10293-10298.

Xue, S., Zhang, X., Ngo, H. H., Guo, W., Wen, H., Li, C., Ma, C. (2019). Food waste based biochars for ammonia nitrogen removal from aqueous solutions. *Bioresource technology*, *292*, 121927.

Yaashikaa, P. R., Kumar, P. S., Varjani, S. J., Saravanan, A. (2019). Advances in production and application of biochar from lignocellulosic feedstocks for remediation of environmental pollutants. *Bioresource technology*, *292*, 122030.

Yahya, M. A., Al-Qodah, Z., Ngah, C. Z. (2015). Agricultural bio-waste materials as potential sustainable precursors used for activated carbon production: A review. *Renewable and Sustainable Energy Reviews*, *46*, 218-235.

Yang, F., Zhang, S., Cheng, K., Antonietti, M. (2019). A hydrothermal process to turn waste biomass into artificial fulvic and humic acids for soil remediation. *Science of the total environment*, *686*, 1140-1151.

Yao, F. X., Arbestain, M. C., Virgel, S., Blanco, F., Arostegui, J., Maciá-Agulló, J. A., Macìas, F. (2010). Simulated geochemical weathering of a mineral ash-rich biochar in a modified Soxhlet reactor. *Chemosphere*, *80*(7), 724-732.

Zazycki, M. A., Borba, P. A., Silva, R. N., Peres, E. C., Perondi, D., Collazzo, G. C., Dotto, G. L. (2019). Chitin derived biochar as an alternative adsorbent to treat colored effluents containing methyl violet dye. *Advanced Powder Technology*, *30*(8), 1494-1503.

Zhang, B., Feng, H., He, Z., Wang, S., Chen, H. (2018). Bio-oil production from hydrothermal liquefaction of ultrasonic pre-treated Spirulina platensis. *Energy Conversion and Management*, *159*, 204-212.

Zhang, S., Su, Y., Xiong, Y., Zhang, H. (2020). Physicochemical structure and reactivity of char from torrefied rice husk: Effects of inorganic species and torrefaction temperature. *Fuel*, *262*, 116667.

Zhou, L., Santomauro, F., Fan, J., Macquarrie, D., Clark, J., Chuck, C. J., Budarin, V. (2017). Fast microwave-assisted acidolysis: a new biorefinery approach for the zero-waste utilisation of lignocellulosic biomass to produce high quality lignin and fermentable saccharides. *Faraday discussions, 202*, 351-370.

Appendix

Table A.1. Process conditions and yield for the biochar, bio-oil, and gas produced from food waste through slow pyrolysis process

Biomass precursors	Temperature (°C)	Reaction Time (min)	Heating rate (°C/min)	Biochar Yield (%)	Bio-oil Yield (%)	Gas Yield (%)
At constant reaction time and heating rate						
Food waste	300	30	5	52.4 ± 1.2	25.5± 2.3	15.7± 2.2
Food waste	400	30	5	34.6±2	29.5±1.1	18.6±2.1
Food waste	500	30	5	32.4±1.4	42.4±2.8	20.1±2.8
Food waste	600	30	5	30.6±0.9	36.3±2.1	22.3±2.3
At constant temperature (optimized) and heating rate						
Food waste	600	40	5	29.0±1.2	35.8±1.4	25.9±1.5
Food waste	600	50	5	28.6±2.1	33.4±2.4	27.05±3.2
Food waste	600	60	5	28.4±1.2	32.35±1.3	30.6±2.1
At constant optimized temperature and reaction time						
Food waste	600	60	10	27.0±2.5	30.5±2	31.5±2
Food waste	600	60	15	24.6±2.1	34.3±3.1	34.3±1.9
Food waste	600	60	20	22±1.5	35.9±2.1	35.9±3
Biochar yield for different agricultural and individual food waste at optimized temperature, reaction time, and heating rate						
Canola Hull	600	60	5	28.8±1.8	33.25±1.3	29.6±2.0
Oat Hull	600	60	5	29.1±1.3	28.8±1.6	32.5±1.9
Pistachio shell	600	60	5	30.1±1.2	34.6±2.1	25.30±1.1
Onion peel	600	60	5	20.5±1.6	22.9±2.7	43.0±2.7
Bell pepper	600	60	5	25.6±1.5	24.5±1.4	29.3±1.7
Carrot	600	60	5	24.3±1.7	25.35±1.8	33.5±1.5

Table A.2. Porous characteristics of the food waste based activated carbons

Activating agent	Temperature ^{o} C	Activation Time (min)	Specific surface area (m^2/g)	Total pore volume (cm^3/g)	Average pore size (nm)	Yield (wt.%)
KOH	700	60	1323	0.67	4.8	62.4
KOH	700	90	1447	0.74	4.1	58.5
KOH	700	120	1398	0.71	4.6	53.8
KOH	800	60	1489	0.75	4.1	52.6
KOH	800	90	1760	0.94	3.7	48.8
KOH	800	120	1723	0.91	3.9	41.4
KOH	900	60	1820	0.95	3.4	50.2
KOH	900	90	1681	0.93	3.8	43.6
KOH	900	120	1407	0.76	3.9	40.3
Steam	700	60	101	0.06	9.13	71.4
Steam	700	90	214	0.11	7.7	63.1
Steam	700	120	262	0.14	5.8	58.7
Steam	800	60	275	0.15	5.2	61.2
Steam	800	90	385	0.28	4.6	54.1
Steam	800	120	529	0.38	3.8	49.3
Steam	900	60	406	0.31	4.2	47.8
Steam	900	90	421	0.32	4.1	43.5
Steam	900	120	348	0.22	4.8	37.4

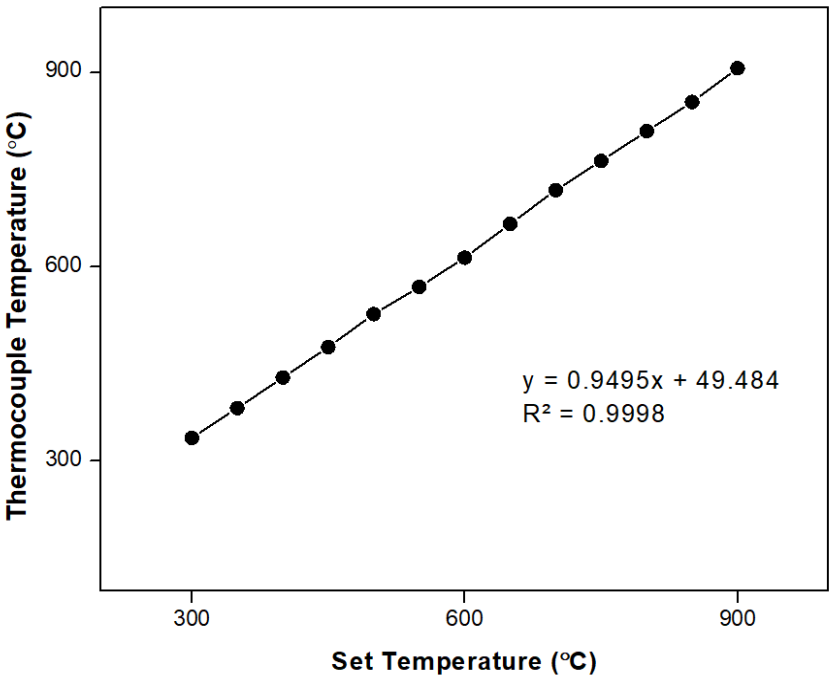

Fig. A.1. Calibration of the reactor temperature

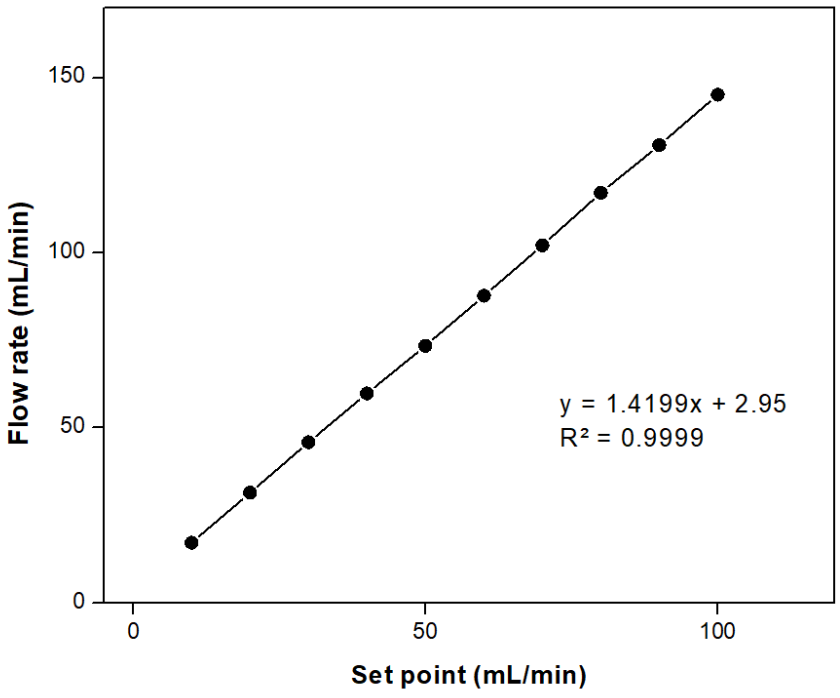

Fig. A.2. Calibration of mass flow meter

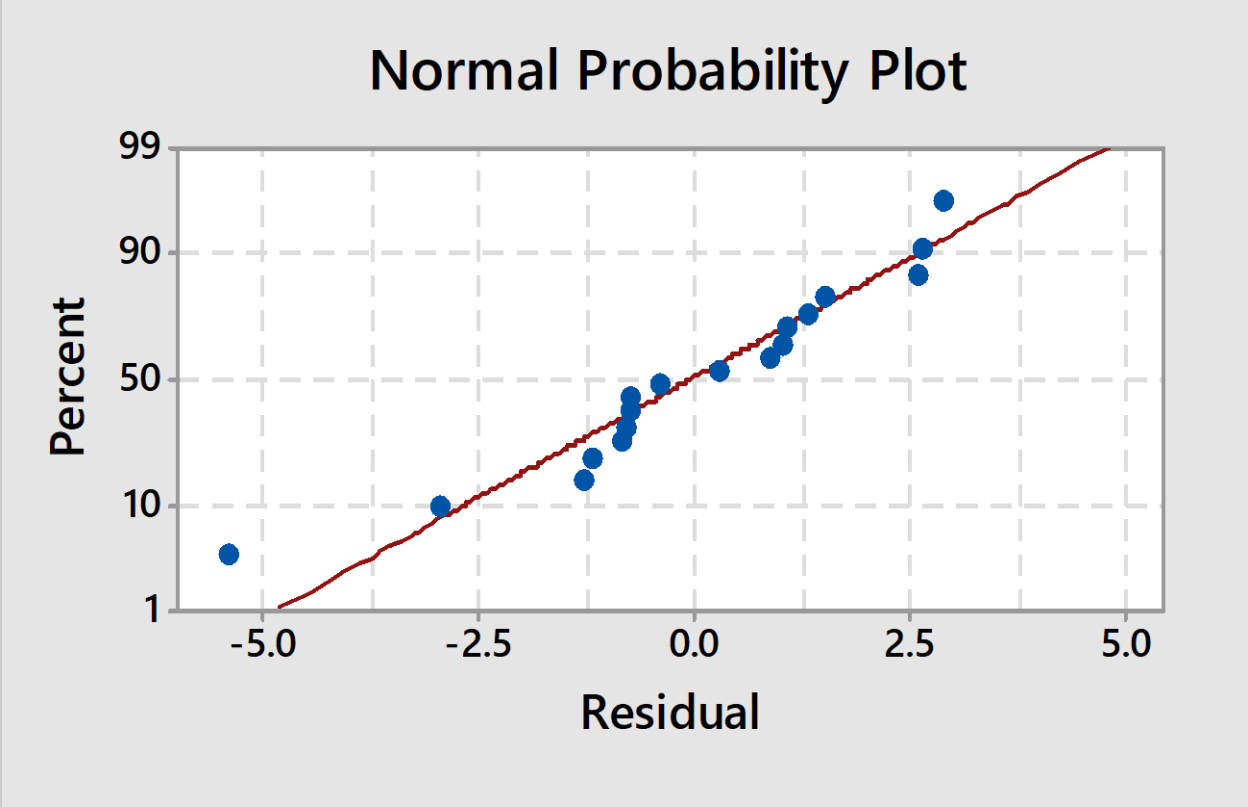

Fig. A.3. Normal probability plot for surface area (m^2/g)